Biomimetic and Estrogenic Plant-Based Nanofibrous Wound Dressings

Biomimetic and Estrogenic Plant-based Nanofibrous Wound Dressings

A dissertation presented

by

Seungkuk Ahn

to

The Harvard John A. Paulson School of Engineering and Applied Sciences

in partial fulfillment of the requirements

for the degree of

Doctor of Philosophy

in the subject of

Engineering Sciences

Harvard University

Cambridge, Massachusetts

March, 2019

Dissertation Advisor: Professor Kevin Kit Parker Author: Seungkuk Ahn

Biomimetic and Estrogenic Plant-based Nanofibrous Wound Dressings

Abstract

Naturally healed wounds do not perfectly regenerate cutaneous connective tissue, which often leads to extensive scarring or unhealed wounds. However, engineering regenerative wound dressings, which is a $10 billion market globally, remains a challenge for primary healthcare. Estrogen, a primary female sex hormone, accelerates wound healing via estrogen receptor (ER)-β but also triggers various breast cancers via ER-α, indicating that the use of estrogen is problematic. A better alternative to estrogen is an estrogenic material that can selectively activate the ER-β signaling pathway for enhanced wound healing without a high risk of triggering ER-α-positive cancers. Soy protein possesses phytoestrogens that have a structure and function similar to estrogen. Interestingly, soy phytoestrogens preferentially induce the ER-β signaling pathway. Moreover, soy phytoestrogens carry bioactive peptides that are similar to extracellular matrix (ECM) proteins in healthy skin. Despite these biological advantages, engineering soy-based scaffolds remains a challenge due to the low molecular weight of soy protein and the lack of studies thoroughly characterizing and optimizing processes for biomedical applications. We therefore propose to engineer estrogenic and ECM-mimetic soy-based nanofibrous scaffolds to accelerate wound healing. The engineered soy nanofibers successfully recapitulated the fiber morphology and diameter, pore diameter, and stiffness of native skin and transported bioactive contents (proteins and phytoestrogens). Moreover, the soy-based nanofibers showed high water retention, which could provide a moist environment to promote healing. As a result, soy

increased *in vitro* fibroblast proliferation and migration on nanofibers compared to those without soy protein. The soy-based scaffolds significantly accelerated tissue restoration in both mouse and human skins. More importantly, these scaffolds promoted re-epithelialization, ECM remodeling, and hair follicle formation via the ER-β pathways. This study confirmed that soy-based dressings enhance wound closure and tissue regeneration via the ER-β pathways by providing a biomimetic and estrogenic microenvironment and by improving the physicochemical properties of scaffolds. We envision that our scaffolds will be the next generation of one-step, cost-effective regenerative scaffolds for primary care of severe cutaneous wounds.

Table of Contents

Table of Figures

Acknowledgments

During my Ph.D. journey, I encountered countless challenges and opportunities that stemmed not only from my research but also from the cultural differences and new relationships throughout my new American life here. During these past years, I went through remarkable academic and personal metamorphoses—everything from publishing 4 first author papers 2 cover articles, presenting my researches at international conferences, being featured in an National Public Radio podcast, and finding the love of my life that led to my new roles as a husband and now an expecting father! I am very grateful that I met my wife, Su-Yeon Angela Choi, here during my time of solitude and struggled research. She is always so energetic, active, and future-oriented to design and execute our life goals together. I am continually inspired by her as she provides me with such different ideas and unique perspectives, coming from her design experiences and larger landscape thinking. I truly know that, without her unwavering support and encouragement, much of what I achieved throughout my studies would not have been possible. I am also greatly indebted to my parents, Sumin An and Hangsook Jung, for always being on my side unconditionally. Their love and support gave me the courage to pursue my dreams. I aspire to become such a parent for my child-to-come. My sister and brother, Jisun Ahn and Munki Jung, also regard me as the family pride and remind me that my hard work is not only for myself but for the honor of my beloved family. In addition, I would like to express my sincere appreciation to my parents-in-law, Byungin Choi and Nanjoo Koh, for their valuable advices and wisdom. The fact that they were also studying here in Cambridge, MA, 30 years ago, while also raising their children and pursing their degrees, gives me much strength and consolation. Their

experiences help broaden my perspectives in planning my own future, balancing both family and career.

I would like to thank my advisor, Professor Kevin Kit Parker. He changed my life after I first met him in 2012 when I joined the Disease Biophysics Group as a visiting master's student. From time to time, he and I collided and passionately discussed regarding research directions and my projects too. Ultimately, his genuine support for my scientific pursuits and life plans was absolutely invaluable. He pushed me to exceed my own limit to become a better scientist and a stronger human being to contribute to my family, my country, and the scientific knowledge. To say that I have learned a lot from him is truly an understatement. I thank him from the bottom of my heart for giving me this opportunity to grow.

I want to acknowledge all members of the Disease Biophysics Group who suffered through the hard times together and overcame many challenges throughout my studies. Especially, I would like to sincerely thank Sung Jin Park, Johan Lind, Herdeline (Digs) Ardoña, Leila Deravi, Chritophe Chantre, Patrick Campbell, Grant Gonzalez, and Ben Pope for their mentorship and friendship. Lastly, I would like to express my gratitude to the Fulbright foundation for their generous offer of fellowship that enabled my study, my previous advisor, Professor Kwanwoo Shin, for his continuous support, and my committee members, Professors Joanna Aizenberg, Katia Bertoldi, and Jennifer Lewis, for their guidance.

1 Introduction

Wounded human skin tissue cannot easily regenerate its original structure and function due to its poor regenerative capacity.[1] Accordingly, development of scaffolds to support and facilitate tissue reconstruction is urgently needed.[2] Animal-derived materials can provide a backbone and/or bioactive moieties for engineered scaffolds, but these substances have various limitations.[3] Alternatively, plant-derived materials have received increased attention. In particular, soy protein has emerged as an interesting biomaterial. Historically, soy protein has been consumed due to its rich nutrients (*e.g.,* proteins and minerals). This protein is biocompatible, plentiful, renewable, and mostly free of immunogenicity and ethical issues, in contrast to animal-derived materials.[4] More importantly, soy protein also carries bioactive molecules similar to those of the extracellular matrix (ECM) or hormones (*e.g.,* estrogen) that can control cell fate.[5] However, engineering soy-based scaffolds and elucidating their underlying biological mechanisms for accelerated skin repair remain limited. Herein, we hypothesized that biomimetic and estrogenic soy-based nanofiber scaffolds can promote wound healing via activation of estrogen receptor β (ER-β). We discuss the biological benefits and limitations of soy-based scaffolds, which are addressed by a sophisticated material design and analysis of the biological mechanism.

1.1 Skin Microenvironment and Wound Healing

Skin is a complex system that is composed of multiple cell types and ECM components (Figure 1-1).[1] Skin consists of two distinctive layers: a thin epidermal layer and the thicker underlying dermal tissues. Epidermal keratinocytes are the major cell type comprising the thin epidermis, which protects skin from exogenous physical and chemical stimuli.[1] Additionally, epithelial stem cells can be differentiated into skin appendages (such as hair follicles and sebaceous glands) that originate from the epidermis and extend to the dermis.[6]

The dermis is composed primarily of dermal fibroblasts embedded within basket-woven collagen fibrous networks that provide structural and biochemical support.[1] Endothelial and fat cells are also present in the dermal layer for nutrition and for hair regeneration, respectively.[7-9] In the context of ECM cues, collagen is the major ECM protein, but other ECM components [*e.g.*, fibronectin (FN) or hyaluronic acid (HA)] are dynamically involved in the development and maintenance of the dermis.[10]

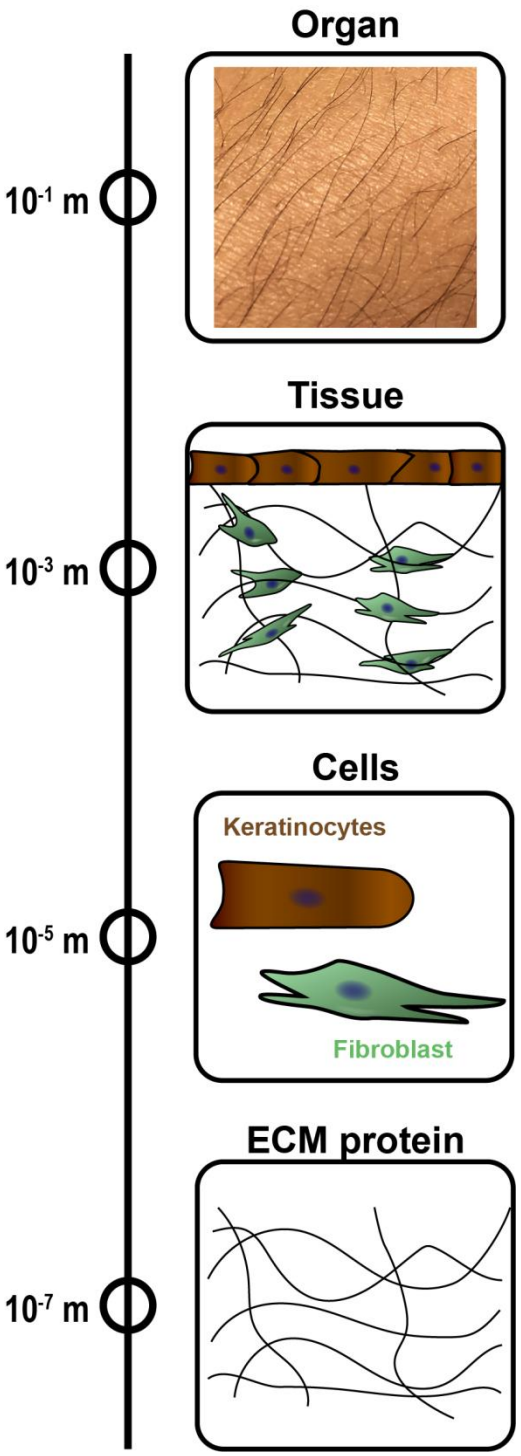

Figure 1-1. Multiscale structure of skin.

Healthy skin consists of skin cells (*e.g.,* keratinocytes and fibroblasts) embedded within ECM protein networks

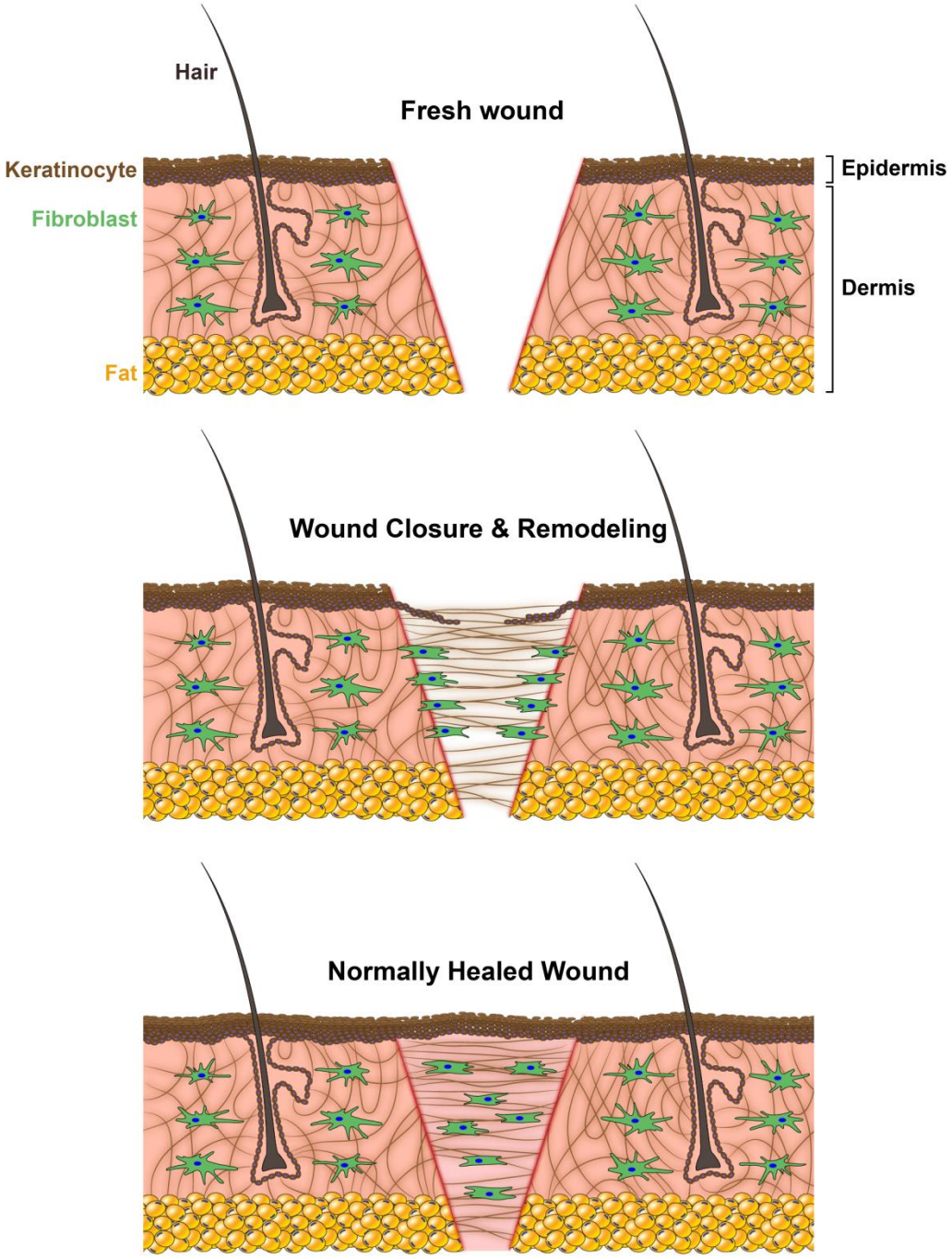

Figure 1-2. Normal cutaneous wound healing

Wound healing in adult humans undergoes wound closure and remodeling phases, usually leading to a scar with loss of basket-woven fiber matrix, hair, and fat.

After a skin wound, repair of the damaged tissues is rapidly initiated, as programmed (Figure 1-2). First, a clot forms in the wound site to act as a temporary shield.[11] The clot contains ECM proteins (*e.g.,* FN or vitronectin) and growth factors [*e.g.,* transforming growth factor (TGF β1) or vascular endothelial growth factor (VEGF)], which attract surrounding inflammatory cells to the wound sites.[12] The recruited inflammatory cells (*e.g.,* neutrophils or macrophages) remove wound debris (coagulated blood clots and bacteria) and secrete proinflammatory cytokines to activate fibroblasts and keratinocytes, promoting tissue regeneration.[1]

The activated epidermal keratinocytes migrate to wound sites to close the wounds and rebuild new epidermal layers; this process is known as re-epithelialization.[1] Furthermore, dermal fibroblasts migrate to wound sites to produce new connective dermal tissues, which are called granulation tissues.[1] Granulation tissues have a granular structure with newly synthesized collagen matrix and vascularization.[2] Re-epithelialization and granulation tissue formation together promote the closure of the wounded tissues. The next and last step is to regenerate skin appendages (hair and sebaceous glands) to restore the original structure and function of the skin. For example, dermal fibroblasts release hair-inducing signals, such as epidermal growth factor (EGF) and fibroblast growth factor (FGF).[13, 14]

Nevertheless, natural skin repair in adult humans leads to aesthetically and functionally imperfect healing outcomes due to the lack of intrinsic regenerative capability.[1] In particular, normal healing in adult humans causes scarring with an extensive and dense collagen matrix in the absence of hair follicles and cutaneous fats.[8] Moreover, diabetes or radiation exposure can result in delayed or non-healing wounds.[2] Accordingly, regenerative medicine therapy, such as biomimetic scaffolds, is needed to regulate wound repair.[2] In the following chapter, we will

discuss how to design regenerative wound dressings for the best healing outcomes, the current limitations of wound dressings, and why we need to develop soy-based wound dressings for the next generation of regenerative biomimetic scaffolds for enhanced skin regeneration.

1.2 Design Criteria for Developing Regenerative Wound Dressings

To develop regenerative medicine applications, particularly biomimetic scaffolds, researchers should consider various criteria for the best healing outcomes. In this chapter, five important parameters for designing regenerative dressings will be discussed.

1.2.1 Nanofibrous Architecture

Over the last two decades, tissue engineers have built increasingly functional tissue constructs by designing scaffolds that guide cell assembly and tissue morphogenesis. Biomimetic tissue analogues are currently used for disease modeling and to support regenerative medicine research.[15] To improve the fidelity of these tissue analogues, researchers have aimed to develop novel scaffolds that effectively recapitulate the mechanical, electrical, and chemical microenvironmental cues of the native ECM. Structurally, native tissue consists of nanofibrous ECM proteins that support mechanical and biochemical functions (Figure 1-1).[7, 16, 17] Accordingly, nanofiber scaffolds have been successfully used as a synthetic ECM to promote the maturation of engineered tissue.[18-20]

Several manufacturing systems have been developed to produce nanoscale fiber scaffolds. First, hydrogels can provide biomimetic nanofiber networks mostly by chemical crosslinking of polymers (*e.g.,* alginate, collagen, or gelatin). This system is easily generated and highly controllable in terms of reaction time, macroscale size, and shape. However, many

hydrogels require crosslinking agents that are toxic and can change the original structure of the bioactive components.[21, 22] In addition, controlling fiber alignment within hydrogels is difficult because crosslinking among polymers is often stochastic in nature. Electrospinning is another common system to produce nanofibers. This system utilizes high-voltage electric fields to induce charged jet elongation and finally generate nanofibers.[23] The fiber morphology, alignments, and physicochemical properties can be easily controlled in electrospinning systems. However, few materials can be processed using electrospinning due to the molecular weight, charge, and/or solubility of the materials.[23] Furthermore, the production rate of electrospinning is very low (<1 mL/hr).[23] As an alternative, force spinning can produce nanoscale fibers under high centrifugal forces generated by rotating a bristle at a high speed and pulling polymeric solution into continuous fibers, similar to a cotton candy machine.[24, 25] This system has a high production rate (~ 20 mL/hr) and good control of fiber qualities without the need for additional treatments and high-voltage electric fields.[22, 26]

1.2.2 Nanofibrous Parameters

The physicochemical properties of nanofibers should be optimized to promote skin reformation. Previous studies have explored the optimal fiber diameter, pore size, stiffness, and roughness for human dermal fibroblasts.[27-35] Briefly, a small fiber diameter (200–400 nm), large pore diameter (6–20 μm), low stiffness (2–600 kPa) and high roughness effectively stimulate attachment and growth of human dermal fibroblasts.[27-35] However, these parameters should be optimized for other cell types (keratinocytes, adipocytes, or endothelial cells) to affect multiple stages of wound healing. Due to the hydrophilic nature of our body, cells prefer hydrophilic

surfaces to adhere and grow.[36] Thus, the hydrophilicity of a material plays a vital role in skin repair because hydrophilic surfaces promote cell adhesion, proliferation, and infiltration.[36]

1.2.3 Bioactive Molecules

The ideal microenvironment for enhanced skin repair should contain relevant bioactive molecules to promote the growth of skin cells and the formation of new tissue.[10, 37-40] There are many different types of bioactive molecules. ECM proteins, such as collagen or FN, are the most common bioactive compounds because they are present in healthy skin. In addition, ECM-mimetic proteins, such as plant-based or synthetic peptides, are often used as cost-effective and/or versatile alternatives to native ECM proteins, which are expensive and unsustainable.[22] Wound dressings are also composed of growth factors, such as TGF-β and VEGF, which are involved in various signaling pathways that affect inflammatory responses and tissue regeneration.[41] Additionally, estrogen and phytoestrogens are integrated into wound dressings to control wound healing via estrogen receptor (ER) pathways and/or other signaling pathways.[42, 43]

1.2.4 Moist Environment

Maintenance of a moist environment in wounds plays an important role in preventing dehydration and cell apoptosis for rapid wound healing without infection and pain.[10, 37-40] Wound dressings that sustain a moist wound environment showed a faster rate of re-epithelialization and better healing outcomes than those that did not.[44] These results led to various moisturizing dressings, such as hydrocolloids and foams, in the commercial market. In research laboratories, hydrogels and swelling nanofibers have been developed to promote a moist wound environment.[22, 45]

1.2.5 Antibacterial Activity

Open wounds are easily infected by bacteria that impair healing processes and thus result in poor cosmetic outcomes. Passive wound dressings can act as physical barriers to prevent bacteria from entering the wound sites. Therefore, the pore size of wound dressings should be smaller than the size of the bacteria. Additionally, antibacterial agents can inhibit bacterial growth in the wounds. Silver is one of the best-known and most commonly used antibacterial molecules and has been used for commercial products (*e.g.,* 3M™ Tegaderm™ Ag Mesh Dressing with Silver). Natural polymers possess antibacterial activities. For example, degraded ECM proteins decreased the activities of Gram-negative *Escherichia coli* and Gram-positive *Staphylococcus aureus*.[46] Phytoestrogens in herbal materials (*e.g.,* soy protein and alfalfa) also possess antibacterial activity.[43]

1.3 Current Wound Dressing Materials and Their Limitations

Approaches based on modern regenerative medicine have recently emerged and have been shown to be effective in managing diseases. Specifically, researchers have extensively investigated new materials for developing wound dressings to support and facilitate skin tissue reconstruction[47] due to the lack of intrinsic regenerative capacity in human tissues.[48] Synthetic and animal-derived materials are most commonly used for engineered scaffolds. Synthetic polymers can form fibrous networks due to their high polymer chain entanglements and can therefore recapitulate the native fibrous architecture of tissues.[49] For example, different types of polyesters [polycaprolactone (PCL),[50] polylactic acid (PLA),[51] and polyglycolic acid (PGA)[52]] have been used as fiber-forming, biodegradable, and biocompatible polymers. However, these

materials are not water-soluble and thus require organic solvents to be dissolved and processed. In addition, they show slow degradation, and thus, the dressings need to be removed after treatment. In contrast, polyvinyl alcohol (PVA)[45] and polyethylene oxide (PEO or polyethylene glycol)[53] are water-soluble polymers with fiber-forming capacities. Nevertheless, they require co-spinning polymers (such as polyesters) or crosslinking agents to increase their structural integrity for wound healing applications due to their high water solubility. Furthermore, all synthetic polymers lack bioactive domains that enhance cell adhesion and growth, requiring these materials to be functionalized with additional bioactive moieties, such as proteins, growth factors, or drugs.

Animal-derived materials (*e.g.*, proteins or hormones) have also been used to develop wound dressings. These substances are rich in cell-binding domains and thus promote cellular behavior and ultimately tissue reconstruction.[49] For example, collagen is one of most commonly used ECM proteins because it is the major component of dermal tissue in healthy skin. Collagen can form both nanofibers and hydrogels but needs to be further crosslinked enzymatically[54] or chemically[55] to enhance the structural stability under physiological conditions. However, the manufacturing processes of collagen dressings can denature its original structure (*e.g.,* protein secondary structure) and thus change its functionality for healing outcomes.[56] Collagen-based dressings might also cause extensive wound contraction and scarring, possibly due to the origin of scar formation by excessive and aligned collagen networks.[10] Moreover, collagen is expensive and unsustainable, has poor mechanical properties, may show immunogenicity and may raise ethical concerns.[10, 49, 57] To overcome the financial burden and the low sustainability of collagen, researchers have introduced gelatin, a denatured collagen type I, as a cheap collagen-like source.[58] The amino acid compositions of gelatins vary according to the sources of gelatins (*e.g.,*

porcine vs. fish).[59] Similar to collagen, gelatin also has poor mechanical properties, may possess immunogenicity and may raise ethical concerns.[60] FN dressings have recently been developed. FN is an ECM protein that is known to be upregulated in fetal scarless healing processes when it is present in a fibrillary form.[61, 62] Inspired by this fetal biology, our laboratory engineered FN fiber dressings.[63] The FN scaffolds promoted wound closure, re-epithelialization, and skin appendage regeneration (hair follicles and adipose tissues).[63] However, these scaffolds are very expensive and may cause immunogenicity and raise ethical concerns; furthermore, the production rate and yield are very low.

To overcome these limitations of synthetic and animal polymers, researchers have recently considered plant-derived materials as alternative bio-building blocks to create cost-effective, sustainable, and regenerative scaffolds.[64,65] In particular, cellulose derivatives enable the formation of a fibrous backbone.[22] Carboxymethyl cellulose (CMC) is one of the most common cellulose derivatives for the development of wound dressings because it is a cheap, water-soluble, sustainable, and FDA-approved biopolymer.[40] CMC-based microfibers and hydrogels have already been commercialized as wound dressing products. These products primarily act as a physical barrier to prevent bacterial penetration and to provide a moist environment in the wound site without potentiating ultimate tissue reconstruction.[40] Cellulose acetate, another cellulose derivative, has been used to generate nanofiber dressings in an electrospinning system using different combinations of organic solvents.[66] This molecule forms nano- to microsized fibers with a high swelling ratio to maintain a moist environment for enhanced healing outcomes.[40] In addition to cellulose, alginate is a well-known plant material that can be used to fabricate dressings. Alginate is a water-soluble polysaccharide extracted from seaweed.[67] In particular, sodium alginate can be ionically crosslinked by replacing sodium ions

with multivalent cations (*e.g.,* calcium ions), forming stable networks within polymer strands.[67] With this reaction, alginate can be easily and quickly reshaped as injectable hydrogels and wet-spun fibers, resulting in various commercial products (*e.g.,* 3M™ Tegaderm™ Alginate Dressing).[67, 68] However, these plant-derived polysaccharides lack bioactive components, such as cell binding moieties, and therefore need to be functionalized with proteins (*e.g.,* collagen or gelatin)[69, 70] or antibacterial agents (*e.g.,* silver or 3M™ Tegaderm™ Alginate Ag Silver Dressing).[71]

Alternatively, among plant materials, soy protein has recently received increased attention as a new type of biomaterial, as soy protein carries bioactive molecules similar to ECM proteins or hormones that control cell fates.[22] Nevertheless, engineering soy-based wound dressings remains largely unexplored due to limited manufacturing platforms and a poor understanding of their regenerative capabilities at different spatial scales (from the molecular to the cellular to the tissue level) during healing processes. In the following chapter, I will review the clinical and molecular studies of soy protein as a new type of wound dressing material as well as the limitations of current soy-based dressings.

1.4 Topical and Oral Administration of Soy Protein in Clinical Trials

Consumption of soy foods was shown to benefit human health, leading to clinical trials to prove their pharmaceutical effects. One clinical study showed that high soy-protein-consuming individuals had a decreased risk of coronary heart disease (CHD), resulting in a decreasing risk of CHD with increasing total soy protein intake, upon FDA approval.[72] Soy protein intake also enhanced the blood lipid levels and bone density in postmenopausal women.[73] Furthermore, cardiovascular diseases (CVDs) were ameliorated by reducing low-density

lipoprotein (LDL)-cholesterol concentrations with soy consumption.[74] The administration of soy foods also decreased the incidence of breast cancer, although the protective mechanism still remains controversial.[75] In the context of skin health, the facial wrinkles and reduced skin elasticity of post-menopausal women were ameliorated after oral intake of soy isoflavones by promoting synthesis of new collagen matrix in the skin.[76, 77] Furthermore, soy isoflavones stimulate hair growth in humans, which is generally absent in wound healing in mice and adult humans,[8] by triggering insulin-like growth factor-I.[78, 79] Soy protein also accelerated wound healing in burn patients (non-healing wounds) by reducing oxidative stress and inflammation.[80] Thus, the administration of soy protein improves wound closure and skin appendage regeneration in clinical trials.

1.5 Bioactive Molecules in Soy Protein

We aimed to further elucidate the mechanism underlying the improved rate of skin tissue regeneration and the specific bioactive components of soy protein responsible for this activity, as soy protein carries various bioactive molecules. Over the centuries, soy protein has been used as an important ingredient in foods due to its rich nutrients, such as proteins, fat, minerals, and vitamins.[74] Herein, I focus on two predominant compounds in soy protein for enhanced wound healing: ECM-mimetic proteins and phytoestrogens (Figure 1-3).

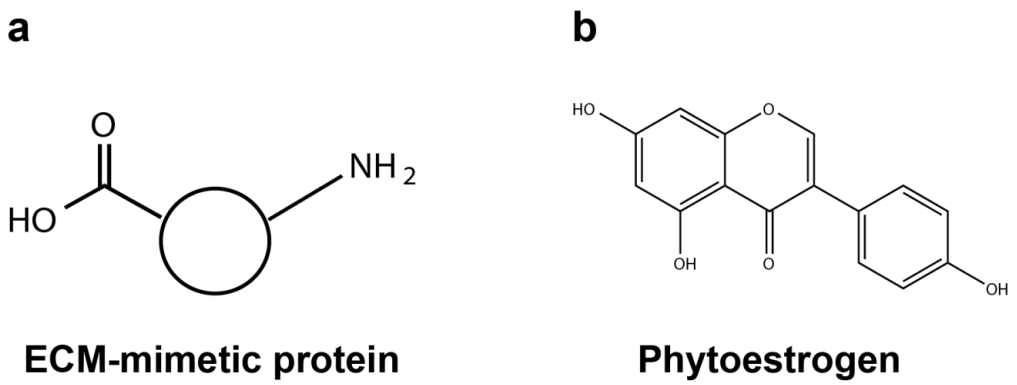

Figure 1-3. Bioactive molecules in soy protein.

a) ECM-mimetic protein and b) phytoestrogen.

1.5.1 ECM-mimetic proteins

Healthy skin consists of a dynamic and complex ECM microenvironment in the epidermis and dermal connective tissues.[1, 2, 81-83] Fibroblasts are the most common cells in connective tissue that produce ECM.[1, 2, 81-91] Specifically, dermal connective tissue is a nanofibrous collagen matrix, offering structural and biological cues to support cell attachment, proliferation, and tissue synthesis.[1, 2, 81-83] Collagen is one of the predominant ECM proteins in all types of tissues. Skin is primarily composed of collagen type I (~ 80%) and III (~ 10%).[92] Soy protein is also a good source of amino acids. Both soy protein and collagen possess similar amino acids, although the ratios of amino acids in soy protein and collagen are different.[93] Various biomaterials have been tested to engineer substrates or scaffolds to improve wound healing and skin regeneration. ECM proteins, extracted from different animals, have traditionally been used to deliver the same proteins in skin. However, these proteins are difficult to customize because they have different biological origins.[94] They also show immunogenicity, raise ethical concerns, and are expensive. Scientists have developed engineered proteins that mimic sequences existing in ECM proteins.[94] However, this strategy requires advanced tools, and

precise engineering of the sequences is difficult. We can utilize ECM-mimetic peptides from soy protein, which do not have these financial and technical burdens, as an alternative bioactive substance to design biomaterials for wound healing.

1.5.2 Phytoestrogens

Post-menopausal women suffer from impaired health status due to decreased levels of a primary sex hormone, estrogen. The estrogen level also declines in old males, which in turn causes slow healing. Hormone replacement therapy (HRT), such as topical estrogen treatment, can reverse the delayed healing processes. After estrogen is administered, it binds to different ERs (ER-α or ER-β) and influences various cellular and molecular mechanisms.[95] Estrogen promotes anti-inflammatory responses, re-epithelialization, and ECM synthesis via the ER-β signaling pathway, especially in skin repair.[43] Oral or topical estrogen therapies can potentially reverse delayed wound healing in post-menopausal women.[96] The cardioprotective roles of estrogen against CHDs and ischemia have been elucidated by utilizing animal models treated with estrogen.[97] However, activation of the ER-α signaling pathway was shown to increase the risk of breast cancer, stroke, and CHDs, indicating that the use of estrogen is problematic.[95] A better alternative to estrogen is an estrogenic material that can selectively activate the ER-β signaling pathway for enhanced wound healing without ER-α activation (Figure 1-4).

Soy protein possesses phytoestrogens that have a structure and function similar to estrogen. One of the main phytoestrogens in soy protein is genistein. Interestingly, genistein preferentially triggers the ER-β signaling pathway, showing much higher affinity for ER-β than ER-α (Figure 1-4). Preclinical and clinical studies have shown that topical and oral intakes of genistein accelerate wound healing in an estrogen-deficient animal model (ovariectomized mice)

and elderly individuals. Specifically, genistein can also bind to ER-β and promote re-epithelialization, new hair follicle formation, and adipose tissue regeneration during wound healing.[43, 79, 98] Furthermore, this molecules is known to modulate inflammation and antibacterial activity.

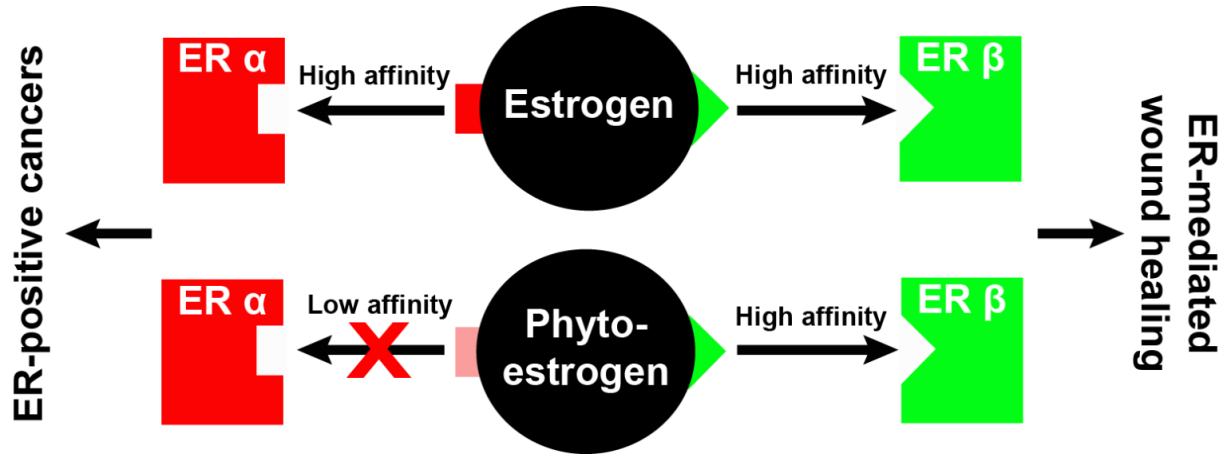

Figure 1-4. Soy phytoestrogen and estrogen receptor-mediated pathways.

Phytoestrogen preferentially triggers the ER-β signaling pathway over the ER-α signaling pathway to selectively enhance wound healing without activating ER-α-positive cancers.

1.6 Current Soy-based Wound Dressings and Their Limitations

Due to the advantages described in Chapters 1.4 & 1.5, soy protein has been used as a building block for developing regenerative scaffolds. There are various types of soy-based scaffolds: film, hydrogel, three-dimensional (3D)-printed and electrospun scaffolds.

1.6.1 Soy Film

Soy film is the simplest form of soy-based scaffolds. Soy film was fabricated via formaldehyde crosslinking with different crosslinker concentrations.[99] This film was transparent

and nontoxic and showed swelling. The film supported the proliferation of both dermal fibroblasts and epidermal keratinocytes with no significant difference in cell viability at different concentrations of formaldehyde. Furthermore, soy film accelerated cytokine expression [interleukin (IL)-6, IL-8, and TNFα] in fibroblasts and keratinocytes.[99] Cytokine secretion mediates macrophage activities that are known to be beneficial for normal wound healing.[100] These results indicate that soy film is nontoxic and facilitates the migration and cytokine expression of skin cells *in vitro*. However, the film lacks 3D, fibrous, and porous structures.[99] The researchers only performed *in vitro* cell culture experiments, not *in vivo* or ex vivo studies that could reveal the healing outcomes mediated by the film.

1.6.2 Soy Hydrogel

Due to the abundant peptides in soy protein, soy-based hydrogels can be produced using different types of crosslinkers [microbial transglutaminase (MTG)[101], calcium chloride ($CaCl_2$)[102], or genipin[102]]. Chien et al. reported a fibrous, porous, and swelling soy hydrogel crosslinked by MTG.[101] Human mesenchymal stem cells (HMSCs) were seeded *in vitro* within the scaffolds for 2 weeks and showed increased cell infiltration, integration, and tissue formation with a minimal dead cell ratio.[101] In another study, Shevchenko and Santin performed a preclinical study of soy-based hydrogel and paste with porcine healing and non-healing wound models.[102] Soy-based dressings were prepared by crosslinking soy protein with $CaCl_2$ or genipin.[102] The soy hydrogels were effective in treating deep and chronic wounds (*e.g.*, chronic foot ulcers) due to their porous structure.[102] They also potentiated acute inflammation, neutrophil growth, neovascularization, and granulation tissue formation with a basket-woven collagen fiber architecture similar to that of healthy skin.[102] These *in vitro* and preclinical data indicated that soy-based dressings can

reduce scar formation and increase angiogenesis, which cannot be achieved by spontaneous healing processes.[102] However, soy hydrogels require the use of crosslinkers that could be toxic or change the original structure of the bioactive molecules in soy protein. Due to the nature of chemical and enzymatic crosslinking, the fiber diameter is on the microscale, and fiber alignment is barely controllable. Furthermore, the structural integrity of soy hydrogels is loose and unstable; therefore, they are not suitable for treating large wounds.[102]

1.6.3 Three-dimensional-printed Soy Scaffold

Recently, 3D printing has emerged as a versatile platform to create 3D objects. Soy protein was also 3D-printed by extruding a mixture of soy slurry and glycerol.[103] Dithiothreitol was added to the printed soy scaffolds to form disulfide bonds between dithiothreitol and soy protein to enhance the stability of the scaffolds.[103] The scaffolds were crosslinked with dehydrothermal (DHT) and 1-ethyl-3-(3 dimethylaminopropyl)carbodiimide (EDC).[103] The microstructure and angles of the layers were easily controllable.[103] However, the 3D-printed soy scaffolds consist of a few hundred micron-scale fibers and have pore diameters that are much larger than the optimal scales. Therefore, these products would not be ideal to facilitate cellular adhesion, growth, and tissue formation. Additionally, the pore size is too large to prevent bacterial penetration. When the scaffolds were cultured with HMSCs, the cells showed good viability.[103] No further *in vitro* or *in vivo* tissue regeneration experiments were performed.

1.6.4 Electrospun Soy Nanofiber

Because the peptides in soy protein have low molecular weights, they cannot form continuous nanofibers alone. Instead, co-spun or carrier polymers that have long chains and can

thus be elongated to form nanofibers via electrospinning processes are required. In current studies, nylon, PVA, PCL, and PEO were used as co-spun polymers for soy protein. The first electrospun soy protein nanofibers were composed of soy protein isolate (SPI)/PEO in hexafluoro-2-propanol (HFIP).[104] The components from soy proteins were homogeneously distributed through single fibers [confirmed by energy-dispersive X-ray spectroscopy (EDS)] and macroscale scaffolds (confirmed by FT-IR).[104] This scaffold showed superhydrophilicity due to the presence of hydrophilic components from soy protein.[104] In another study, SPI/PEO blend nanofibers were cultured with human dermal fibroblasts *in vitro* for 8 days.[105] SPI/PEO nanofibers supported cell adhesion, proliferation, and growth of fibroblasts similar to gelatin, collagen type I, and poly(lactic-co-glycolic acid) (PLGA) substrates, which are common cell culture substrates.[105] Furthermore, similar to the type I collagen scaffold, SPI/PEO scaffolds upregulated the gene expression of cell binding receptors (*e.g.,* integrin β1) and ECM deposition proteins (collagen and laminin), indicating non-fibrotic dermal ECM remodeling in the dermis, which enhances healing outcomes.[105] SPI/PEO nanofibers also showed antibacterial activity and promoted wound closure in a rat model.[106] In addition to co-spun PEO polymers, soy protein nanofibers were also spun with PVA, PCL, or nylon. These fibers possess nanoscale fiber diameters and pore sizes small enough to prevent fungal penetration.[107] However, the current electrospun soy nanofiber scaffolds still used non-optimal materials, such as synthetic polymers as a backbone and toxic solvents such as HFIP. Furthermore, these scaffolds did not recapitulate the native skin microenvironment. Thus, rigorous *in vitro* and *in vivo* studies on their regenerative capability (*e.g.,* mechanistic studies and studies of skin tissue regeneration, such as hair follicle or adipose tissue reformation) are needed.

1.7 Unanswered Questions and Perspectives

Recent studies have utilized soy protein as wound dressing materials. Nevertheless, there are still important questions that need to be answered to improve soy-based dressings.

1.7.1 Can Soy Dressings Effectively Mimic the Native Microenvironment?

To obtain the best healing outcomes, we need to effectively recapitulate the composition and structure of the native ECM microenvironment in skin. Current soy-based dressings were engineered to partially mimic these properties. As described in Chapter 1.2, soy-based dressings should be further improved to have basket-woven or isotropic fibrous architecture with an optimal fiber diameter (200–400 nm), pore diameter (6–20 μm), and stiffness (2–600 kPa). In addition, the scaffolds should be highly hydrophilic to enhance cell adhesion and growth as well as sustain a moist environment.

Furthermore, the composition of soy-based scaffolds can be improved. Current soy-based dressings mostly rely on synthetic polymers to produce fibrous structures with soy protein. However, some synthetic polymers (*e.g.,* PCL or PU) are insoluble in water, necessitating the use of toxic organic solvents (*e.g.,* HFIP or chloroform). These solvents are often derived from petroleum oils, raising environmental and sustainability concerns. As an alternative, plant-derived polymers such as cellulose derivatives can be used as carrier polymers without the use of toxic crosslinkers. Furthermore, ECM components [*e.g.,* glycosaminoglycans (GAGs)] can be used to form a stable fibrous backbone similar to that in native skin. In particular, HA, a GAG in skin, enables the formation of hydrogel or nanofibers.[108] HA is observed not only in animals but also in bacteria.[109] HA synthesized from bacteria has similar physicochemical properties to animal-derived HA but reduces the cost by an order of magnitude.

1.7.2 Can We Generate High-Throughput Biomimetic Soy Dressings?

As mentioned in Section 1.5, current soy-based fibrous 3D scaffolds are low throughput in terms of manufacturing scale. Specifically, the production rate of electrospun soy-based nanofibers is very low (<1 mL/hr).[23, 104-107] Soy hydrogels require a few hours to a few days for the crosslinking reaction and freeze-drying prior to use.[101, 102] Although 3D printing is very efficient in terms of throughput, it is unable to produce nanoscale structures due to its spatial resolution limitation (a few microns at the lowest).[110] To overcome the limitation of the current low-throughput platforms, we hypothesize that force spinning [*e.g.,* rotary jet spinning (RJS)] can produce biomimetic soy-based nanofiber dressings in a high-throughput system (>1 mL/min).[25] If a volatile solvent, such as an electrospinning system, is used, RJS can increase the throughput 50 times higher than that of the current electrospinning system for the development of soy nanofibers. Additionally, the modified version of RJS, called immersion rotary jet spinning (iRJS), enables the production of nanofibers from water.[68] Therefore, water-soluble ECM components (*e.g.,* HA) can be adopted into the high-throughput spinning system to optimize the soy-based dressings.

1.7.3 Can Soy Dressings Activate Estrogen Receptor β?

As mentioned in Chapter 1.5, soy protein has two important bioactive molecules for wound healing: ECM-mimetic peptide and phytoestrogens. Current studies have only explored the effects of soy peptides in wound healing *in vitro* and *in vivo*. Accordingly, the existence and delivery of soy phytoestrogens via engineered soy dressings as well as the effect of soy phytoestrogens on healing processes remain unexplored. Nevertheless, most *in vitro*, *in vivo*, and

clinical studies have indicated that the medicinal benefits of soy protein largely stem from soy phytoestrogens (see more details in Chapter 1.5.2).

First, spinning materials and systems should be optimized to deliver phytoestrogens with soy scaffolds. Most phytoestrogens (*e.g.,* genistein and daidzein) are partially soluble in water but highly soluble in dimethyl sulfoxide (DMSO).[111] Accordingly, phytoestrogen-dissolving solvents should be incorporated, and the use of DMSO or equivalent strong solvents should be acceptable in the spinning system. In addition, the amount of soy phytoestrogens in the scaffolds should be quantified. For this purpose, liquid chromatography-mass spectrometry (LC-MS) will be a useful tool to analyze phytoestrogens because it can first separate molecules based on their polarities, and then, each molecule is ionized and analyzed based on the mass of each ionized segment.[112] The time-dependent release kinetics of phytoestrogens from the scaffolds can also be determined by LC-MS analysis.

The next step is to investigate the effect of phytoestrogens in soy scaffolds on cutaneous wound healing via ER signaling pathways. As described in Chapter 1.5.2, clinical studies indicated that oral and tropical administration of soy phytoestrogens accelerated healing processes via ER-β. However, current studies only examined the engineering capability for soy-based dressings and their potential as wound dressings without elucidating the mechanisms of wound repair mediated by ER signaling pathways. To study the ER-related mechanisms, researchers introduced ER-specific antagonists (*e.g.,* 4-[2-phenyl-5,7-bis(trifluoromethyl)pyrazolo[1,5-a]pyrimidin-3-yl]phenol (PHTPP) for ER-β or 8-benzylsulfanylmethyl-1,3-dimethyl-3,7-dihydro-purine-2,6-dione, 8-[(benzylthio)methyl]theophylline, theophylline, and 8-[(benzylthio)methyl] (TPBM) for ER-α) to block ER pathways *in vitro* and *in vivo*.[5] Moreover, ER knockout animal models in combination

with ovariectomy surgery and a soy-free diet can be used to determine how phytoestrogens in soy dressings affect healing processes via the ER signaling pathways without other ER stimulants (such as endogenous estrogen and soy-based diets).[43]

1.7.4 Can Soy Dressings Stimulate Improved Healing Outcomes?

Healing shows various stages, from early inflammatory responses to wound closure (or re-epithelialization) to regeneration of the dermis and epidermis. Although clinical evidence has shown that soy protein and/or soy phytoestrogens could enhance the healing outcomes (*e.g.,* hair follicles and adipose tissue reconstruction), current studies of soy wound dressings have only explored the simple aftereffects, such as wound closure, re-epithelialization, or granulation tissue formation. To further verify the potential of soy wound dressings, researchers should examine advanced healing outcomes (*e.g.,* minimal scar formation and regeneration of new hair follicles and adipose tissues).[8] Furthermore, the applicability of soy wound dressings for hard-to-heal wounds, such as chronic ulcers, should also be tested.[40]

1.7.5 What Else Can We Do with Soy Scaffolds?

If the above questions are answered, soy-based scaffolds can be applied to treat not only cutaneous wounds but also other diseases. As described in Chapter 1.4, clinical reports indicated the pharmaceutical effects of soy protein in treating CHD, CVDs, osteoporosis, and breast cancer. Based on these proven health benefits, the engineered soy scaffolds can be further implanted into the damaged regions of heart, bone, or breast to provide biochemical and physical support to enhance tissue regeneration. Additionally, biomimetic soy scaffolds can be used as a substrate for disease modeling. Recent studies showed that fibrous scaffolds were engineered to provide a

3D biomimetic microenvironment to study the cause and treatment of diseases *in vitro* without sacrificing animals and utilizing suboptimal 2D models.[113, 114]

1.8 Conclusions

In this chapter, we address the following question: *how can we engineer soy-based scaffolds to improve the treatment of cutaneous wounds while reducing financial, environmental, and ethical burdens?* Severe cutaneous wounds caused by burns or chronic skin ulcers are a global health problem, affecting 6 million patients worldwide.[10] Naturally healed wounds do not perfectly regenerate cutaneous connective tissue, and they can often lead to extensive scarring (non-chronic) or can remain unhealed (chronic). As a result, engineering regenerative and cost-effective wound dressings, which is a $10 billion market globally, still remains a challenge for primary healthcare.[10]

Current regenerative dressings rely on synthetic and/or animal-derived materials that are suboptimal for healing outcomes and commercialization, and thus, improved dressing materials are needed. We argue that biomimetic and estrogenic soy nanofiber scaffolds can overcome the limitations of current wound dressings by providing a well-recapitulated microenvironment and triggering ER-β signaling pathways for high-quality healing outcomes. In addition, we reviewed the microenvironmental cues to direct the design criteria of ideal dressings as well as the current status and limitations of soy-based dressings. The biomimetic and estrogen soy scaffolds will be a new generation of regenerative, cost-effective, and versatile scaffolds for wound healing and further biomedical applications.

2 Soy Protein/Cellulose Nanofiber Scaffolds Mimicking Skin Extracellular Matrix for Enhanced Wound Healing

Historically, soy protein and extracts have been used extensively in foods due to their high protein and mineral content. More recently, soy protein has received attention for a variety of its potential health benefits, including enhanced skin regeneration. It has been reported that soy protein possesses bioactive molecules similar to extracellular matrix (ECM) proteins and estrogen. In wound healing, oral and topical soy has been heralded as a safe and cost-effective alternative to animal protein and endogenous estrogen. However, engineering soy protein-based fibrous dressings, whilst recapitulating ECM microenvironment and maintaining a moist environment, remains a challenge. Here, we describe the development of an entirely plant-based nanofibrous dressing comprised of cellulose acetate (CA) and soy protein hydrolysate (SPH) using rotary jet spinning. The spun nanofibers successfully mimic physicochemical properties of the native skin ECM and exhibit high water-retaining capability. *In vitro*, CA/SPH nanofibers promote fibroblast proliferation, migration, infiltration, and integrin β1 expression. *In vivo*, CA/SPH scaffolds accelerate re-epithelialization and epidermal thinning as well as reduce scar formation and collagen anisotropy in a similar fashion to other fibrous scaffolds, but without the use of animal proteins or synthetic polymers. These results affirm the potential of CA/SPH nanofibers as a novel wound dressing.

2.1 Introduction

Soy protein is a dietary protein extracted from the soy beans, which have received considerable attention in the last couple of decades for their potential health benefits. Epidemiological and clinical studies supporting this claim ultimately enabled US Food and Drug Administration (FDA) approval in 1999 of soy protein for protective effects on coronary heart disease.[73, 74] Alternatively, soy protein has also been explored more recently as a "green" and renewable substitute for petroleum- or animal-derived polymers in biomedical applications.[4, 105] It was found that soy protein has bioactive peptides similar to extracellular matrix (ECM) proteins, present in human tissues.[93] These ECM-mimetic peptides can promote cell adhesion, proliferation, and migration critical for supporting tissue regeneration.[93, 101, 103] Furthermore, soy protein carries phytoestrogens that act as a structural and functional analogue to the female sex hormone estrogen,[5, 115] which affects the regulation and development of various organs by binding to estrogen receptors (ERs).[95] Binding of estrogen to ERs forms dimers that perform as co-activators to stimulate transcription of target gene expressions in various regions [116]. Interestingly, soy phytoestrogens preferentially bind to an ER that has been shown to have positive effects on age-related diseases, including delayed wound healing.[43, 117, 118] In cutaneous wound healing, soy protein has attracted increased attention as a safe and cost-effective alternative to animal protein and endogenous estrogen.[43, 93, 119-121] Previous studies have shown that cryptic peptides in soy protein improved wound healing by increasing dermal ECM synthesis and stimulating re-epithelialization.[93, 120, 121] Soy phytoestrogens have demonstrated to accelerate the healing process via ER-mediated signaling pathways.[43, 118, 122, 123] They also possess anti-bacterial,[4, 124, 125] anti-inflammatory,[126] and anti-oxidant properties [80, 127] that support and enhance wound healing. Moreover, clinical trials have reported that oral intake of soy (both

protein and phytoestrogens) accelerates skin regeneration in aged women and burn patients.[76, 77, 80]

Nanofibrous scaffolds have emerged as a promising approach to develop wound dressings,[60, 128] as they can replicate the fibrous dermal ECM microenvironment that provides structural support for wound healing and functional cues for directing tissue regeneration.[37, 60, 128] Biodegradable synthetic polymers such as polycaprolactone (PCL) have been widely used to produce nanofibers due to their versatile spinning capabilities.[37, 60, 128] Yet, they remain poorly-suited building blocks for developing wound dressings as they are much stiffer than natural skin.[129, 130] Furthermore, many of them are hydrophobic, limiting their ability to keep wounds hydrated.[129, 130] Synthetic polymers also lack cell binding domains and therefore cannot enhance cellular attachment or functionality.[131] Nanofibers spun from animal-sourced ECM proteins, such as gelatin and collagen in combination with synthetic polymers, have been previously reported in literature to contain bioactive molecules which support healing.[60, 130] Whilst adding ECM proteins to a nanofibrous scaffold enhances its biological and mechanical properties, ECM proteins are costly and susceptible to common liabilities of animal-derived products: immunogenicity, antigenicity, disease transmission, and pathogen contamination.[4, 132, 133] Furthermore, the utilization of collagen alone, the most common ECM protein used in wound dressings, has been shown to cause extensive wound contraction and scarring.[10]

Because of its pro-regenerative traits, soy protein-based nanofiber wound dressings have recently been developed as an alternative to the animal-derived ECM protein nanofibers.[99, 105, 106, 121] By mimicking the fibrous dermal ECM microenvironment, they can provide potent structural and functional cues for directing tissue regeneration.[10, 134] However, current methods for engineering soy protein nanofibers require the use of synthetic polymers as carriers, due to

the low molecular weight of soy protein that inhibits the production of nanofibers alone.[104-107, 135] As described above, synthetic polymers are not ideal for developing wound dressings as they possess physicochemical properties different from the native skin.[129, 130] Soy protein hydrogels necessitate additional crosslinking agents that can be toxic and can alter the original structure of soy peptides.[99, 101, 103] As such, the development and validation of effective soy protein-based nanofiber scaffolds for wound healing applications remain an essential challenge.

In this study, we report the fabrication of plant hybrid cellulose acetate (CA) / soy protein hydrolysate (SPH) nanofibers for wound healing applications. We hypothesized that CA/SPH nanofibers could recapitulate the dermal ECM microenvironment and maintain a moist environment while delivering soy protein to potentiate skin regeneration. Cellulose acetate was selected as a co-spinning polymer because it readily dissolves in various solvents and self-assembles into nanofibers, enabling recapitulation of the native ECM fibrous structure and high water retention ability.[136-139] It is also abundant and exhibits low immunogenicity to humans because of its non-animal origins.[4, 119, 136, 138] Dermal ECM-mimetic CA and SPH nanofibers were manufactured via rotary jet spinning (RJS) system that utilizes centrifugal forces to extrude fibers in the nanometer range. We optimized physicochemical properties of the spun nanofibers by functionalizing the CA nanofibers with SPH. The RJS-spun CA/SPH nanofibers have higher production rate and better control of fiber morphology without an additional modification or high-voltage electric fields in the system, when compared to the existing electro-spun soy-based nanofibers.[25, 50] Lastly, *in vitro* and *in vivo* functionalities of our dressings were tested by investigating dermal fibroblast behaviors and then further assessing wound closure rate and skin regeneration in an excisional wound splinting mice model, respectively. In comparison with the current fibrous scaffolds, the CA/SPH nanofibers have a healing ability similar to or better than

other fibrous dressings, but our scaffolds are free of animal-derived proteins or synthetic polymers that are suboptimal. Our results underscored the potential of such soy-based nanofiber scaffolds as potent and cost-effective alternative to existing pro-regenerative strategies.

2.2 Results and Discussion

2.2.1 Fabrication of Plant Hybrid Nanofibers

Plant-based hybrid nanofibers were fabricated by co-spinning CA and SPH in hexafluoroisopropanol (HFIP) using a RJS system, which produces defect-free nanofibers under centrifugally induced shear forces (Figure 2-1).[25, 50, 68, 140-142] CA was chosen to supplement the low molecular weight of soy protein, and SPH was chosen as the soy protein source. SPH is a mixture of amino acids, peptides, phytoestrogens, and soy derivatives obtained by hydrolyzing soy protein isolate to minimize inorganic ions and to maximize protein content.[143] Continuous CA and CA/SPH nanofibers were spun at a centimeter scale by extruding polymer solution from a rotating reservoir (Figure 2-1a-b).

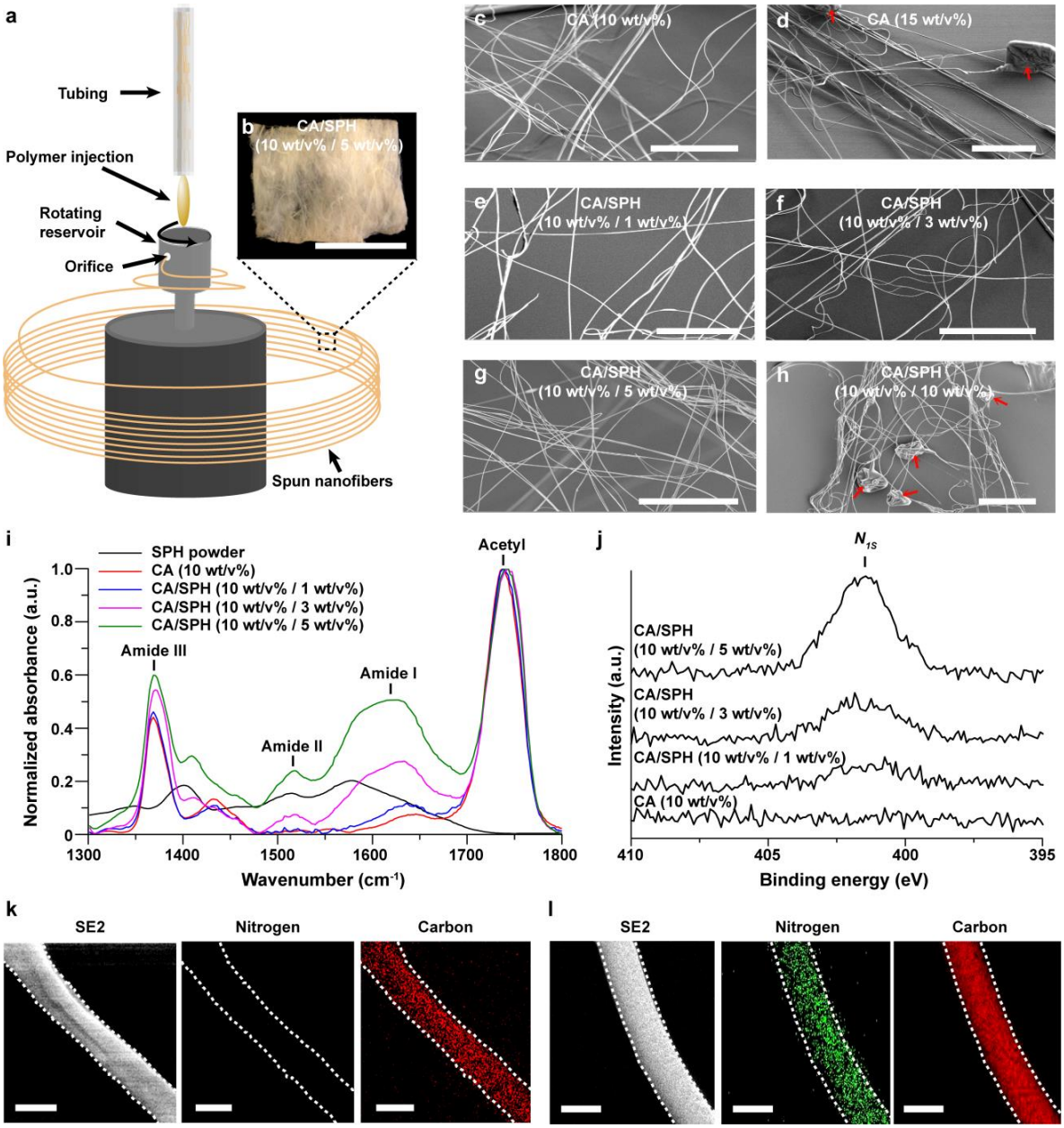

Figure 2-1. Fabrication and chemical composition of plant hybrid nanofiber.

(a) Schematic for nanofiber fabrication by RJS. (b) Bright field image of CA/SPH (10:5) nanofiber scaffolds. Scales are 5mm. (c–h) SEM images of CA and CA/SPH. The red arrows indicate beading. Scales are 50 μm. (i) FT-IR spectrum of different CA/SPH nanofibers and SPH powder. (j) High resolution XPS spectra of N1s for different CA/SPH nanofibers. (k–l) Elemental analysis by Energy-dispersive X-ray spectroscopy (EDS) for nitrogen (NK) and

(continued) carbon (CK) together with corresponding secondary electron (SE2) images in (k) CA (10 wt/v%) and (l) CA/SPH (10 wt/v% / 5 wt/v%) nanofibers. The white dots indicate the shape of nanofibers. Scales are 500 nm.

For the RJS system, the spinnability and beading of CA and SPH nanofibers were significantly influenced by their polymer concentrations (w/v%). It was found that SPH alone could not be spun into nanofibers because its molecular weight is too low. The short chains of SPH molecules cannot overlap and entangle, suggesting that SPH would require a co-spinning polymer with longer chains.[25, 104] Experimentation with fixed rotation and injection speeds showed that adding 10 w/v% of CA to various concentrations of SPH (1, 3, 5 w/v%) resulted in continuous nanofiber formation without beading (Figure 2-1c-d). A higher concentration of SPH (10 w/v%) in contrast showed beading in fibers (Figure 2-1e-h). Moving forward, 10 w/v% of CA was therefore selected as the carrier polymer for SPH. The developed continuous nanofibers had an intercalated nanofibrous structure that resembles the native extracellular matrix. This morphological similarity supports cell–fiber interactions that promote wound healing.[10, 134]

2.2.2 Chemical Characterization of Plant Hybrid Nanofibers

To ensure a uniform structure, elements must be homogenously dispersed at the nanofiber surface.[19] ATR-FTIR spectroscopy was performed to determine the relative amounts of proteins in the spun nanofibers. In the FTIR spectrum, amide I peaks (1600–1700 cm^{-1}) are representative of the secondary structure of amino acids in SPH, and acetyl peaks (1700–1800 cm^{-1}) are representative of C=O stretching of acetyl groups in CA (Figure 2-1i). After subtracting background intensity from CA in the amide I peak, the peak area-to-peak area ratios (amide I

peak over acetyl peak) were linearly related to the amounts of SPH, showing that SPH can be added into fibers in an amount up to 5 w/v% without causing the loss of soy protein molecules.

XPS was performed to confirm the elemental composition of the nanofiber surfaces. The nitrogen content gradually increased as the concentration of SPH increased (Figure 2-1j), confirming that SPH was incorporated into CA nanofibers. High resolution analysis of the C_{1s} peaks additionally confirmed the increasing protein content on the nanofiber surface. This peak was deconvoluted, into four peaks corresponding to the following chemical bonds: C–C, C–O, O–C–O/N–C=O, and O–C=O. Increasing SPH content thus led to relatively higher concentrations of C–C and O–C–O/N–C=O bonds. More amino acids and phytoestrogens in higher concentration of SPH ascribe to the increase of C–C and O–C–O/N–C=O bonds. These results demonstrated that SPH successfully integrated with CA.

To analyze the distribution of CA and SPH in individual fibers, EDS was performed to obtain an elemental mapping of nitrogen and carbon atoms (Figure 2-1k-l). Carbon mapping showed uniform distribution of carbon atoms on the spun nanofibers, matching the corresponding secondary electron (SE2) images. Nitrogen atoms appeared exclusively on CA/SPH nanofibers owing to the presence of SPH and were homogeneously distributed throughout individual fibers. This confirms and concludes that spinning CA at 10 w/v% and SPH at 5 w/v% improved fiber spinnability and yielded fibers with high concentrations of uniformly distributed protein. In the following studies, CA (10 w/v%) and CA/SPH (10 w/v% / 5 w/v%) nanofibers were selected as pure CA nanofibers and CA/SPH nanofibers, respectively.

2.2.3 Characterization of Mechanical Properties and Surface Chemistry

The physico-mechanical properties of nanofibers—fiber diameter, pore diameter, and stiffness—influence wound healing. Recent studies have shown that fiber diameter (200–400 nm) and scaffold pore diameter (6–20 μm), similar to the native ECM, enhance adhesion, proliferation, and infiltration of human dermal fibroblasts, while minimizing bacterial infiltration.[27, 28, 144] Fiber stiffness has also been shown to affect cell behavior.[145, 146] To encourage assembly of new ECM, the stiffness of wound dressing materials should mimic the stiffness of the native ECM microenvironment (5–600 kPa),[29-33] however the stiffness of common synthetic polymer nanofiber scaffolds is usually one to several orders of magnitude higher.[129, 130]

It was observed that fiber diameter ranges from 300.30 ± 0.76 nm in CA nanofibers and to 396.66 ± 0.90 nm in CA/SPH nanofibers (Figure 2-2a-b). In contrast, PCL nanofibers showed thicker fiber diameter (644.04 ± 5.20 nm) than CA-based nanofibers. Pore diameter ranges from 6.63 ± 0.14 μm in CA scaffolds to 6.13 ± 0.17 μm in CA/SPH scaffolds, while for PCL scaffold pore size decreased to 3.82 ± 0.38 μm. Next, scaffold thickness can be controlled by spinning a different amount of polymer solution. Our system is able to produce fiber scaffolds with thickness ranging from a couple hundred micrometers to several millimeters. However, scaffold thickness does not significantly change pore diameters of nanofiber scaffolds. The stiffness of the CA and the CA/SPH nanofibers was between 100 and 600 kPa in the longitudinal and transverse directions respectively (Figure 2-2c). On the other hand, the stiffness of the PCL nanofibers was in a MPa range, much stiffer when compared to native skin or CA-based nanofibers. These results suggest that fiber and pore diameter of both CA and CA/SPH nanofibers are well suited to support growth and migration of human dermal fibroblasts and that their stiffness resembles that of human skin ECM.[29-33]

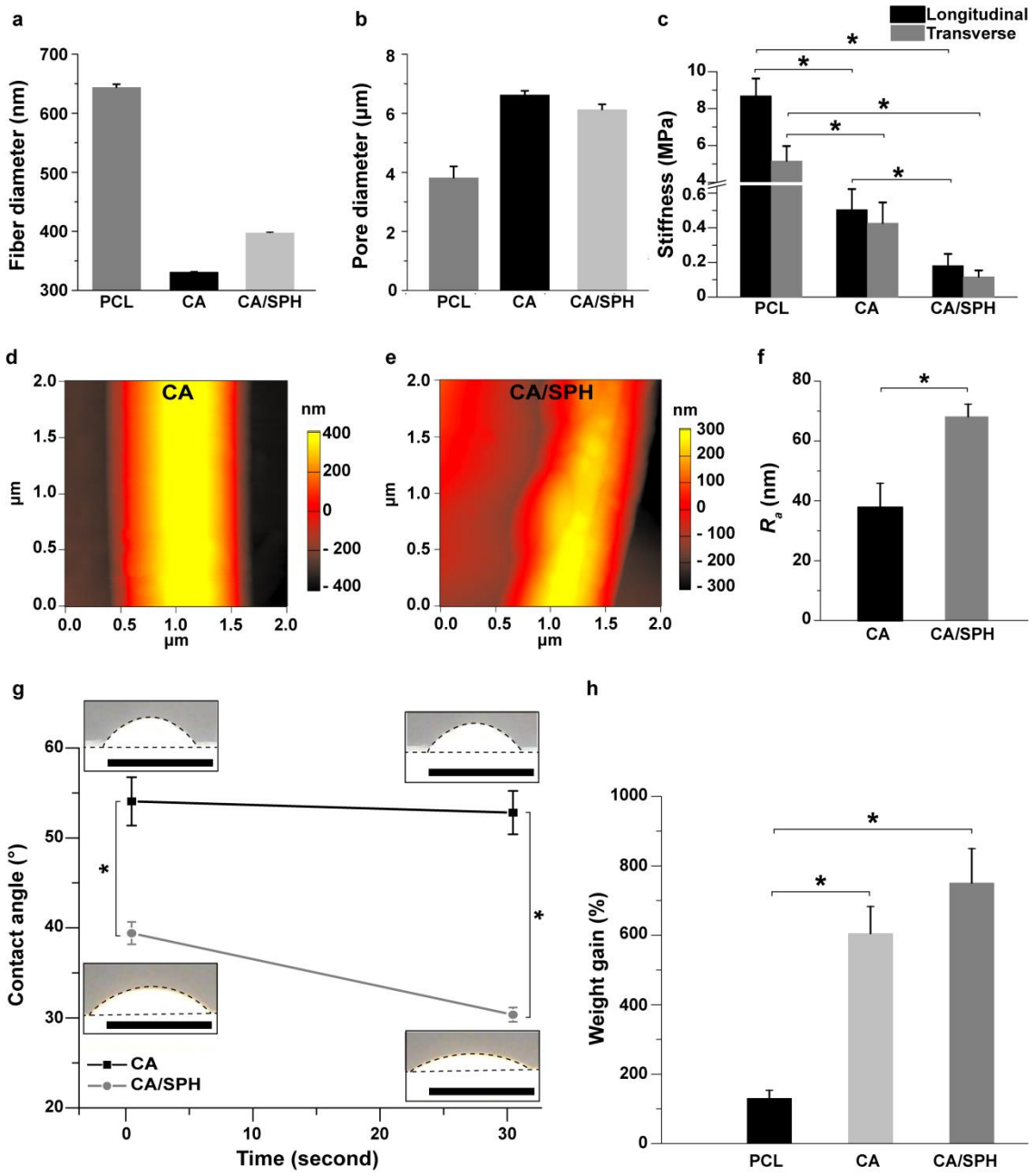

Figure 2-2. Characterization of mechanical properties and surface chemistry.

(a–b) Fiber diameter and pore diameter analysis for PCL (6 wt/v%), CA (10 wt/v%), and CA/SPH (10 wt/v% / 5 wt/v%) nanofiber scaffolds. Bars represent standard error, n=10 from 3 productions. (c) Stiffness measurement for PCL (6 wt/v%), CA (10 wt/v%), and CA/SPH (10 wt/v% / 5 wt/v%) nanofibers in the wet state on the longitudinal and transverse directions. Bars represent standard error, n=5 from 3 productions, * indicates $p < 0.05$. (d–f)AFM images of (d)

(continued) CA (10 wt/v%) and (e) CA/SPH (10 wt/v% / 5 wt/v%) nanofibers with (f) roughness (R_a) of nanofibers (n=3, FOV=3 from 3 productions). (g) Bright field images of water droplets on CA (10 wt/v%) and CA/SPH (10 wt/v% / 5 wt/v%) cast films with contact angle analysis (n=3 from 3 productions). Dots delimit water droplet and film. Scales are 5 mm. (h) *In vitro* water absorption measurements by weight gain (n=6 from 3 productions). Bars represent standard error, * indicates $p < 0.05$.

Next, we investigated the fiber surface roughness that affects cellular behaviors at both nano- and micro-scales since cells sense and react differently on various micro-topographies.[34, 35] Current studies have reported that rough surfaces enhance cell adhesion, migration, and growth by triggering expression of integrin receptors and production of growth factors and ECM proteins.[34, 35] To estimate the effect of the addition of SPH on the surface roughness of CA nanofibers, the average deviation (R_a) of the surface roughness was calculated from atomic force microscopy images (Figure 2-2d-e). Figure 2-2f showed that the R_a value for the CA/SPH nanofibers (68.19 ± 4.13 nm) was significantly higher than that of the CA nanofibers (38.06 ± 7.98 nm). Several factors may account for the effect of SPH on fiber roughness: the distribution of proteins throughout the surface and inside the nanofibers (Figure 2-1i-l), the aggregation of different materials within the nanofibers, and the short peptides that SPH carries.

The incorporation of SPH introduces polar moieties such as hydroxyl, amino, and carboxylic groups into the fibers. This increases the hydrophilicity as well as improves cell attachment by providing cell-binding functional groups.[39, 104] High hydrophilicity and water retaining properties are vital for removing wound exudates and providing a moist environment for cell growth.[37, 39] To evaluate the chemical composition influence on the hydrophilicity of the

materials, we performed contact angle measurement of uniform cast films (Figure 2-2g). The contact angles were significantly reduced by raising the ratio of SPH in the films, indicative of increased hydrophilicity. A similar trend was seen for fibrous samples, though rapid diffusion of water into the samples was seen for all samples. The increased hydrophilicity was reflected by an increased water absorption capacity (Figure 2-2h). When CA was used as a backbone in nanofibers, their water-absorbing capabilities were significantly greater than that of hydrophobic PCL nanofibers which are frequently used as a backbone polymer to spin nanofiber scaffolds. The addition of SPH to the CA backbone further increased the water uptake.

An ideal nanofibrous scaffolds should be highly biodegradable so that it is gradually replaced by natural tissues during wound healing.[147, 148] Over a 15-day period CA/SPH nanofibers lost significantly more mass than CA or PCL nanofibers due to hydrolysis of soy proteins. The rate of soy protein hydrolysis within the hybrid nanofibers resulted in the degradation, which correlates with the rate of protein breakdown.[105, 148] The lower mechanical strength and higher surface wettability of the hybrid nanofibers also contributed to their rate of degradation.[105, 148] In addition, the release kinetics of soy protein from CA/SPH nanofiber scaffolds resulted in a burst release of soy protein within 24 hours due to the fast hydrolysis of soy protein and high hydrophilicity. After the initial burst release, a sustained soy release over 2 weeks was observed. The two phases of *in vitro* release (the initial burst and the sustained release over a long period) are typical release profiles of nanofiber-loaded molecules.[149] Therefore, a dressing made from plant-based hybrid nanofibers could provide structural cues until wound healing is completed and be naturally replaced by native tissue.

2.2.4 *In Vitro* Fibroblast Study

We hypothesized that the addition of SPH into CA nanofibers could promote wound healing-relevant cellular activity of human dermal fibroblasts (HNDF) via the presence of bioactive molecules, increased roughness, and enhanced water-retaining capabilities. In an effort to test this hypothesis, we began by analyzing several indicative markers for wound closure and tissue regeneration, including proliferation, surface coverage, migration, and infiltration of HNDFs (Figure 2-3).[2, 85, 150, 151] The behaviors of dermal fibroblasts were tested *in vitro* because they are a critical skin cell type that remodels the dermal ECM, communicates with other skin cells (such as keratinocytes), and thus regulates dermal function.[81, 82, 85, 91] Cytotoxicity tests of the nanofiber scaffolds were likewise conducted as a standard pre-clinical experiment.[152] PCL nanofibers were used as a reference since it is one of the most common biocompatible and biodegradable synthetic polymers in nanofiber fabrication for biomedical applications.[19]

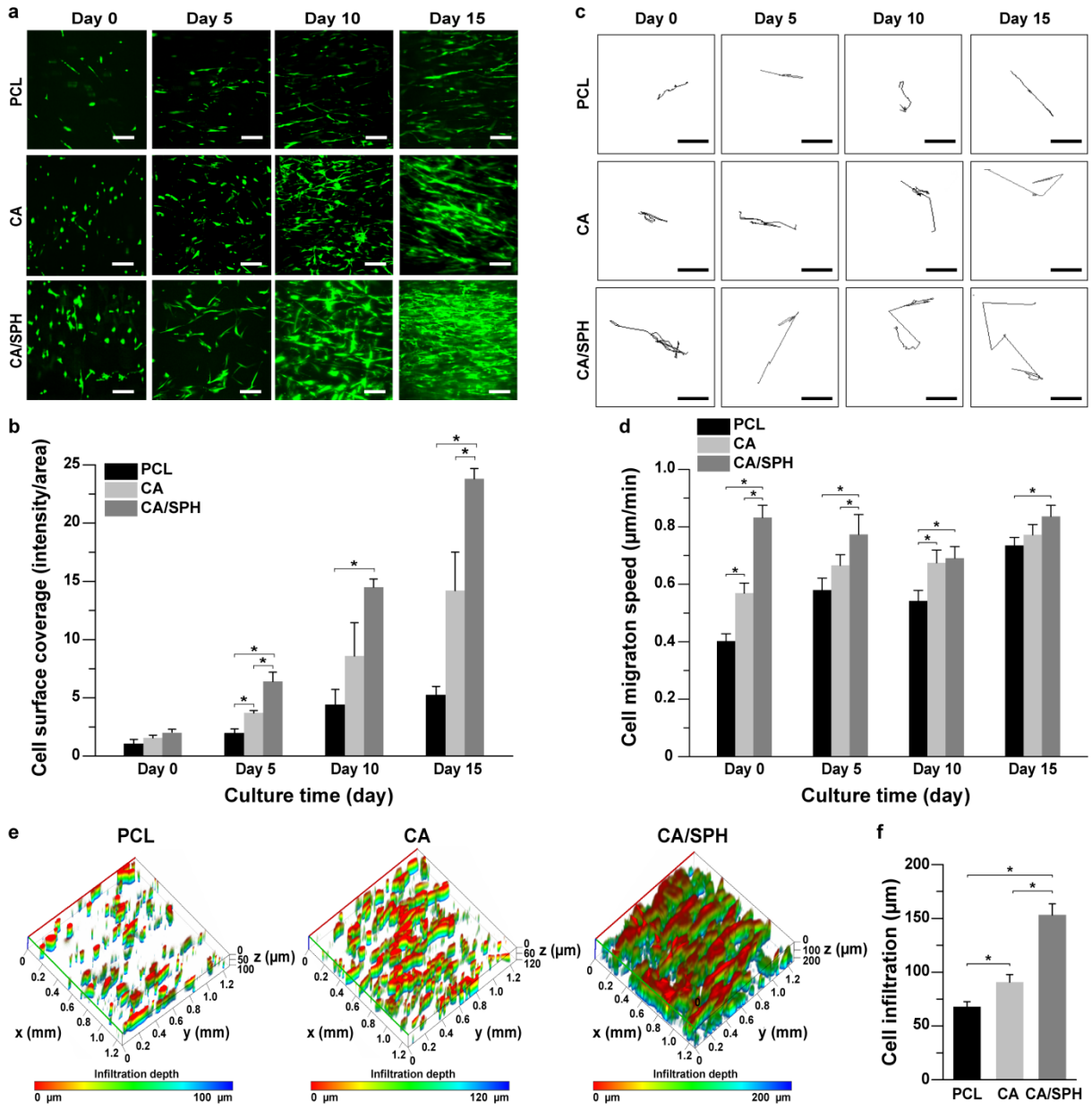

Figure 2-3. *In vitro* fibroblast coverage, migration, and infiltration.

(a–b) (a) Representative confocal microscopy images of GFP-expressing human neonatal dermal fibroblasts (HNDF) on nanofibers with (b) analysis of surface area covered by cells at day 0, 5, 10, and 15. Scales are 50 μm. Bars represent standard error, n=5, FOV=5 from 3 productions, * indicates $p < 0.05$. (c–d) (c) Representative binary images of tracking a single cell on nanofibers at day 0, 5, 10, and 15 for calculating (d) migration speed of HNDF. Scales are 50 μm. Bars

(continued) represent standard error, *n*=5, FOV=5 from 3 productions, * indicates $p < 0.05$. (e-f) (e) Representative 3D-recontructed confocal microscopy images of HNDF on nanofibers after 15 days of cell culture with (f) quantitative analysis of cell infiltration depth. Bars represent standard error, *n*=5 for PCL and *n*=8 for CA and CA/SPH, FOV=3 from 3 productions, * indicates $p < 0.05$.

Immunostaining analysis with the Ki-67 antibody – a marker specific to proliferative nuclei [153] – showed that CA/SPH nanofibers induced higher cell proliferation than PCL or CA nanofibers. Nanofiber cytotoxicity was calculated by using a common LDH assay.[50, 152] Both CA and CA/SPH nanofiber scaffolds exhibited low cytotoxicity, with similar values to PCL nanofibers. Furthermore, we observed that the cell surface coverage on the CA/SPH nanofibers was significantly higher than on the PCL and CA nanofibers after 5 days in culture (Figure 2-3a-b). The CA nanofibers showed greater cell coverage at day 5 and day 15 versus the PCL nanofibers. HNDFs migrated faster on CA-based nanofibers than on PCL nanofibers (Figure 2-3c-d), whilst the addition of bioactive SPH into CA nanofibers resulted in increased cell migration compared to pure CA nanofibers. These results reflect the preferential properties of dermal ECM-mimetic CA-based nanofibers (fiber diameter, pore diameter, and stiffness as shown in Figure 2-2), and underscore the suboptimal properties of PCL. In addition, soy protein has been reported to trigger the expression of extracellular signal-regulated kinase (ERK), transforming growth factor (TGF β1), and integrin β1 that promote cell migration.[105, 120] In an effort to assess cell infiltration, cells were seeded on the surface of nanofiber scaffolds. Cells adhered to nanofibers and started to grow. At day 0, there is no significant difference in cell infiltration between different nanofibers. After 15 days of cell culture, CA-based nanofibers

showed an increase in cell infiltration depth compared to PCL nanofibers (Figure 2-3e-f) which was again further increased by functionalizing CA nanofibers with SPH. As CA-based nanofiber scaffolds have higher pore diameters than PCL nanofibers (Figure 2-2b), cells infiltrate faster on CA-based nanofibers.[28] However, there is no significant difference in pore diameters between CA and CA/SPH nanofiber scaffolds, suggesting that the existence of SPH promoted cell migration (Figure 2-3c-d) and thus cells on CA/SPH nanofibers penetrated faster than CA nanofibers.

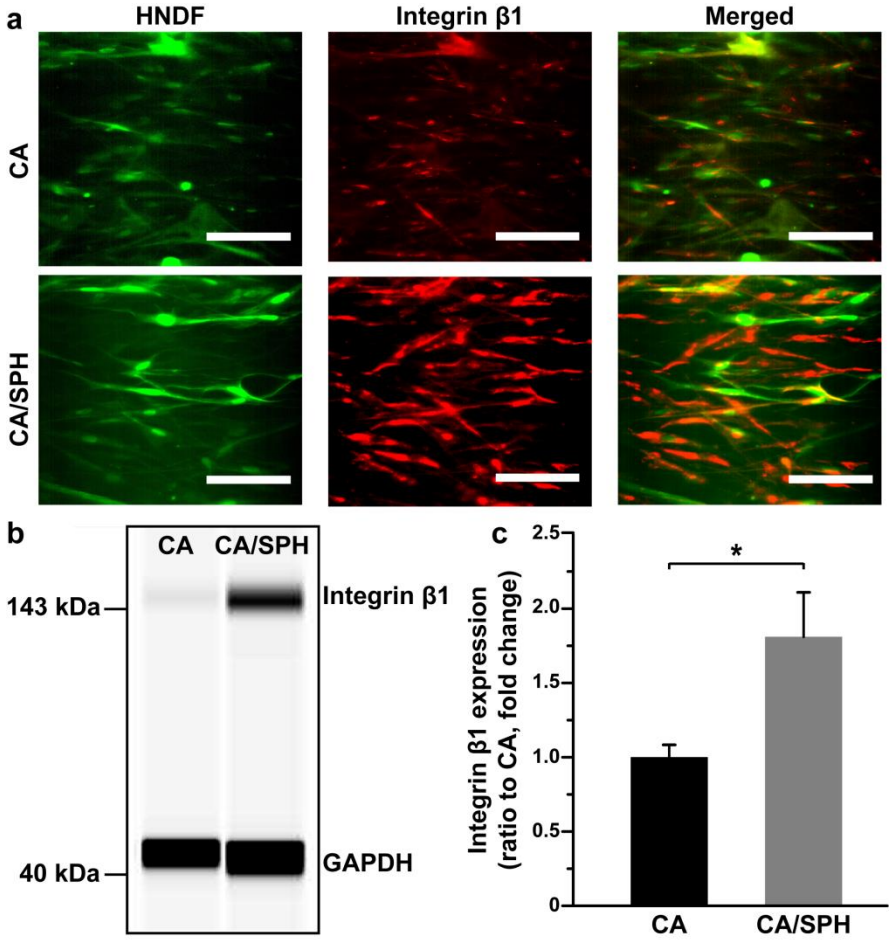

Figure 2-4. *In vitro* integrin β1 expression by fibroblast.

(continued) (a) Representative immunostaining and (b) Western blotting images for integrin β1 with (c) quantitative analysis from Western blotting. Scales are 100 μm. Bars represent standard error, n=6 for CA and n=7 for CA/SPH from 3 productions, * indicates $p < 0.05$.

Next, immunocytochemical and WSestern blot analysis for integrin β1 were performed to understand the effect of SPH on cell growth and migration. The integrin β1 is ECM protein receptors which regulates the behavior of ECM proteins and cells.[89, 154-156] It also enables crosstalk with other growth factors and plays a crucial role in tissue repair [157]. During wound healing, dermal fibroblasts migrate to the wound site and express integrin β1 to mature the developing matrix.[157] It has been found that decreased expression of integrin β1 reduces the ability of fibroblasts and keratinocytes to migrate, lay down a collagen matrix, and ultimately enable wound closure.[89, 154-156] After 15 days of cell culture, immunocytochemical (Figure 2-4a) and western blot (Figure 2-4b-c) analysis indicated that the integrin β1 expression was significantly increased on CA/SPH nanofibers, compared to CA nanofibers. These results indicate that soy protein in our scaffolds can trigger the expression of integrin β1 that in turn accelerates the cell migration and the production of new ECM proteins for wound closure. The increased integrin β1 expression by functionalizing CA nanofibers with SPH is in line with previously published work that reported that soy protein peptides up-regulated the expression of integrin β1 in fibroblasts.[105]

In summary, our *in vitro* fibroblast study demonstrated that CA nanofibers supported stronger cell growth, proliferation, migration, and infiltration than PCL nanofibers. These enhanced cellular activities occurred because CA provides a soft and hydrophilic backbone similar to that of a collagen matrix found in native dermal tissue. Further functionalization of CA

nanofibers with SPH accelerated proliferation, growth, migration, infiltration, and integrin β1 expression of HNDFs. Accordingly, it can be extrapolated that CA/SPH nanofibers should possess the ability to provide structural and biological cues to promote wound healing *in vivo*.

2.2.5 *In Vivo* Wound Healing Study in a Rodent Model

To investigate the potency of CA/SPH *in vivo*, we tested our nanofiber scaffolds on a mouse excisional wound splinting model.[158] Wound contraction was inhibited by suturing a silicon splint to the peripheral edge of the wound in an effort to study the healing process via re-epithelialization and thus improving recapitulation of the wound healing process of humans (Figure 2-5a).[159, 160] Nanofiber scaffolds were held in place with a Tegaderm™ film. The control group wounds received no nanofiber treatment and were only covered with the Tegaderm™ film. It was observed that CA/SPH nanofibers significantly accelerated wound closure (Figure 2-5b-c). On Day 7 after surgery, CA nanofibers showed 42% faster wound closure than our control. The addition of SPH in the CA nanofibers further accelerated wound closure by 21% and showed an overall 72% increase when compared to the non-treated control. After 14 days, the wounds treated with CA/SPH nanofibers were fully closed (Figure 2-5b-c). Moreover, the wound closure potentiated by CA/SPH nanofibers significantly higher than both the control and CA nanofibers.

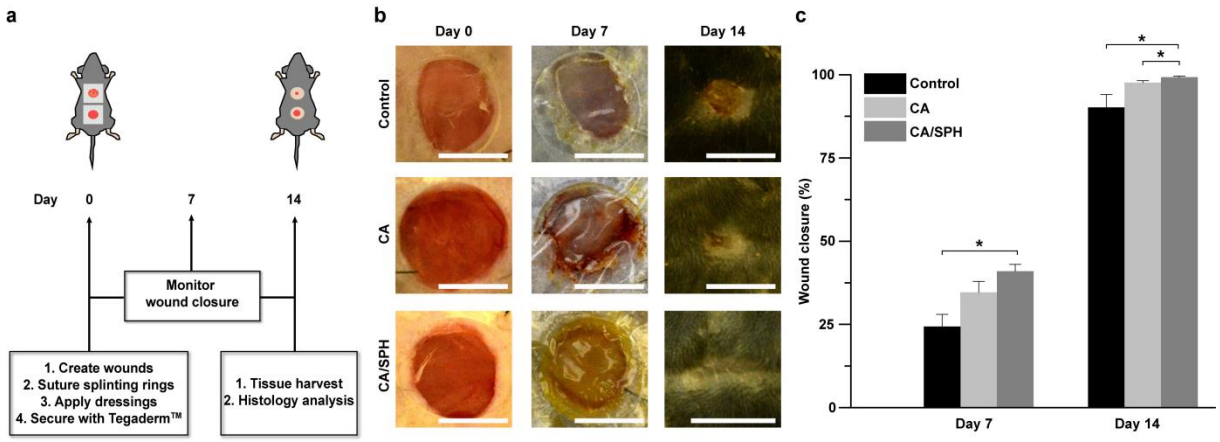

Figure 2-5. *In vivo* wound healing study with a mouse excisional wound splinting model. All wounds were covered with the Tegaderm™ film. Control wounds received no nanofibers. (a) Schematic representation of *in vivo* wound healing experiment. (b) Representative images of wounds from the study groups: untreated control, treated with CA nanofibers, and treated with CA/SPH nanofibers at Day 0, 7, and 14. Scales are 5 mm. (c) Analysis of wound closure. Fiber wound dressings were prepared from 3 productions for each condition. Bars represent standard error, n=4 wounds and 3 mice for control, n=5 wounds and 3 mice for CA and CA/SPH. * indicates $p < 0.05$.

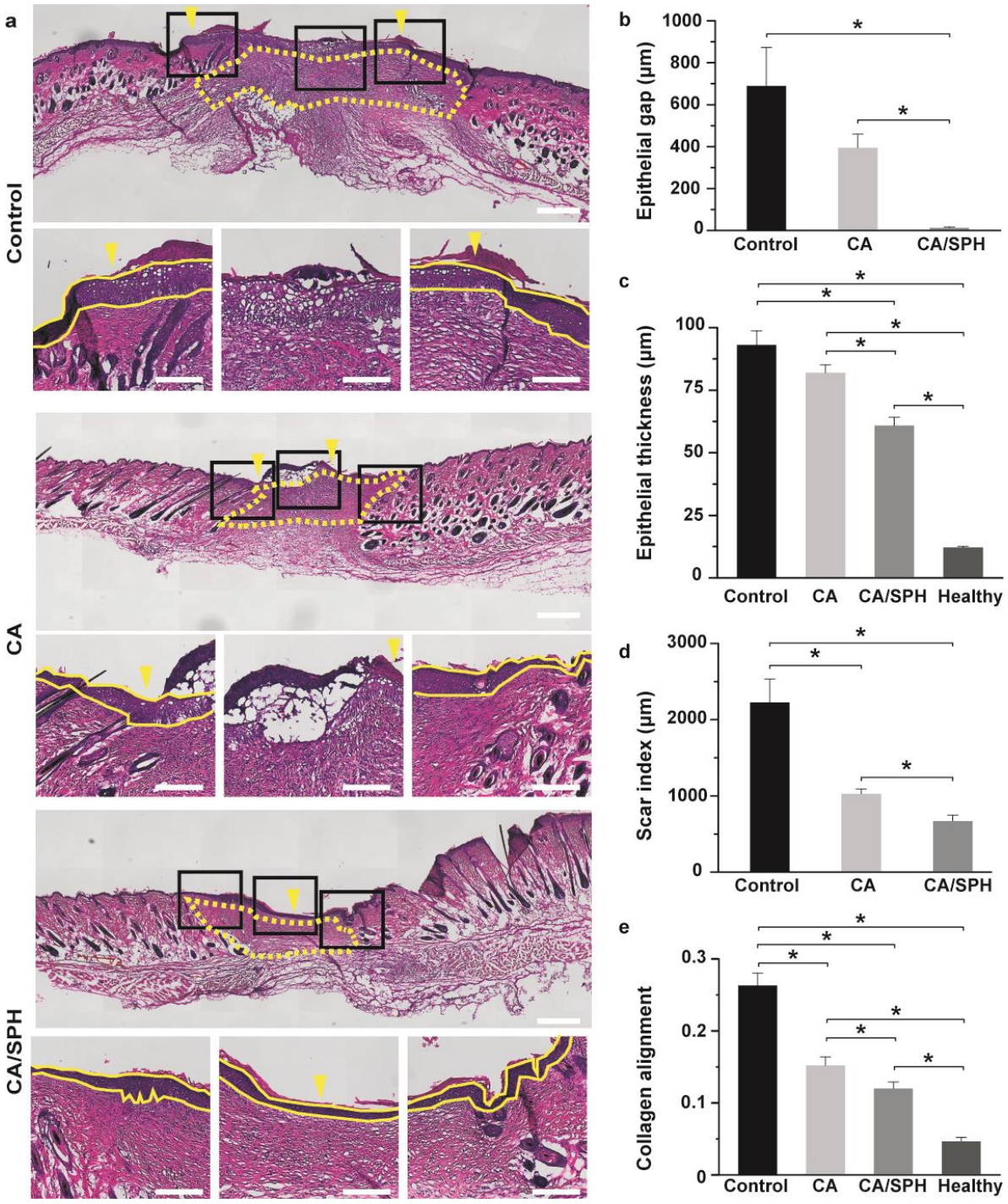

Figure 2-6: Histology analysis.

(a) H&E staining of wounds after 14 day post-surgery (untreated control, treated with CA nanofibers, and treated with CA/SPH nanofibers). In the top panel, the yellow arrows indicate the edge of the epidermal layer and the yellow dots outline the scar area. The yellow lines in the

(continued) bottom panels of the zoom-in images delimit the epidermal layer in the skin tissue. Scales in the top and bottom panels are 500 μm and 200 μm, respectively. (b–e) Quantitative analysis of b) epithelial gap, c) epithelial thickness, d) scar index, and e) collagen alignment from H&E staining images. Fiber wound dressings were prepared from 3 productions for each condition Bars represent standard error, n=3 wounds and 3 mice for control, n=4 wounds and 3 mice for CA and CA/SPH nanofibers, n=5 wounds and 5 mice for healthy tissue, at least 3 sections per wound, * indicates $p < 0.05$.

In an effort to further assess the regenerative capacity of our treatment conditions, histological analysis of healed tissues was performed at day 14 post surgery (Figure 2-6a). Restoration of the dermal and epidermal layers are key parameters for evaluating wound healing and tissue regeneration.[158, 161] It is commonly analyzed by quantifying the epithelial gap, epithelial thickness, and scar size.[158, 161] H&E staining confirmed our previous macroscopic observation that CA/SPH nanofiber-treated wounds were re-epithelialized at day14 post-surgery. However, wounds from the control and CA nanofiber-treated groups remained open, resulting in epithelial gaps a few hundred micrometers in diameter after 14 days of treatment (Figure 2-6b). In addition, the control or CA nanofibers-treated wounds exhibited significantly thicker epidermises than CA/SPH nanofibers-treated wounds, indicating slower regeneration of the epidermis (Figure 2-6c). It should nonetheless be noted that the epidermal thicknesses of CA/SPH nanofibers-treated wounds were still higher than that of healthy tissues (Figure 2-6c). We also measured the scar size using a quantitative scar index (Figure 2-6d),[161] which found that CA/SPH nanofibers significantly reduced the scar size compared to the control or CA nanofibers after 14 days treatment. Lastly, the alignment of the newly synthesized collagen in the dermis

was calculated (Figure 2-6e). The dermal collagen was significantly less aligned in CA/SPH nanofiber-treated wounds than control or CA nanofiber-treated wounds. However, the alignment of CA/SPH nanofiber–treated wounds was still higher than that of healthy tissues that possess typically basket-woven fiber organization. In line with our *in vitro* results, the *in vivo* data supported our hypothesis that both a nanofibrous architecture and bioactive soy protein accelerated wound closure and supported regeneration of the dermal and epidermal layers. These observation also corroborate previously published results in which ECM-mimetic peptide [80, 121] and phytoestrogens [43, 111, 162, 163] in soy protein promoted re-epithelialization and dermal tissue regeneration. When comparing our results to other reports of pro-regenerative fibrous scaffolds that consist of natural materials (such as ECM proteins, silk, and chitosan),[164-168] similar trends can be established for both wound closure rate and tissue regeneration (re-epithelialization, epidermal thinning, collagen alignment, and scar formation). Yet our scaffolds present a significant advantage gained by their inherent plant-based origin as they are free of animal-derived materials or synthetic carrier polymers that raise manufacturing cost, immunogenicity, and ethical concerns.

2.3 Conclusions

To the best of our knowledge, the present study reports the first fabrication and optimization of CA/SPH nanofibers produced using an RJS system. CA and SPH molecules were homogeneously distributed along the nanofibers for equal functionality at the fiber surface. Using CA as a co-spinning polymer enabled recapitulation of fiber morphology, fiber diameter, pore diameter, and stiffness of the native ECM thus creating optimal conditions for dermal fibroblasts to thrive. Functionalization of CA nanofibers with SPH enhanced surface roughness,

hydrophilicity, and water absorption capacity. The *in vitro* study indicated that CA/SPH nanofibers increased proliferation, growth, migration, and infiltration of fibroblasts and exhibited low cytotoxicity, compared to both PCL and CA nanofibers. The addition of SPH into CA nanofibers further up-regulated the expression of integrin β1, which has been attributed to enhanced cell migration and tissue regeneration. Finally, the *in vivo* mouse study revealed that CA/SPH nanofibers accelerated wound closure and tissue regeneration in comparison to CA nanofibers or the non-treated control. Altogether, these findings confirmed the utility of CA/SPH nanofibers for enhanced wound healing. We envision that our one-step, cost-effective, and regenerative scaffolds comprised of plant-based materials will be the next generation of regenerative dressings to push the envelope of nanofiber technology and the wound care market.

2.4 Material and Methods

2.4.1 Materials

PCL (M_n 70,000-90,000; Sigma-Aldrich), CA (M_n 50,000; Sigma-Aldrich), SPH (Amisoy^{TM}; Sigma-Aldrich), and Hexafluoroisopropanol (HFIP, Oakwood Chemical) were used as received.

2.4.2 Fiber Fabrication by Rotary Jet Spinning

Nanofibers were spun by using rotary jet spinning (RJS) system as described in previous studies.[25, 50, 140, 141] Briefly, CA and CA/SPH with different compositions and concentrations (weight per volume percent, wt/v %) were dissolved in HFIP and stirred for overnight. As a reference group, PCL (6 wt/v %) was also dissolved in HFIP. After mixing, solutions were flowed to the rotating reservoir through polyfluoroalkoxy alkane tubing (Saint-Gobain) at 2 mL/min by using an automatic syringe pump (Harvard Apparatus). Then, the

solutions (10 mL in total) were sprayed from the reservoir at at 60,000 rpm for 5 min, elongating polymers into nanofibers and evaporating HFIP rapidly in the air from the orifice (diameter of 360 μm). The spun nanofibers were dried overnight in a desiccator to fully remove excess solvent. For cell culture, the spun nanofibers were collected on coverslips and sterilized overnight under UV-light.

2.4.3 Scanning Electron Microscopy (SEM)

Fiber samples were imaged by using a field emission scanning electron microscopy (FESEM, Carl Zeiss). The fiber samples were mounted on sample stubs, sputter-coated with 5 nm thickness of Pt/PD (Denton Vacuum), and imaged by using FESEM.

2.4.4 Characterization of Chemical Compositions

Attenuated Total Reflectance-Fourier Transform Infrared spectroscopy (ATR-FTIR, Bruker) was used to obtain FT-IR spectra of nanofibers over 600–4000 cm^{-1} at a resolution of 2 cm^{-1} with 16 scans. The samples were mounted on sample stage and contacted with ATR-crystal for measurement. The FT-IR spectrum of the dried samples were measured and normalized from 0 to 1. For Gaussian curve fitting and area analysis, OriginPro 8.6 software (Origin Lab Corporation) was used. For statistical analysis, n=3 from 3 productions for each condition. X-ray photoelectron spectrometer (XPS, K-Alpha XPS system, Thermo Scientific) was used to further evaluate fiber surface composition. Fibrous test samples were prepared on silicon wafer substrates. Survey and high resolution elemental spectra were obtained using monochromatized aluminum Kα radiation (pass energy 200 eV). An argon flood gun was applied to offset sample charging. Peak detection and high resolution C_{1s} peaks were deconvoluted using Lorentzian/Gaussian product mix (30% L) functions. For statistical analysis, n=3 from 3 productions for each condition. Energy-dispersive X-ray spectroscopy (EDS) in FESEM was

used to investigate elemental mapping of nitrogen (N_K near 0.392 eV) and carbon (C_K near 0.277 eV) atoms, together with corresponding type II secondary electron (SE2) images. The fiber sample was also sputter-coated with Pd/Pt on sample stub and imaged by using EDS.

2.4.5 Characterization of Structural Properties

Fiber diameter, pore diameter, and fiber thickness were analyzed by using SEM images of the nanofibers and ImageJ (NIH) with the plug-in DiameterJ.[169] For fiber thickness analysis, nanofiber scaffolds were prepared from different injection volume (10, 30, and 60 mL in total) and the cross-sectioned scaffolds were imaged and analyzed. DiameterJ was used to determine fiber and pore diameters by using algorithm as described in previous study.[169] Here, the pore diameters refer to the pores of the fibrous scaffolds (between fibers). For statistical analysis, n=10 from 3 productions for each condition.

2.4.6 Biaxial Tensile Test for Stiffness Measurement

The stiffness in the wet state was determined by using biaxial tensile tester (CellScale). The spun fiber scaffolds were loaded by using clamps to hold the samples and immersed in phosphate buffered saline (PBS, ThermoFisher Scientific) at 37°C. Sample was loaded equibiaxially at a strain rate of 5% per second to 20% strain. A built-in software (CellScale) was used to record force/displacement measurements and images at 15 Hz. By using these measurements and the thickness of the samples, stress-strain curves were then produced. Stiffness was determined by calculating the slope of the stress-strain curves. For statistical analysis, n=5 from 3 productions for each condition.

2.4.7 Atomic Force Microscopy (AFM) for Roughness Measurement

Roughness (average deviation, R_a) was calculated by using built-in software in atomic force microscopy (AFM, MFP-3D^{TM}, Asylum). The fiber samples were mounted on sample

stage and imaged with tapping mode.[170] For statistical analysis, *n*=3 (field of view (FOV)=3) from 3 productions for each condition.

2.4.8 Contact Angle and Water Absorption Measurements

The cast film samples were prepared on coverslips using spin coater (at 2000 rpm for 1 min). The nanofiber samples were directly spun onto coverslips. A camera was used to record water droplet formation on the surfaces of the substrates. Contact angle was calculated by using ImageJ with the plug-in Drop Shape Analysis.[171] For statistical analysis, *n*=3 from 3 productions for each condition. Water absorbency was measured as % mass gain like a standard method reported before.[172] First, dry weight of the samples was recorded. The samples were immersed in PBS for 24 h at 37°C. The excess PBS on the wet samples was removed by placing it on a paper towel. Then, weight of the water-absorbing samples was measured. The water absorption ability was defined as described below;

$$A = 100 \times (W2 - W1)/W1 \quad (1)$$

where A is the water absorption ability (%), $W1$ is the weight before wet, and $W2$ is the weight after wet. For statistical analysis, *n*=3 from 3 productions for each condition.

2.4.9 Biodegradation Measurement

In vitro biodegradation was measured as % mass loss as detailed in previous studies.[105, 148, 173] The initial weight of the scaffold was measured, after which the samples were immersed in PBS at 37°C and 5% CO_2. At day 5, 10, and 15, the samples were washed three times with fresh PBS and dried in an oven at 60°C overnight. After complete dehydration, the weight of the dried samples was measured. The *in vitro* biodegradation was defined as follows:

$$D = 100 \times (W3 - W1)/W1 \quad (2)$$

where *D* is the *in vitro* biodegradation (%), *W1* is the initial weight, and *W3* is the final weight after degradation. For statistical analysis, *n*=3 from 3 productions for each condition.

2.4.10 Soy Protein Release Kinetics

In vitro release profile of soy protein from the nanofibers was measured as % loss of amide I peaks. The samples were immersed in PBS at 37°C and 5% CO_2. At day 0, 3, 5, 7, and 15, the samples were washed three times with fresh PBS and freeze-dried. The FT-IR spectrum of the dried samples were measured and normalized from 0 to 1. The relative areas of amide I peaks were analyzed from the normalized spectrum to calculate the % release of soy protein from the scaffolds. For statistical analysis, *n*=3 from 3 productions for each condition.

2.4.11 Cell Culture

Green fluorescent protein (GFP)-expressing human neonatal dermal fibroblasts (HNDFs, Angio-Proteomie) were properly treated as described in protocol from the manufacturer (Angio-Proteomie) for cell culture. Briefly, HNDFs were delivered at passage 3 in a frozen vial and stored in a liquid nitrogen tank before use. Cells were subcultured to passage 7 with Dulbecco's modified eagle medium (DMEM, ThermoFisher Scientific) containing Fetal Bovine Serum (FBS, 5%) and antibiotics (penicillin-streptomycin, ThermoFisher Scientific, 1%) in a T25 flask at 37°C incubator with 5% CO_2 and 21% O_2. Once the cells reach passage 7, trypsin/ ethylenediaminetetraacetic acid solution (trypsin/EDTA, Lonza, 2 mL) was added to the T25 flask. Seeding density was fixed at 30,000 cells per sample. Cell media was changed every 2 days before imaging and fixation.

2.4.12 Analysis of *In Vitro* Cell Behavior

GFP-expressing HDNFs on the fibers were imaged by using confocal microscopy (Zeiss LSM 5 LIVE) at 37 °C in a temperature controlled chamber. 4-(2-hydroxyethly)-1-

piperazineethanesulfonic acid (HEPES, ThermoFisher Scientific, 2.5 %) buffer was added to the media during imaging in an effort to keep the pH constant. For cellular growth study, the intensity of GFP-expressing HNDF per area was calculated from the confocal images by using ImageJ. For cellular migration study, the migration of GFP-expressing cells on fibers was tracked (1 frame/10 min for at least 40 frames). Once all images were collected, ImageJ plug-in StackReg was used to correct the center of each image.[174] For statistical analysis, *n*=5 (field of view (FOV)=5) from 3 productions for each condition. Migration of each cell was analyzed by using the plug-in Mtrack2 in ImageJ.[175] The Mtrack2 calculates the total distance each cell has migrated. Migration speed of cells was calculated by dividing the total distance by total imaging time. For statistical analysis, *n*=5 (field of view (FOV)=5) from 3 productions for each condition. In cellular infiltration study, z-stack confocal images of GFP-expressing cells on fibers were captured at 15 days of cell culture. The cell infiltration depth from the z-stack images was calculated using the z-axis profile function in ImageJ as previously reported.[142] The cross-sectional view (in *yz* plane) of cells was processed from ImageJ by using the orthogonal view function. For statistical analysis, *n*=5 for PCL and *n*=8 for CA and CA/SPH nanofibers (field of view (FOV) =3) from 3 productions for each condition.

2.4.13 Cytotoxicity Measurement

In vitro cytotoxicity of cells on the fibers was measured by using lactate dehydrogenase (LDH) cytotoxicity assay (Promega) as described previously.[50, 152] Briefly, HNDFs were cultured on nanofibers for 15 days and successively incubated with reaction solution and stop solution (1 M acetic acid) from the assay kit. A commercial plate reader was used to measure absorbance at 490 nm. The % cytotoxicity was defined as follows;

$$\% \text{ Cytotoxicity} = 100 \times (S - C)/(M - C) \quad (3)$$

where S is the readout from the sample, C is the readout from the control (medium only without cell), and M is the readout from maximum LDH release.[50, 152] For statistical analysis, n=17 in triplicate from 3 productions for each condition. For box plot, the box range is 25–75%, the whisker range is 10–90% using OriginPro 8.6 software.

2.4.14 Immunocytochemical Analysis

After 15 days of culture, HNDFs grown on nanofibers were fixed in paraformaldehyde (PFA, 4%) and Triton-X (0.05%) for 10 min. Following fixation, samples were incubated with primary antibody (rabbit polyclonal anti-Ki67 with 4′ ,6-diamidino-2-phenylindole dihydrochloride (DAPI) for proliferation study or rabbit monoclonal anti-integrin β1 antibody, Abcam) and with secondary antibody (goat anti-rabbit IgG (H+L) secondary antibody with Alexa fluor® 546, Invitrogen) during 1 h at room temperature for both primary and secondary antibody incubation. Following immunostaining, samples were mounted on glass slides by using Prolong Gold anti-fade agent (Invitrogen) and imaged on the confocal microscopy. Cell proliferation was calculated by dividing the number of Ki-67 positive cells by the number of DAPI-positive cells. For statistical analysis, n=5 for PCL and n=6 for CA and CA/SPH (field of view (FOV)=25) from 3 productions for each condition.

2.4.15 Western Blot Analysis

HNDFs were cultured on nanofibers for 15 days and were lysed at 4 ºC using radioimmunoprecipitation assay (RIPA) lysis buffer (SLBG8489, Sigma) with Complete Mini (11836153001, Roche Diagnostic) and Halt-Protease and Phosphotase Inhibitor (1861281, ThermoFisher Scientific). A capillary-based Wes Simple Western (ProteinSimple) was used to

detect and quantify the expression of integrin β1 in cell lysates following the manufacturer's protocol. In brief, each capillary loaded 5 μg of sample lysates and separated proteins by size. The samples were incubated with primary antibodies for Integrin β1 and Glyceraldehyde 3-phosphate dehydrogenase (GAPDH) as a loading control (ab52971 and ab9485 respectively, ABCAM). Target proteins were labeled with secondary antibodies and chemiluminescent reagents provided by the manufacturer (ProteinSimple). Signals were detected and quantified using CompassSoftware (ProteinSimple). Expression of integrin β1 was normalized to GAPDH loading control and compared across sample conditions. For statistical analysis, n=6 for CA and n=7 for CA/SPH from 3 productions for each condition.

2.4.16 Mouse Excisional Wound Splinting Model

All mouse wound healing experiments were performed using IACUC approved protocols (Protocol ID 11-11). Based on the previous publications,[159, 160] the mouse excisional splinting model was carried out in order to analyze cutaneous wound closure in murine skin by excluding wound contraction. Briefly, splinting rings were prepared by cutting 8 mm holes in a 0.5 mm-thick silicon sheet (Grace Bio-Labs) using a sterile biopsy punch (Integra® Miltex®). The prepared rings were washed and sterilized by ethanol (70 % vol/vol), and then were air-dried in a sterile culture hood before surgery. C57BL/6 male mice (Charles River Laboratories, 52 days old) were anesthetized with isofurane through the duration of procedure. Once anesthesia was confirmed by a toe pinch test, the dorsal side of mice was shaved using electric and manual razor. After hair removal, the skin was cleaned with betadine (Santa Cruz Biotechnology) and ethanol (70 % vol/vol). The full-thickness excisional wounds were created on the midline by punching through the skin with a 6-mm-diameter sterile biopsy punch. The punched tissues were used for histological analysis of healthy skin (Day 0). An instant-bonding adhesive (Krazy glue)

was put on one side of a splint. The splints were fixed into place around the wound with instant bonding adhesive followed by suturing with nylon suture (Ethicon). Nanofiber wound dressings were applied to the wound and covered with Tegaderm™ (Nexcare™) patches to keep the scaffolds in place and the surgical area clean. Control wounds received no nanofibers and were covered with Tegaderm™ patches only. Tegaderm™ is a clinical standard wound dressing.[159, 160] The mice were monitored daily. Before tissue harvest on Day 7 and 14, mice were sacrificed via IACUC approved methods.

2.4.17 *In Vivo* Wound Closure Analysis

Wound area was photographed with a digital camera on Day 0, 7, and 14. The wound area was manually quantified using ImageJ. Wound closure was defined as described below;[159]

$$\text{Wound closure } (\%) = 100 \times (O - A)/O \quad (4)$$

where O is the area of the original wound and A is the area of the wound at a given time point. Fiber wound dressings were prepared from 3 productions for each condition. For statistical analysis, n=4 wounds and 3 mice for control, n=5 wounds and 3 mice for CA and CA/SPH.

2.4.18 Histological Analysis

Histological analysis was preformed based on previously published methods.[159] Tissues were harvested from Day 0 and 14 and fixed with PFA (4%) at 4 ºC overnight. The fixed tissue was washed using PBS five times for 30 min each. The tissue was incubated with sucrose (Sigma, 20% and 40% wt/vol) in PBS at room temperature for 2 h each. Then, the tissue was embedded in O.C.T. compound (Electron Microscopy Science) with cryomold (Tissue-Tek®). The frozen wound tissues were sectioned with 10 μm thickness, stained with hematoxylin and eosin (H&E), and imaged by slide scanner (Olympus VS120). Re-epithelialization was analyzed by manually calculating distance among the newly synthesized epithelial layers from H&E staining tissue

sections (marked as yellow arrows in Figure 2-6a).[158] Epithelial thickness was also manually measured using ImageJ. Scar index was quantified by using a previously published method.[161] Briefly, scar area (yellow dotted area in Figure 2-6a) and dermal thickness were manually measured using ImageJ. Then, scar index was defined as described below;[161]

$$\text{Scar index } (\mu m) = S/D \tag{5}$$

where S is the scar area (μm^2) and D is the average dermal thickness (μm). Dermal collagen alignment in the wounds was calculated by using OrientationJ in ImageJ as previously published.[176] The OrientationJ computes the coherency that is between 0 (isotropic) and 1 (anisotropic). Fiber wound dressings were prepared from 3 productions for each condition. For statistical analysis, n=3 wounds and 3 mice for control, n=4 wounds and 3 mice for CA and CA/SPH nanofibers, n=5 wounds and 5 mice for healthy tissue, at least 3 sections per wound.

2.4.19 Statistical Analysis

All data is displayed as mean ± standard error of mean (SEM). One-way analysis of variance (ANOVA) in OriginPro 8.6 software was used for statistical comparisons. Statistical significance was determined at * $p < 0.05$.

3 Biomimetic and Estrogenic Fibers Promote Regeneration in Mice and Human Skin via Estrogen Receptor β

Morbidity associated with cutaneous wound healing has become a major challenge in global healthcare as aging populations increase.[2] Estrogen has been used to promote healing processes via the estrogen receptor (ER) β pathway.[42, 177] However, this hormone could also increase the risk of other diseases via the ER-α pathway, indicating that the use of estrogen is problematic.[95] Recently, soy phytoestrogens have been suggested as a better alternative to estrogen to preferentially trigger the ER-β pathway.[5] However, the development and evaluation of regenerative soy-based dressings as ER-β modulators remain largely unexplored. Here, we engineered biomimetic and estrogenic hyaluronic acid (HA)/soy protein nanofiber dressings. The engineered scaffolds successfully recapitulated the native dermal microenvironment. We confirmed the presence of an ER-β-triggering phytoestrogen (genistein) within our scaffolds. We demonstrated that the scaffolds promoted wound closure and skin appendage regeneration via the ER-β pathway in both mouse and human skins.

3.1 Introduction

Estrogen, a primary female sex hormone, affects the regulation and development of various organs by binding to different estrogen receptors (ERs, ER-α or ER-β).[117] This hormone has been used in hormone replacement therapy (HRT) to treat age-related diseases, including delayed wound healing.[178] Estrogen accelerates normoxic and ischemic wound healing via the ER-β signaling pathway.[118, 177] ER-α, another signaling pathway activated by estrogen, triggers

certain breast cancers, indicating that the use of estrogen is problematic.[179] A better alternative to estrogen is an estrogenic material that can selectively activate the ER-β signaling pathway for enhanced wound healing without a high risk of triggering ER-α-positive cancers.

Soy protein possesses phytoestrogens that have a structure and function similar to estrogen.[74] Interestingly, among phytoestrogens, genistein preferentially triggers the ER-β pathway and is known to modulate inflammation and antibacterial activity.[43] Preclinical and clinical studies have shown that topical and oral intakes of genistein accelerate skin tissue regeneration (*e.g.*, new granulation tissue and hair follicle formation) in an estrogen-deficient animal model (*e.g.,* ovariectomized mice) and skin samples from patients with chronic conditions.[78, 80, 102] While these studies elucidated the protective roles of genistein in healing, engineering soy phytoestrogen scaffolds remains largely unexplored. Nanofibers have attracted interest because they can provide an extracellular matrix (ECM)-mimetic microenvironment and efficiently deliver molecules into a target region.[10] Studies on the current soy-based nanofiber scaffolds have only focused on the effects of peptide contents in soy on fabricating wound dressings.[4] Accordingly, validation of phytoestrogens within dressings and elucidation of the physiological effects of phytoestrogens in soy-based scaffolds on skin regeneration through ER-β are lacking. The functionality of the engineered dressings has been assessed for minimal healing outcomes (*e.g.,* wound closure, re-epithelialization, and granulation tissue formation), but their effects on major healing outcomes, such as new hair follicle formation, which is absent during normal wound healing, have not been fully elucidated. The animal wound models used for evaluating current wound dressings are mostly limited to rodent or porcine models that cannot fully simulate the healing processes and results in humans.[180]

Herein, we hypothesized that plant, estrogenic, and ECM-mimetic soy fiber scaffolds will promote cutaneous wound healing by providing a suitable biomimetic microenvironment and altering the ER-β-mediated signaling pathways in both mouse and human skins. We developed a force-induced nanofiber fabrication technology (immersion rotary jet spinning or iRJS) to design fibrous scaffolds that can integrate soy phytoestrogens and carrier polymers.[68] Specifically, we used HA as a carrier polymer. HA is a water-soluble glycosaminoglycan that forms fibrous networks to provide structural support and retain moisture in the native skin microenvironment.[181] HA/soy protein isolate (SPI) composite fibers were successfully spun from water-based solvents and chemically crosslinked, resulting in biostable microfibers composed of nanofibrils similar to collagen fibrils in skin. The physicochemical properties of the scaffolds were characterized under different fabrication conditions. Furthermore, we verified the presence of proteins and phytoestrogens (genistein) in the scaffolds. When applied to ovariectomized mice, HA/SPI scaffolds reduced epidermal thickness and scar formation and promoted new hair follicle formation. The correlation between ER-β expression and hair follicle formation was further confirmed by quantifying the immunofluorescence intensity of ER-β and keratin 14 (K14) expression. Finally, HA/SPI scaffolds promoted re-epithelialization in human skin *ex vivo*, but this beneficial effect was prevented by inhibiting the ER-β signaling pathway with an ER-β antagonist. These data support our hypothesis that biomimetic and estrogenic HA/SPI fibrous scaffolds enhance skin regeneration via ER-β.

3.2 Results and Discussion

3.2.1 Fiber Scaffold Fabrication and Characterization

We developed a force-induced nanofiber fabrication technology (iRJS, Figure 3-1a), enabling us to design fibrous scaffolds that can integrate soy phytoestrogens and carrier polymers.[68] Specifically, we used HA as a carrier polymer for SPI, which possesses bioactive molecules, including genistein. HA is a water-soluble glycosaminoglycan that forms fibrous networks to provide structural support and retain moisture in the native skin microenvironment.[181] HA and SPI were dissolved in water/dimethyl sulfoxide (DMSO) (6:1) to fully dissolve soy phytoestrogens prior to the spinning processes because phytoestrogens are only slightly soluble in pure water.[182, 183] The polymer solution was ejected at a high injection rate (10 mL/min) and high centrifugal forces (15,000 rpm) to form a polymer jet, the jet entered a precipitate bath (80% ethanol), and the solidified nanofibers were collected on a rotating mandrel (Figure 3-1a). The spun fibers were then freeze-dried for further characterization, resulting in a scaffold with a scale of a few millimeters developed in a high-throughput process (Figure 3-1b).

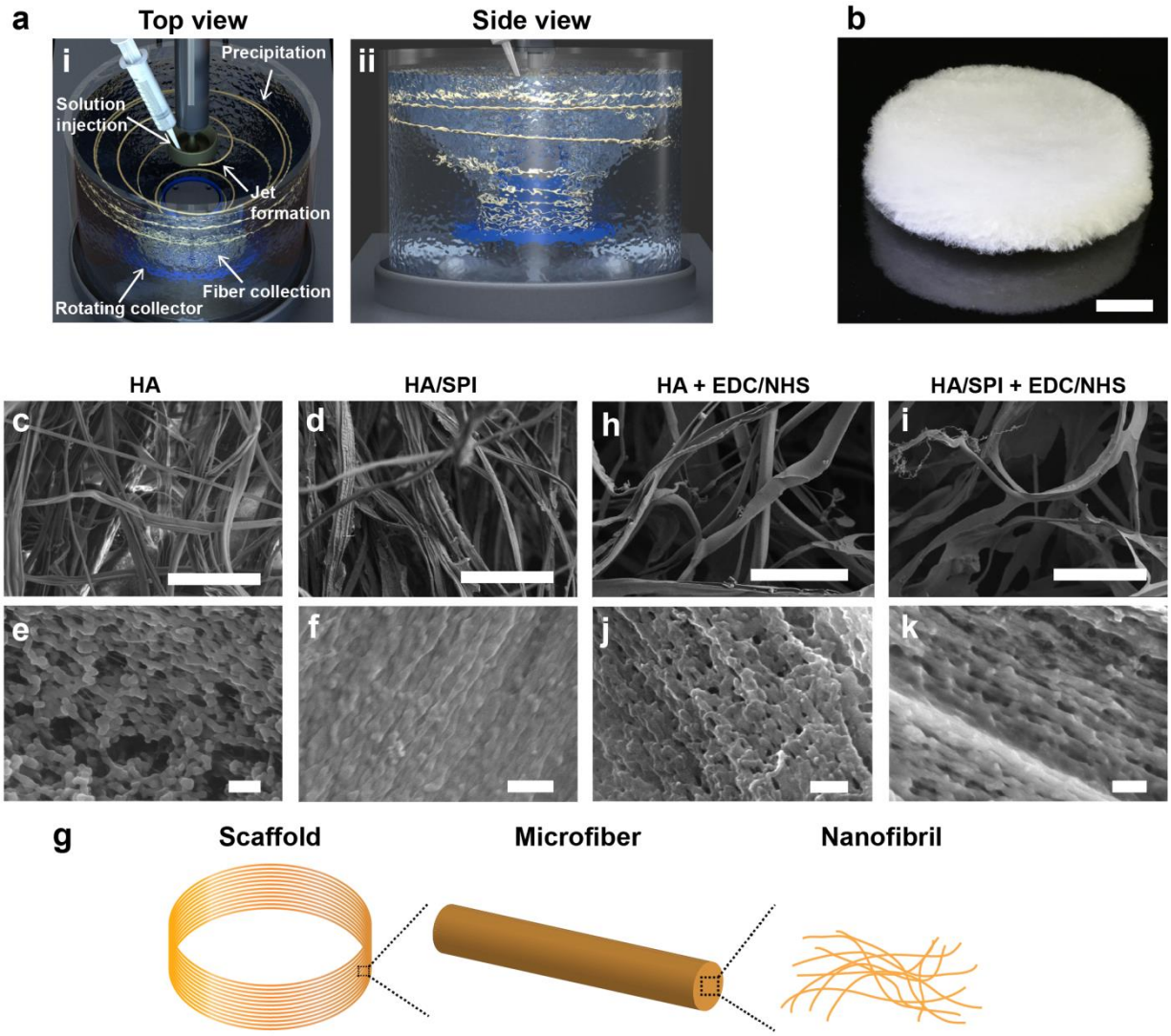

Figure 3-1. Fiber fabrication.

(a) Schematic illustration of the iRJS machine. (b) Spun, crosslinked, and freeze-dried HA/SPI fiber scaffold. The scale is 1 mm. (c–k) SEM images of the engineered fibers. The scales of the top and bottom panels are 50 μm and 500 nm, respectively. (g) Schematic illustration of the fibrillary structure of the engineered scaffold at different spatial scales.

We varied the concentration of SPI (0, 2, and 4 wt/v %) to identify an optimal concentration for continuous and bead-free fibers with a fixed concentration of the HA backbone (2 wt/v %). Pure HA (2 wt/v %) and HA/SPI (2 wt/v %/2 wt/v %) solutions exhibited bead-free microfibers (Figure 3-1c-d), whereas HA/SPI (2 wt/v %/4 wt/v %) solution showed beading in the microfibers. Accordingly, for further characterization and assessment, we used HA/SPI (2 wt/v %/2 wt/v %) fibers as our sample and pure HA (2 wt/v %) fibers as a control. Interestingly, the spun microfibers were composed of nanofibrils whose diameters were a few tens of nanometers (Figure 3-1e-f), mimicking the multiscale architecture of collagen fibers in the native skin microenvironment (Figure 3-1g).[184] However, the spun fibers were quickly dissolved in physiological conditions [phosphate-buffered saline (PBS) and cell culture medium] due to the lack of strong bonds among the molecules. The spun fibers were crosslinked using 1-ethyl-3-(3-dimethylaminopropyl) carbodiimide (EDC) and N-hydroxysuccinimide (NHS) to improve their biostability.[185] The crosslinked fibers were stable in the physiological medium for at least a few days. The biomimetic fibrillary structure was also preserved in the crosslinked fibers (Figure 3-1h-k).

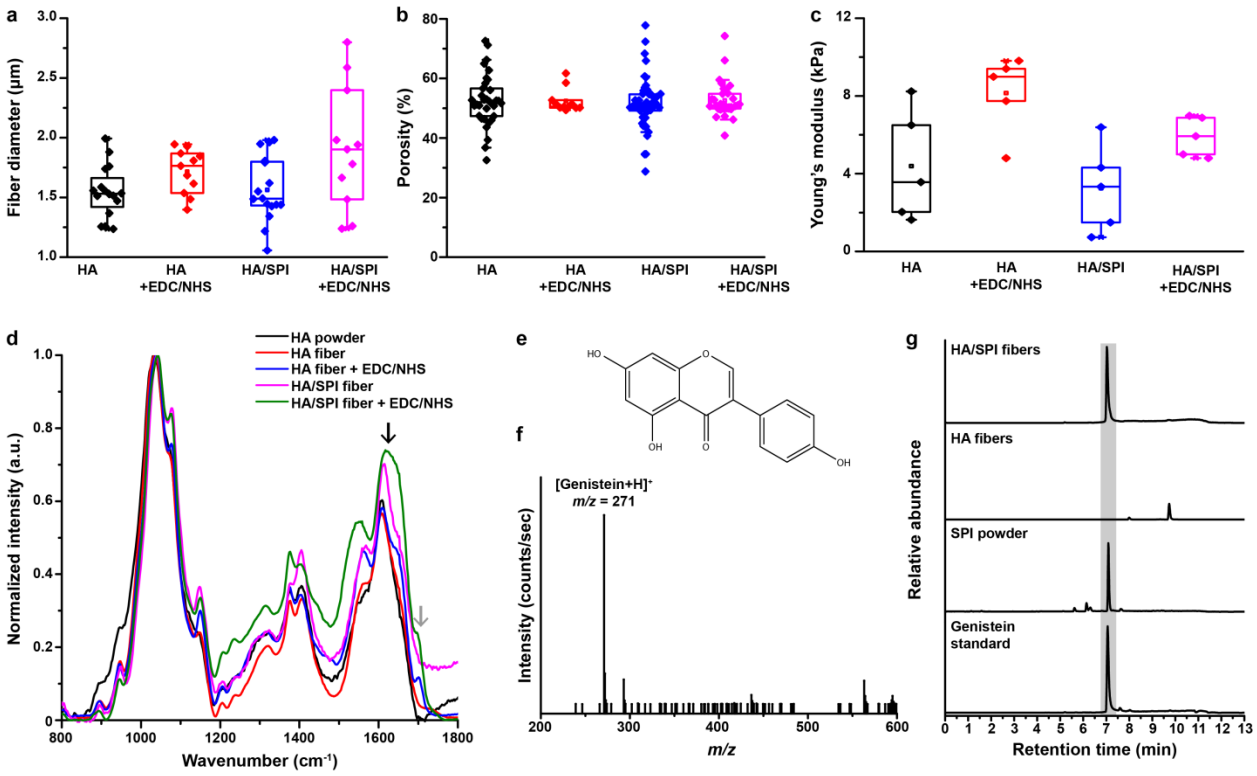

Figure 3-2. Scaffold characterization.

(a–b) Fiber diameter and scaffold porosity analysis by the Diameter J plug-in. For statistical analysis, $n \geq 5$, field of view (FOV) ≥2. (c) Mechanical strength of scaffolds. For statistical analysis, $n=5$. (d) FT-IR spectra of HA powder and scaffolds. The black and gray arrows indicate amide and ester bond-specific peaks, respectively. (e–g) LC-MS analysis of genistein in scaffolds. (e) Chemical structure of genistein. (f) Full MS spectra of genistein showing the major peak at *m/z* 271. (g) LC-MS spectra of samples with SIM mode. The gray area indicates the genistein-specific peaks that were found at a retention time of 7 min.

We further characterized the structural properties of the engineered fiber scaffolds to study the effects of the addition of SPI to the HA backbone and EDC/NHS crosslinking on fiber diameter, porosity, and mechanical strength, which are known to be crucial for determining skin cell fate during wound healing.[28, 145] First, fiber diameters increased after the crosslinking

reaction, whereas the addition of SPI to the fibers barely influenced the fiber diameter (Figure 3-2a). In all cases, fiber diameters ranged from 1 to 3 μm, similar to that of *in vivo* collagen microfibrils.[184] Regardless of the presence of SPI and the use of the crosslinker, the engineered scaffolds possessed a highly porous morphology (>50% porosity) that promoted cell infiltration and growth and inhibited bacterial penetration (Figure 3-2b).[28] Moreover, Young's modulus of the scaffolds increased after crosslinking and slightly decreased after the addition of SPI due to hydrophilic molecules from SPI (Figure 3-2c).[22] The Young's modulus of the scaffolds was between 1 and 10 kPa, similar to that of healthy human skin.[30] Due to the favorable biostability and structural cues, the crosslinked HA and HA/SPI fiber scaffolds were used as our controls and samples in the following studies.

Next, we analyzed the biochemical components in the scaffolds. In particular, we performed FT-IR measurements to confirm the chemical crosslinking among molecules and the macroscopic distribution of SPI within the scaffolds (Figure 3-2d). The EDC/NHS reagent enables the formation of ester bonds from carboxylic groups and hydroxyl groups (between HA-HA, HA-SPI, or SPI-SPI) and amide bonds from carboxylic groups and amine groups (between HA-SPI or SPI-SPI). The increase in peaks specific to ester (at 1700–1800 cm^{-1}) and amide (at 1600–1700 cm^{-1}) bonds confirmed the crosslinking reaction among HA and SPI. In addition, the increase in the amide peak in HA/SPI fiber scaffolds compared to pure HA fiber scaffolds indicated that SPI was successfully integrated into the HA backbone. More importantly, we detected phytoestrogens in the scaffolds by using liquid chromatography–mass spectrometry (LC-MS) (Figure 3-2e-g). Specifically, we focused on measuring genistein, which is one of the main soy phytoestrogens known to trigger ER-β signaling pathways to enhance skin regeneration (*e.g.,* ECM synthesis and hair reformation). The major peak of the positively ionized genistein

molecule was observed at *m/z* 271 (Figure 3-2f). The genistein standard produced a peak at a retention time of 7 min in LC (Figure 3-2g). The genistein peak was found in raw SPI powder and HA/SPI fiber scaffolds but not in pure HA fiber scaffolds. These data revealed that HA/SPI scaffolds possess genistein and therefore can induce ER-β signaling pathways.

3.2.2 Enhanced Skin Regeneration in Mice Skin via Estrogen Receptor β

Due to the biomimetic and estrogenic cues of our scaffolds, we hypothesized that HA/SPI scaffolds will promote skin regeneration via the ER-β signaling pathways. To test our hypothesis, we used full-thickness excisional splinting wounds in ovariectomized mice (Figure 3-3a). The mouse wound splinting model helps to recapitulate the healing processes occurring in humans by preventing local wound contraction in mice.[159] Moreover, all mice underwent ovariectomy (OVX) surgery and were fed soy-free special diets to hinder endogenous and external sources of estrogen and phytoestrogens except our scaffolds in an effort to study the effects of our scaffolds on cutaneous regeneration via the ER-β signaling pathways. We created 6 mm wounds on Day 0 and collected tissues on Day 20 to assess skin reformation. As a control, wounds received no treatment. Twenty days after the surgery, all wounds were fully closed. The HA/SPI scaffolds significantly reduced epidermal thickness and scar formation and accelerated new hair follicle formation compared to control and HA scaffolds (Figure 3-3b-g).

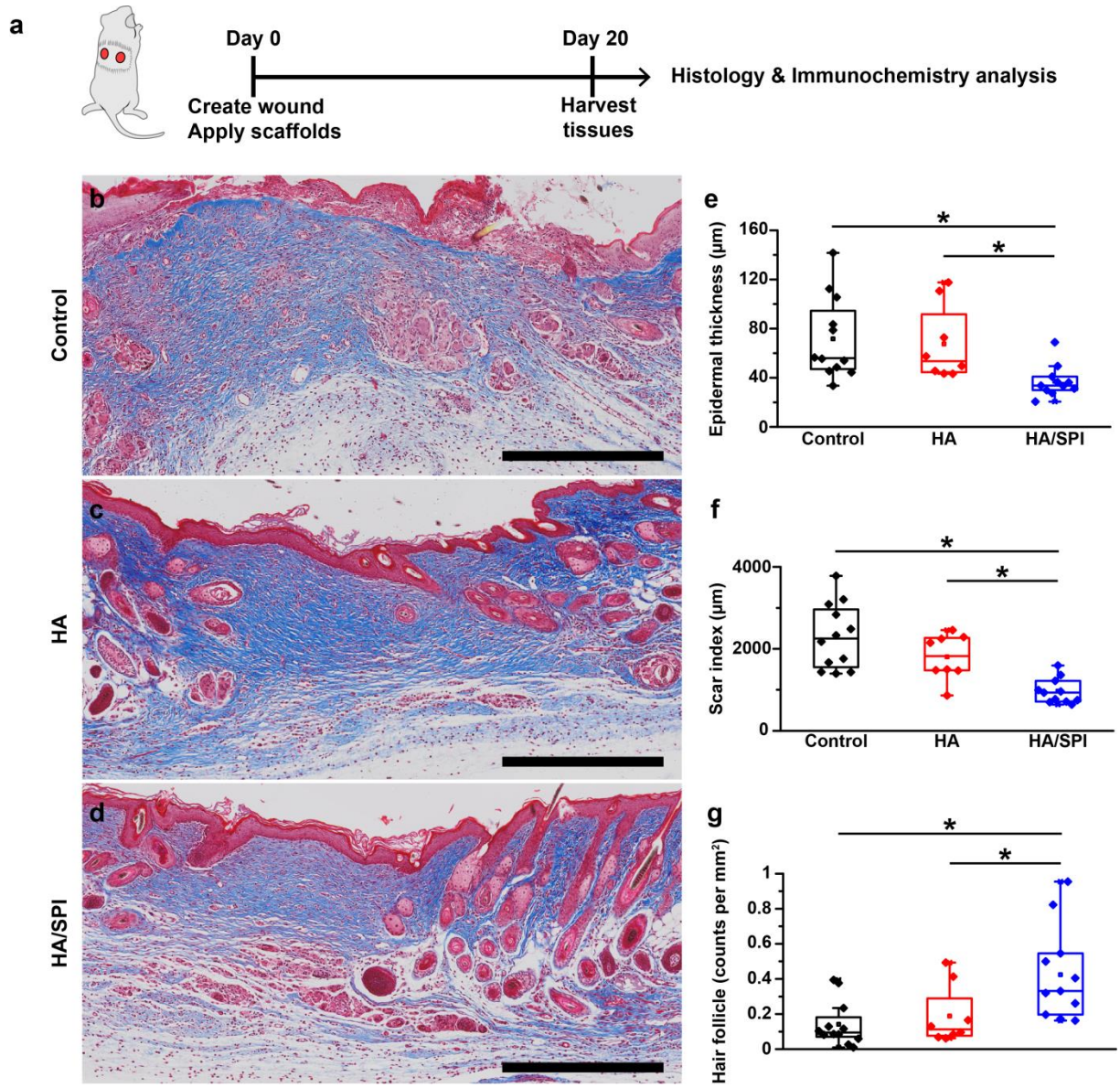

Figure 3-3. ***In vivo*** **mouse wound healing and histological studies.**

(a) Schematic illustration of the experimental timeline. (b–d) Masson's trichrome images of day 20 post-injury tissues. Scales are 500 μm. (e–g) Quantitative analysis of skin appendage regeneration (f, epidermal thickness, g, scar index, and h, hair follicle density). For statistical analysis, *p<0.05, n=12 for the control group, n=8 for the HA group, and n=11 for the HA/SPI group.

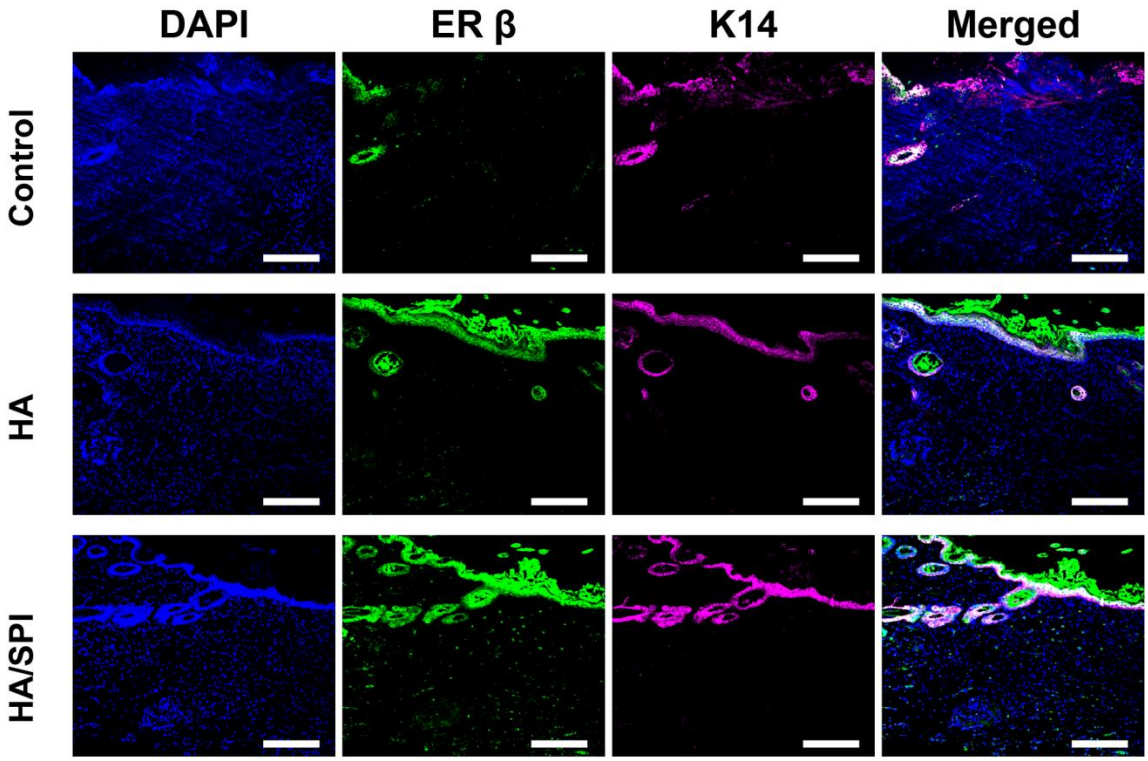

Figure 3-4. Hair follicle formation via estrogen receptor β in mouse skin.

Immunofluorescence images of day 20 post-injury mouse skin stained with DAPI (for nuclei), anti-ER-β antibodies, and anti-K14 (for epidermal keratinocytes and hair follicles) antibodies. Scales are 100 μm.

To further analyze the correlation of ER-β and hair follicle expression, we conducted ER-β and cytokeratin 14 (K14) staining (Figure 3-4) because K14 is expressed in epidermal keratinocyte layers and hair follicles.[186] Consistent with the histological analysis (Figure 3-3), HA/SPI scaffolds accelerated hair follicle and germ regeneration compared to control and HA scaffolds, as shown by K14-positive staining. In addition, we observed that ER-β was highly expressed in the epidermal keratinocyte layer and the hair follicles (Figure 3-4). Accordingly, the

ER-β-positive and K14-positive areas were highly overlapped. In addition, HA/SPI scaffolds exhibited the highest expression of ER-β in the wound site.

3.2.3 Enhanced Human Skin Regeneration via Estrogen Receptor β

Although human-mimetic mouse wound healing studies confirmed the efficacy of our scaffolds, the mouse model cannot fully recapitulate the healing processes and outcomes in human skins.[180] Therefore, we questioned whether HA/SPI scaffolds can promote tissue regeneration in human skins. To test this premise, we investigated wound healing in *ex vivo* human skins with 2 mm wounds for 7 days (NativeSkin®, Figure 3-5a-b).[180] Unlike tissue-engineered human skin constructs with limited ECM components and cell types, the *ex vivo* human skin model entirely mimics the cutaneous microenvironment, resulting in accurate assessment of the regenerative performance of wound dressings in human skin prior to clinical analysis.[180] In addition, ER-β signaling pathways were selectively inhibited by an ER-β antagonist (4-[2-phenyl-5,7-bis(trifluoromethyl)pyrazolo[1,5-a]pyrimidin-3-yl]phenol, PHTPP) to study the effect of the scaffolds on *ex vivo* healing processes via ER-β.[177]

Seven days after the injury, the HA/SPI scaffolds significantly promoted re-epithelialization compared to control and HA scaffolds (Figure 3-5c-g). However, following treatment with PHTPP, the re-epithelialization rate by the HA/SPI scaffolds was significantly reduced (Figure 3-5e-g). We also explored the expression of ER-β in the healed skins by immunofluorescence. Consistent with the *in vivo* results (Figure 3-3 and 3-4), human skin treated with HA/SPI scaffolds had the largest ER-β-positive area among all the conditions (Figure 3-5h-j). However, the expression of ER-β in the wound bed and newly formed epithelial tongues was retarded by PHTPP (Figure 3-5k).

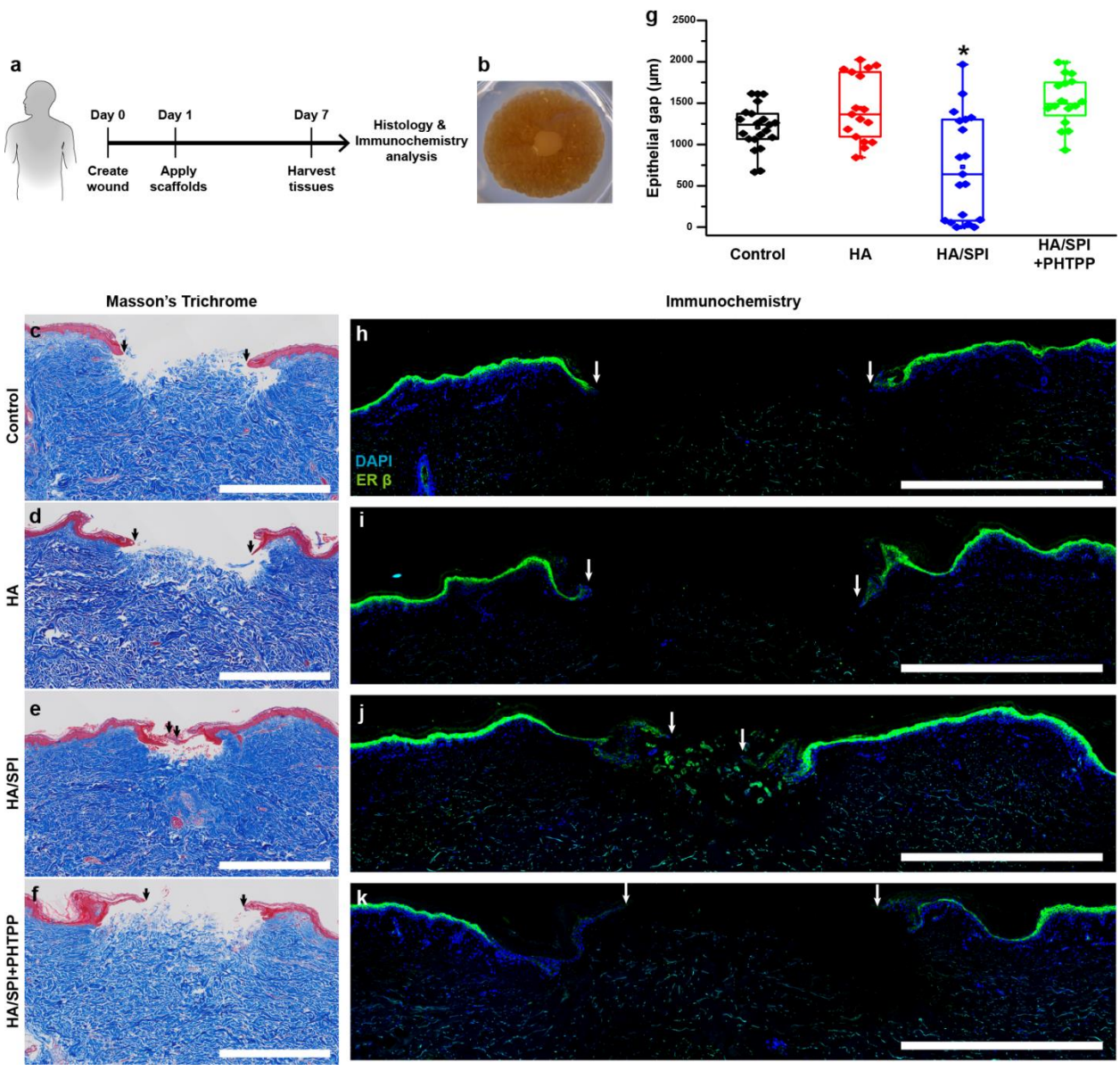

Figure 3-5. *Ex vivo* human skin wound healing via estrogen receptor β.

(a) Schematic illustration of the experimental timeline. PHTPP was introduced on day 1 to block the ER-β pathway. (b) Photograph of a wounded human skin biopsy on day 1 prior to scaffold application. (c–f) Masson's trichrome images of day 7 post-injury tissues. The black arrows indicate the edges of the new epithelial tongues. Scales are 1 mm. g, Re-epithelialization analysis. For statistical analysis, *p<0.05, n=11 for the control group, n=9 for the HA group, n=10 for the HA/SPI group, and n=8 for the HA/SPI+PHTPP group, 2 sections per tissue from 3 different

(continued) patients. (h–k) Immunofluorescence images of day 7 post-injury tissues stained with DAPI (for nuclei) and anti-ER-β antibody. The white arrows indicate the edges of the new epithelial tongues. Scales are 1 mm.

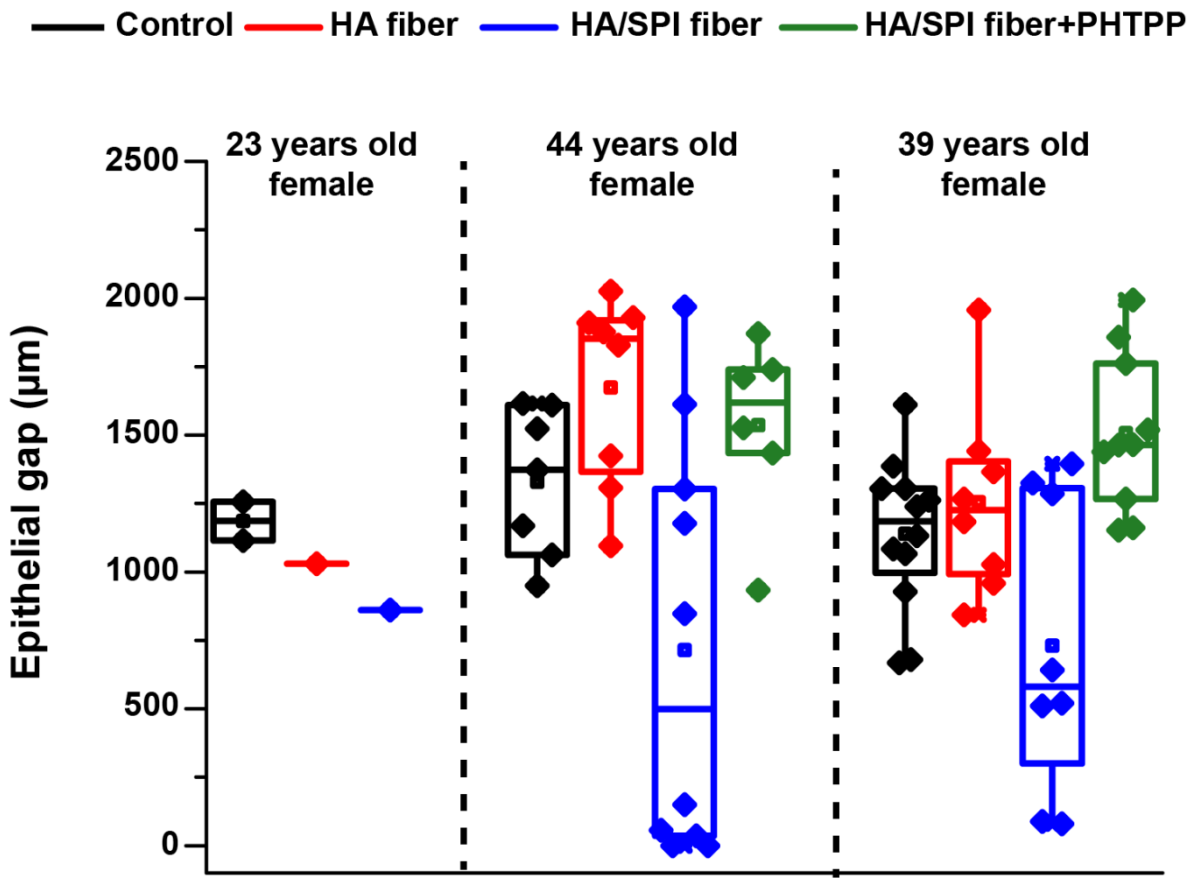

Figure 3-6. Age-dependent re-epithelialization in *ex vivo* human skin

Re-epithelialization analysis based on the same data set in Figure 3-5g, but separately plotted per each patient.

Moreover, we further analyzed re-epithelialization in human skin across the different ages of the donors. To this end, we separately plotted the data according to the ages of the donors (Figure 3-6). It was found that there was no difference in the tendency of re-epithelialization between the different ages, although there were not enough samples from the 23 years old female donor. This result is in a line with published results showing that re-epithelialization in *ex vivo* human skin model is barely affected by sex and age of the donor.[187]

3.3 Conclusions

In conclusion, the HA/SPI fibrous scaffold presented herein overcomes the limitations of current soy-based dressings that use suboptimal solvents (*e.g.,* toxic organic solvents) and co-spinning materials (*e.g.,* stiff and/or hydrophobic synthetic polymers derived from crude petroleum) as well as the lack of knowledge of the regenerative capacity in mouse and human skins via ER-β.[119] Our spinning platform enables us to engineer nanofiber scaffolds from water. In particular, water-soluble HA provides a biodegradable and water-absorbing fibrous architecture similar to that in native skin, making it an optimal backbone to develop high-throughput wound dressings. We affirmed that our scaffolds carry genistein to trigger the ER-β pathway. For the first time, we confirmed that HA/SPI scaffolds accelerate cutaneous reconstruction in both mouse and human skins via the ER-β pathway. We envision that HA/SPI fiber scaffolds can be used as a regenerative tissue construct for not only cutaneous wound healing but also ER-β-modulated diseases, such as breast cancer or cardiovascular diseases. Accordingly, our soy-based nanofiber fabrication approach opens new avenues for tissue engineering and regenerative medicine research.

3.4 Materials and Methods

3.4.1 Fiber Fabrication

Soy protein isolate (PRO-FAM® 974, ADM) and hyaluronic acid sodium salt (Sigma) were dissolved in deionized water (Invitrogen) and DMSO (Sigma) (6:1) solution with 10 mg/mL of sodium chloride (Sigma) and stirred overnight. The nanofibers were spun from the polymer solution by using iRJS as previously reported [68]. The polymer solution were injected at

a speed of 10 mL/min in to the reservoir and extruded through the orifices (with a diameter of 300 μm) into the precipitation bath (80 % ethanol) at 15,000 rpm. The precipitated fibers were collected on the rotating mandrel in the bath. The spun fibers were crosslinked with 10 mM EDC and 4mM NHS in 80% ethanol for 24 hrs on a shaker. The crosslinked fibers were washed by running DI water for 1 hr, frozen in DI water at -80 ºC, and freeze-dried using lyophilizer (SP Scientific) for further characterization and wound healing studies.

3.4.2 Scanning Electron Microscopy (SEM) and Fiber Analysis

The freeze-dried samples were mounted on SEM stubs and sputter-coated with Pt/Pd (Denton Vacuum) prior to imaging. The samples were then imaging by using a field emission scanning electron microscopy (FESEM, Carl Zeiss). The SEM images of fiber samples were used to calculate the fiber diameter and porosity in ImageJ (NIH) software with the plug-in DiameterJ.

3.4.3 Uniaxial Tensile Testing

The freeze-dried samples were loaded by using clamps and uniaxially pulled at a strain rate of 5 %/s up to 60 % strain in a tensile tester (CellScale). The data were recorded by using a built-in software (CellScale) and analyzed by using OriginPro 8.6 software (OriginLab).

3.4.4 Fourier-transform Infrared Spectroscopy (FTIR)

FTIR spectra of samples were obtained by using attenuated total reflectance (ATR)-FTIR (Bruker) in a range between 600 and 4000 cm^{-1} with 16 scans at a resolution of 2 cm^{-1}. The recorded data were normalized to C-O-C stretching peak of HA at around 1050 cm^{-1} by OriginPro 8.6 software.

3.4.5 Liquid Chromatography-mass Spectrometry (LC-MS)

LC-MS (Agilent) was utilized to quantify the amount of genistein within scaffolds. Samples were dissolved in DMSO, filtered with polytetrafluorethylene (PTFE) membranes (Pall Corporation), and loaded in the system. For the LC part, we used C18 LC column (ZORBAX RRHD C18) with a gradient of H_2O and acetonitrile (ACN) at a flow rate of 0.25 mL/min. The chromatographically separated molecules then underwent electrospray ionization (ESI) to detect the charged ions according to their molecular weights. The hydrogenized genistein ions ($[genistein+H]^+$) were detected at *m/z* 271 with the selected ion monitoring (SIM) mode. The chemical structure of genistein molecule in Fig. 2e was drawn by using ChemDraw software (PerkinElmer).

3.4.6 Biostability Test

Biostability of scaffolds were tested by submerging the scaffolds in PBS or a cell culture medium (Dulbecco's Modified Eagle's medium (DMEM, Thermo Fischer Scientific) in 6 well plates at 37 ºC and 5 % CO_2. We tracked the complete degradation time.

3.4.7 Mouse Excisional Wound Splinting Model

All animal experiments were approved by Harvard Institutional Animal Care and Use Committee (IACUC). As previously reported[159], we performed the mouse excisional splinting model to recapitulate human-mimetic healing processes in mouse by preventing wound contraction in mouse skin. In short, normal female mice (7 weeks old, C57BL/6, Charles River Laboratories) were fed by soy-free special diets (LabDiet 5V5R 50/IF, PMI® Nutrition International) and ovariectomized by manufacturers. After the ovariectomy surgery, mice were delivered and familiarized at the vivarium for a week. Following a week post ovariectomy surgery, wound clips were removed and mice recovered for a week before wound healing surgery. On the wound healing surgery day, isoflurane was used to anesthetize the mice during

all procedure. We shaved hairs on the dorsal side of mice by using electric razor and cleaned their skin with betadine (Santa Cruz Biotechnology) and 70% ethanol (v/v). The full thickness wounds were performed by using a 6-mm diameter sterile biopsy punch (Integra Miltex). Before the surgery, splinting rings were prepared from a silicon sheet (Grace Bio-Labs) by cutting 8 mm inner holes using a 8-mm sterile biopsy punch (Integra Miltex) and sterilized with 70% ethanol (v/v) and under UV light in a sterile cell culture hood. We applied the splinting rings to the wound site with an adhesive (Krazy glue) and sutures (Ethicon). Nanofiber scaffolds were placed to the wounds and secured with Tegaderm (Nexcare) patches. Control wounds got no treatment, but covered with Tegaderm. At day 20 post-injury, mice were scarified and skin tissues were harvested via IACUC approved protocols.

3.4.8 Human Skin Wound Model

Human skin biopsies with 2 mm wounds (NativeSkin®, Genoskin) were prepared by the manufacturer as previously reported[180]. Briefly, the skin biopsies were obtained from the abdomen of three different patients (23 years old, 44 years old, and 39 years old females), wounded with 2-mm diameter biopsy punch, and embedded within nourishing hydrogel in transwell inserts of 12 well plates at day 0. Upon overnight delivery, the human skin biopsies were incubated with dedicated culture medium for 1 h at 37 ºC, 5% CO_2, and humidity. Afterward, nanofiber scaffolds were cut with 2-mm diameter biopsy punch and applied to the wound sites. Control had no treatment. The skin biopsies were cultured for 7 days (the maximum possible culture time) by changing the culture medium daily. At day 7 post-injury, tissues were harvested. In an effort to specifically block ER β pathway in vitro, we added ER β antagonist (4-[2-Phenyl-5,7-bis(trifluoromethyl)pyrazolo[1,5-a]pyrimidin-3-yl]phenol, PHTPP, Sigma) to the culture medium. In particular, 10^{-2} M PHTPP stock solution was prepared in DMSO and 1 μL of

the stock solution was added to 1 mL of the culture medium per well, resulting in the final concentration of 10^{-5} M PHTPP in the culture medium that has been previously used in vitro[188]. To eliminate the effect of the vehicle (DMSO) on the healing processes, the same concentration of the vehicle solution was also added to the culture medium of all samples.

3.4.9 Histological Analysis of Skin Tissues

The harvested skin tissues were fixed by 4 % paraformaldehyde (PFA, v/v) in phosphate-buffered saline (PBS, Invitrogen) solution overnight at 4 ºC and washed by PBS 3 times. The fixed tissues were processed for paraffin embedding, sectioning, and Masson's trichrome staining at Harvard specialized histopathology core. We used slide scanner (Olympus VS120) to image the Masson's trichrome stained tissues. The Masson's trichrome images along with image J software were used to calculate epidermal thickness, scar index, and hair follicle regeneration for mouse skin as well as re-epithelialization for human skin. The epidermal thickness was analyzed by measuring the thickness of newly formed epithelial layers in the wound sites (μm). Following the previously established method[161], the scar index was measured by dividing the scarred area (μm^2) by the average dermal thickness (μm). We also quantified the reformation of hair follicles by dividing the number of hair follicles in the wound sites (counts) by the area of the wound sites (mm^2). The re-epithelialization was calculated by measuring distance among the edges of newly formed epithelial layers.

3.4.10 Immunofluorescent Analysis of Skin Tissues

The paraffin-processed sections were de-paraffinized washing the sections by xylene, a gradient of ethanol, and water sequentially. The de-praffinized sections were incubated with 5% bovine serum albumin (BSA, Jackson Immunoresearch) in PBS for 2 hrs at room temperature and then primary antibodies (anti-cytokeratin 14 (K14) and/or anti-ER β, Abcam) in 1% BSA in

PBS overnight at 4 ºC. After the primary antibody incubation, the samples were washed by PBS 3 times, followed by secondary antibody incubation (Alexa Fluor 488-conjugated anti-rabbit IgG (H+L) secondary antibody, Alexa Fluor 594-conjugated anti-mouse IgG (H+L) secondary antibody, and/or 4rse IgG (H+L) sephenylindole (DAPI), Thermo Fisher Scientific)) in 1% BSA in PBS for 1hr at room temperature. Subsequently, the samples were washed by PBS 3times and mounted with Prolong Gold anti-fade agent (Invitrogen) on glass coverslips. A spinning disc confocal microscope (Olympus ix83) was utilized to take the immunofluorescent images. For coverage analysis, the positively stained area in the wound sites were measured by using ImageJ software and divided by the area of the wounds.

3.4.11 Statistical Analysis

Mean ± standard error (SEM) was used to present all data in box plots with all data overlap. In the box plots, the edges, middle bars, and whiskers indicated 25^{th} and 75^{th} percentiles, median, 5^{th} and 95^{th} percentiles, respectively. One-way analysis of variance (ANOVA) with the post-hoc Tukey's test was used to assess the statistical difference among samples using OriginPro 8.6 software. *p value lower than 0.05 was counted statistically significant.

4 Conclusions

4.1 Engineering Biomimetic and Hydrating Plant-hybrid Nanofiber Dressing

In Chapter 1, we reviewed the current state of soy-based dressings. In particular, the use of synthetic polymers or animal-derived proteins in wound dressing development is a limiting factor.[4] Additionally, most synthetic polymers are hydrophobic and stiff, resulting in substandard physicochemical properties and healing performance.[128] Although animal proteins are effective in terms of healing outcomes,[2] due to their origin, they raise financial, ethical, and immunogenic concerns.[3]

In Chapter 2, we aimed to improve the dressing material and thus its performance by developing a plant-derived nanofiber scaffold using soy protein and cellulose acetate. Due to the fiber-forming capability of cellulose acetate, the resulting scaffold did not require additional materials or toxic crosslinkers. The plant-hybrid scaffold exhibited high hydrophilicity and high water retention due to the homogeneous distribution of hydrophilic soy protein compounds throughout the scaffold. *In vitro* dermal fibroblast studies showed that the scaffold promoted cell growth, migration, and infiltration. Additionally, the scaffold helped stimulate the expression of integrin β1, which is required for cell mobility and ECM remodeling.[155] The functionality of the scaffold was further confirmed *in vivo* using a mouse model of wound healing. We utilized an excisional mouse splinting model known as the "human-relevant mouse wound healing model" by preventing wound contraction in mice to mimic healing processes in humans with minimal wound contraction.[159] When tested with this mouse model, the scaffold accelerated wound

closure and re-epithelialization. Furthermore, the scaffold reduced collagen alignment and scar formation.

Collectively, these results revealed the potential of plant hybrid nanofiber dressings for enhanced wound healing. Nanofibers exhibited well-established microenvironmental cues (optimal fiber diameter, porosity, stiffness, and water absorption) were manufactured in a high-throughput manner. The resulting wound dressing costs approximately $1 per product with performance well compared to existing commercial dressings. Accordingly, we conclude that the questions discussed in Chapters 1.7.1 and 1.7.2 can be solved by the research described in Chapter 2. However, we still needed to elucidate the underlying ER-related mechanisms for high-quality (*e.g.*, hair regrowth) healing.

4.2 Biomimetic and Estrogenic Soy/Hyaluronic Acid Fiber Scaffold to Promote Skin Regeneration via Estrogen Receptor β

In Chapter 1, we noted that the effect of soy dressings on wound healing should be studied in greater detail.[8] Previous studies on soy-based dressings focused simply on protein content and healing outcomes mediated by the dressings. Although dressings enhanced re-epithelialization and granulation tissue formation in rodent and porcine models, additional outcomes such as hair follicle or cutaneous fat tissue regeneration should be explored in engineered or biopsied human skin to study long-term and cosmetic impacts. In Chapter 2, we introduced plant-hybrid scaffolds to effectively recapitulate the native microenvironment and to maintain a moist environment. Although our scaffold exhibited optimal physicochemical properties and enhanced wound healing, we did not fully elucidate how phytoestrogens in the scaffolds activate ER signaling pathways. In addition, HFIP was used to dissolve cellulose

acetate and soy protein prior to fiber spinning and is toxic. Thus, we explored alternative solvents for fiber spinning.

In Chapter 3, we hypothesized that biomimetic and estrogenic soy scaffolds will promote skin generation via the ER-β signaling pathway. In this study, water-soluble HA was used as a co-spun polymer to provide a structural cue because it is part of the native skin ECM network.[62] By using iRJS, we eliminated the use of toxic organic solvents (*e.g.*, HFIP).[68] In iRJS, the polymer solution (water/DMSO mixture in this case) was extruded at high centrifugal forces and then precipitated into an 80% ethanol bath, resulting in microfibers composed of nanofibrils similar to native collagen fiber bundles. A small portion of DMSO was added to the water solvent to completely dissolve soy phytoestrogens that are partially soluble in pure water. As a result, the fiber scaffold possessed soy protein components (confirmed by FT-IR) and soy phytoestrogens (*e.g.,* genistein; confirmed by LC-MS). The genistein level was quantified because it is one of the main phytoestrogens known to provide health benefits.

Due to these beneficial properties, we aimed to investigate healing outcomes. To test our hypothesis, we again used an excisional mouse splitting model that enables us to study human-relevant healing in mice.[159] To observe healing results, we monitored the mice longer (20 days) than that of common wound healing studies (14 days). In particular, hair follicle regeneration was examined because hair follicles do not regenerate in normal mouse and human wound healing. Moreover, hair follicles are important for skin function and cosmetics.[8] In addition, recent preclinical and clinical studies showed that oral and topical administration of soy phytoestrogens can initiate hair regrowth,[78, 79] although the ER-related mechanism underlying enhanced hair reformation remains unexplored. Soy-based scaffolds promoted both hair follicle

and ER-β expression as well as re-epithelialization and dermal ECM remodeling in a mouse model.

Although mouse wound model can help elucidate the healing outcomes of our scaffolds, it is unable to fully recapitulate the physiological healing capability of human skin.[180] Accordingly, we sought to explore the effects of our scaffolds on human skin using a commercially available human skin biopsy wound model. The 2-mm wounds were treated with our scaffolds and harvested at day 7 post-injury for histological analysis. We found that soy-based scaffolds accelerated re-epithelialization in human skins. After treatment with an ER-β antagonist, enhanced re-epithelialization by our scaffolds was not observed. These data confirmed that our soy-based scaffolds promote wound healing in human skin via the ER-β pathway.

4.3 Limitations and Future Directions

This dissertation has demonstrated the development of biomimetic and estrogenic soy-based nanofiber scaffolds for enhanced skin regeneration via the ER-β pathway. Notably, there are some limitations for future applications. In this study, we focused only on the ER-β pathway. Although soy phytoestrogens were reported to preferentially activate ER-β, the effect of our soy-based scaffolds on wound healing via the ER-α pathway should be investigated. Furthermore, the binding affinity of the scaffolds for both ER-α and ER-β should be studied to alleviate the potential risk of ER-α-positive diseases. More importantly, due to nature of human skin wound models, we could only study short-term healing effects of our scaffolds in human skin. Therefore, long-term and advanced healing outcomes (*e.g.,* hair follicle and adipose tissue reconstruction) by our scaffolds in human skin should be explored.

Additionally, future studies can expand the use of our scaffolds as ER-β-modulators in different diseases. For example, soy phytoestrogens were shown to prevent ischemic diseases and breast cancer.[189] Therefore, our scaffolds can be used to partially replace damaged tissues or to prevent the progression of carcinogenic cells. For this purpose, fibers can be collected onto a premade mandrel with the 3D morphology of the target tissue. Similarly, solutions for fiber spinning can potentially be used for 3D printing organ-level constructs.

4.4 Funding Sources

This work was funded by the Wyss Institute for Biologically Inspired Engineering at Harvard University. I received Fulbright Scholarship (Fulbright Foreign Student Program for 2014–2015) from the U.S. Department of State to accomplish this research. This research was supported by the Harvard University Materials Research Science and Engineering Center (MRSEC), NSF Award No. DMR-1420570. This research was also performed in part at the Center for Nanoscale Systems (CNS), a member of the National Nanotechnology Infrastructure Network (NNIN), which is supported by the National Science Foundation under NSF award no. 1541959. CNS is part of Harvard University. This study was partly supported by the Harvard University Materials Research Science and Engineering Center (MRSEC), NSF Award No. DMR-1420570. We thank Dana-Farber/Harvard Cancer Center in Boston, MA, for the use of the Specialized Histopathology Core, which provided tissue preparation and histology staining services. Dana-Farber/Harvard Cancer Center is supported in part by an NCI Cancer Center Support Grant # NIH 5 P30 CA06516. I thank the Neurobiology Department and the Neurobiology Imaging Facility for consultation and instrument availability that supported this work. This facility is supported in part by the Neural Imaging Center as part of an NINDS P30

Core Center grant #NS072030. I also appreciate the graphic works provided by Su-Yeon Choi and Michael Rosnach.

5 Bibliography

1. Martin P. Wound healing--aiming for perfect skin regeneration. *Science*. 1997;276:75-81

2. Gurtner GC, Werner S, Barrandon Y, Longaker MT. Wound repair and regeneration. *Nature*. 2008;453:314-321

3. Lutolf MP, Gilbert PM, Blau HM. Designing materials to direct stem-cell fate. *Nature*. 2009;462:433

4. Tansaz S, Boccaccini AR. Biomedical applications of soy protein: A brief overview. *J. Biomed. Mater. Res., Part A*. 2016;104:553-569

5. Cederroth CR, Nef S. Soy, phytoestrogens and metabolism: A review. *Mol. Cell. Endocrinol.* 2009;304:30-42

6. Ohyama M. Hair follicle bulge: A fascinating reservoir of epithelial stem cells. *J. Dermatol. Sci.* 2007;46:81-89

7. Frantz C, Stewart KM, Weaver VM. The extracellular matrix at a glance. *J. Cell Sci.* 2010;123:4195-4200

8. Plikus MV, Guerrero-Juarez CF, Ito M, Li YR, Dedhia PH, Zheng Y, Shao M, Gay DL, Ramos R, Hsi T-C. Regeneration of fat cells from myofibroblasts during wound healing. *Science*. 2017;355:748-752

9. Tonnesen MG, Feng X, Clark RA. Angiogenesis in wound healing. *J. Investig. Dermatol. Symp. Proc*. 2000;5:40-46

10. Zhong S, Zhang Y, Lim C. Tissue scaffolds for skin wound healing and dermal reconstruction. *Wiley Interdiscip. Rev.: Nanomed. Nanobiotechnol.* 2010;2:510-525

11. Clark RA. Fibrin and wound healing. *Ann. N. Y. Acad. Sci.* 2001;936:355-367

12. Singer AJ, Clark RA. Cutaneous wound healing. *N. Engl. J. Med.* 1999;341:738-746

13. Guo L, Degenstein L, Fuchs E. Keratinocyte growth factor is required for hair development but not for wound healing. *Genes Dev.* 1996;10:165-175

14. Rosenquist TA, Martin GR. Fibroblast growth factor signalling in the hair growth cycle: Expression of the fibroblast growth factor receptor and ligand genes in the murine hair follicle. *Dev. Dyn.* 1996;205:379-386

15. Parker KK, Ingber DE. Extracellular matrix, mechanotransduction and structural hierarchies in heart tissue engineering. *Philos. Trans. Royal Soc. B*. 2007;362:1267-1279

16. Geiger B, Bershadsky A, Pankov R, Yamada KM. Transmembrane crosstalk between the extracellular matrix and the cytoskeleton. *Nat. Rev. Mol. Cell Biol*. 2001;2:793-805

17. Hynes RO. The extracellular matrix: Not just pretty fibrils. *Science*. 2009;326:1216-1219

18. Capulli A, MacQueen L, Sheehy SP, Parker K. Fibrous scaffolds for building hearts and heart parts. *Adv. Drug Del. Rev.* 2016;96:83-102

19. Pham QP, Sharma U, Mikos AG. Electrospinning of polymeric nanofibers for tissue engineering applications: A review. *Tissue Eng*. 2006;12:1197-1211

20. Cui W, Zhou Y, Chang J. Electrospun nanofibrous materials for tissue engineering and drug delivery. *Sci. Technol. Adv. Mater*. 2010;11

21. Hennink WE, van Nostrum CF. Novel crosslinking methods to design hydrogels. *Adv. Drug Del. Rev.* 2012;64:223-236

22. Ahn S, Chantre CO, Gannon AR, Lind JU, Campbell PH, Grevesse T, O'Connor BB, Parker KK. Soy protein/cellulose nanofiber scaffolds mimicking skin extracellular matrix for enhanced wound healing. *Adv. Healthcare Mater.* 2018;7:e1701175

23. Li D, Xia Y. Electrospinning of nanofibers: Reinventing the wheel? *Adv. Mater.* 2004;16:1151-1170

24. Deravi LF, Sinatra NR, Chantre CO, Nesmith AP, Yuan H, Deravi SK, Goss JA, MacQueen LA, Badrossamy MR, Gonzalez GM. Design and fabrication of fibrous nanomaterials using pull spinning. *Macromol. Mater. Eng.* 2017;302

25. Badrossamay MR, McIlwee HA, Goss JA, Parker KK. Nanofiber assembly by rotary jet-spinning. *Nano Lett.* 2010;10:2257-2261

26. Ahn S, Ardoña HAM, Lind JU, Eweje F, Kim SL, Gonzalez GM, Liu Q, Zimmerman JF, Pyrgiotakis G, Zhang Z. Mussel-inspired 3d fiber scaffolds for heart-on-a-chip toxicity studies of engineered nanomaterials. *Anal. Bioanal. Chem.* 2018:1-14

27. Hodgkinson T, Yuan X-F, Bayat A. Electrospun silk fibroin fiber diameter influences in vitro dermal fibroblast behavior and promotes healing of ex vivo wound models. *J. Tissue Eng.* 2014;5:2041731414551661

28. Lowery JL, Datta N, Rutledge GC. Effect of fiber diameter, pore size and seeding method on growth of human dermal fibroblasts in electrospun poly (ε-caprolactone) fibrous mats. *Biomaterials*. 2010;31:491-504

29. Agache P, Monneur C, Leveque J, De Rigal J. Mechanical properties and young's modulus of human skin in vivo. *Arch. Dermatol. Res.* 1980;269:221-232

30. Liang X, Boppart SA. Biomechanical properties of in vivo human skin from dynamic optical coherence elastography. *IEEE Trans. Biomed. Eng.* 2010;57:953-959

31. Kuwazuru O, Saothong J, Yoshikawa N. Mechanical approach to aging and wrinkling of human facial skin based on the multistage buckling theory. *Med. Eng. Phys.* 2008;30:516-522

32. Pailler-Mattei C, Bec S, Zahouani H. In vivo measurements of the elastic mechanical properties of human skin by indentation tests. *Med. Eng. Phys.* 2008;30:599-606

33. Pan J-f, Liu N-h, Sun H, Xu F. Preparation and characterization of electrospun plcl/poloxamer nanofibers and dextran/gelatin hydrogels for skin tissue engineering. *PLoS One*. 2014;9:e112885

34. Chung T-W, Liu D-Z, Wang S-Y, Wang S-S. Enhancement of the growth of human endothelial cells by surface roughness at nanometer scale. *Biomaterials*. 2003;24:4655-4661

35. Xu C, Yang F, Wang S, Ramakrishna S. In vitro study of human vascular endothelial cell function on materials with various surface roughness. *J. Biomed. Mater. Res., Part A*. 2004;71:154-161

36. Yoo HS, Kim TG, Park TG. Surface-functionalized electrospun nanofibers for tissue engineering and drug delivery. *Adv. Drug Del. Rev.* 2009;61:1033-1042

37. Boateng JS, Matthews KH, Stevens HN, Eccleston GM. Wound healing dressings and drug delivery systems: A review. *J. Pharm. Sci.* 2008;97:2892-2923

38. Zahedi P, Rezaeian I, Ranaei-Siadat SO, Jafari SH, Supaphol P. A review on wound dressings with an emphasis on electrospun nanofibrous polymeric bandages. *Polym. Adv. Technol.* 2010;21:77-95

39. Jin G, Prabhakaran MP, Kai D, Annamalai SK, Arunachalam KD, Ramakrishna S. Tissue engineered plant extracts as nanofibrous wound dressing. *Biomaterials*. 2013;34:724-734

40. Abrigo M, McArthur SL, Kingshott P. Electrospun nanofibers as dressings for chronic wound care: Advances, challenges, and future prospects. *Macromol. Biosci.* 2014;14:772-792

41. Werner S, Grose R. Regulation of wound healing by growth factors and cytokines. *Physiol. Rev.* 2003;83:835-870

42. Ashcroft GS, Dodsworth J, vAN BoxTEL E, Tarnuzzer RW, Horan MA, Schultz GS, Ferguson MW. Estrogen accelerates cutaneous wound healing associated with an increase in tgf-β1 levels. *Nat. Med.* 1997;3:1209-1215

43. Emmerson E, Campbell L, Ashcroft GS, Hardman MJ. The phytoestrogen genistein promotes wound healing by multiple independent mechanisms. *Mol. Cell. Endocrinol.* 2010;321:184-193

44. Wigger-Alberti W, Kuhlmann M, Ekanayake S, Wilhelm D, Buettner H, Callaghan T, Wilhelm K. Using a novel wound model to investigate the healing properties of products for superficial wounds. *J Wound Care*. 2009;18

45. Kamoun EA, Kenawy E-RS, Chen X. A review on polymeric hydrogel membranes for wound dressing applications: Pva-based hydrogel dressings. *J. Adv. Res.* 2017;8:217-233

46. Sarikaya A, Record R, Wu C-C, Tullius B, Badylak S, Ladisch M. Antimicrobial activity associated with extracellular matrices. *Tissue Eng.* 2002;8:63-71

47. Dvir T, Timko BP, Kohane DS, Langer R. Nanotechnological strategies for engineering complex tissues. *Nat. Nanotechnol.* 2011;6:13

48. Griffith LG, Naughton G. Tissue engineering--current challenges and expanding opportunities. *Science*. 2002;295:1009-1014

49. Ma PX. Biomimetic materials for tissue engineering. *Adv. Drug Del. Rev.* 2008;60:184-198

50. Badrossamay MR, Balachandran K, Capulli AK, Golecki HM, Agarwal A, Goss JA, Kim H, Shin K, Parker KK. Engineering hybrid polymer-protein super-aligned nanofibers via rotary jet spinning. *Biomaterials*. 2014;35:3188-3197

51. Toncheva A, Spasova M, Paneva D, Manolova N, Rashkov I. Polylactide (pla)-based electrospun fibrous materials containing ionic drugs as wound dressing materials: A review. *Int J Polym Mater.* 2014;63:657-671

52. Athanasiou KA, Niederauer GG, Agrawal CM. Sterilization, toxicity, biocompatibility and clinical applications of polylactic acid/polyglycolic acid copolymers. *Biomaterials*. 1996;17:93-102

53. Yoshii F, Zhanshan Y, Isobe K, Shinozaki K, Makuuchi K. Electron beam crosslinked peo and peo/pva hydrogels for wound dressing. *Radiat. Phys. Chem.* 1999;55:133-138

54. Chau DY, Collighan RJ, Verderio EA, Addy VL, Griffin M. The cellular response to transglutaminase-cross-linked collagen. *Biomaterials*. 2005;26:6518-6529

55. Wissink M, Beernink R, Pieper J, Poot AA, Engbers G, Beugeling T, Van Aken W, Feijen J. Immobilization of heparin to edc/nhs-crosslinked collagen. Characterization and in vitro evaluation. *Biomaterials*. 2001;22:151-163

56. Zeugolis DI, Khew ST, Yew ES, Ekaputra AK, Tong YW, Yung L-YL, Hutmacher DW, Sheppard C, Raghunath M. Electro-spinning of pure collagen nano-fibres–just an expensive way to make gelatin? *Biomaterials*. 2008;29:2293-2305

57. Chan G, Mooney DJ. New materials for tissue engineering: Towards greater control over the biological response. *Trends Biotechnol.* 2008;26:382-392

58. Gorgieva S, Kokol V. Collagen-vs. Gelatine-based biomaterials and their biocompatibility: Review and perspectives. *J Biomater Appl*. InTech; 2011.

59. Zhang F, Xu S, Wang Z. Pre-treatment optimization and properties of gelatin from freshwater fish scales. *Food Bioprod. Process.* 2011;89:185-193

60. Hassiba AJ, El Zowalaty ME, Nasrallah GK, Webster TJ, Luyt AS, Abdullah AM, Elzatahry AA. Review of recent research on biomedical applications of electrospun polymer nanofibers for improved wound healing. *Nanomedicine*. 2016

61. Ahn S, Deravi LF, Park SJ, Dabiri BE, Kim JS, Parker KK, Shin K. Self-organizing large-scale extracellular-matrix protein networks. *Adv. Mater.* 2015;27:2838-2845

62. Larson BJ, Longaker MT, Lorenz HP. Scarless fetal wound healing: A basic science review. *J Plast Reconstr Surg Nurs*. 2010;126:1172

63. Chantre CO, Campbell PH, Golecki HM, Buganza AT, Capulli AK, Deravi LF, Dauth S, Sheehy SP, Paten JA, Gledhill K. Production-scale fibronectin nanofibers promote wound closure and tissue repair in a dermal mouse model. *Biomaterials*. 2018;166:96-108

64. Reddy N, Yang Y. Potential of plant proteins for medical applications. *Trends Biotechnol.* 2011;29:490-498

65. Liu W, Burdick JA, van Osch GJ. Plant-derived recombinant human collagen: A strategic approach for generating safe human ecm-based scaffold. *Tissue Eng., Part A*. 2013;19:1489-1490

66. Han SO, Youk JH, Min KD, Kang YO, Park WH. Electrospinning of cellulose acetate nanofibers using a mixed solvent of acetic acid/water: Effects of solvent composition on the fiber diameter. *Mater. Lett.* 2008;62:759-762

67. Rowley JA, Madlambayan G, Mooney DJ. Alginate hydrogels as synthetic extracellular matrix materials. *Biomaterials*. 1999;20:45-53

68. Gonzalez GM, MacQueen LA, Lind JU, Fitzgibbons SA, Chantre CO, Huggler I, Golecki HM, Goss JA, Parker KK. Production of synthetic, para-aramid and biopolymer nanofibers by immersion rotary jet-spinning. *Macromol. Mater. Eng.* 2017;302

69. da Cunha CB, Klumpers DD, Li WA, Koshy ST, Weaver JC, Chaudhuri O, Granja PL, Mooney DJ. Influence of the stiffness of three-dimensional alginate/collagen-i interpenetrating networks on fibroblast biology. *Biomaterials*. 2014;35:8927-8936

70. Cullen B, Watt PW, Lundqvist C, Silcock D, Schmidt RJ, Bogan D, Light ND. The role of oxidised regenerated cellulose/collagen in chronic wound repair and its potential mechanism of action. *Int. J. Biochem. Cell Biol*. 2002;34:1544-1556

71. Opasanon S, Muangman P, Namviriyachote N. Clinical effectiveness of alginate silver dressing in outpatient management of partial-thickness burns. *Int Wound J*. 2010;7:467-471

72. Zhang X, Shu XO, Gao Y-T, Yang G, Li Q, Li H, Jin F, Zheng W. Soy food consumption is associated with lower risk of coronary heart disease in chinese women. *J. Nutr*. 2003;133:2874-2878

73. Potter SM, Baum JA, Teng H, Stillman RJ, Shay NF, Erdman J. Soy protein and isoflavones: Their effects on blood lipids and bone density in postmenopausal women. *Am. J. Clin. Nutr.* 1998;68:1375S-1379S

74. Sacks FM, Lichtenstein A, Van Horn L, Harris W, Kris-Etherton P, Winston M. Soy protein, isoflavones, and cardiovascular health. *Circulation*. 2006;113:1034-1044

75. Messina M. Soy and health update: Evaluation of the clinical and epidemiologic literature. *Nutrients*. 2016;8:754

76. Izumi T, Saito M, Obata A, Arii M, Yamaguchi H, Matsuyama A. Oral intake of soy isoflavone aglycone improves the aged skin of adult women. *J. Nutr. Sci. Vitaminol.* 2007;53:57-62

77. Jenkins G, Wainwright L, Holland R, Barrett K, Casey J. Wrinkle reduction in post-menopausal women consuming a novel oral supplement: A double-blind placebo-controlled randomized study. *Int. J. Cosmet. Sci.* 2014;36:22-31

78. Harada N, Okajima K, Arai M, Kurihara H, Nakagata N. Administration of capsaicin and isoflavone promotes hair growth by increasing insulin-like growth factor-i production in mice and in humans with alopecia. *Growth Horm IGF Res*. 2007;17:408-415

79. Zhao J, Harada N, Kurihara H, Nakagata N, Okajima K. Dietary isoflavone increases insulin-like growth factor-i production, thereby promoting hair growth in mice. *J. Nutr. Biochem.* 2011;22:227-233

80. Babajafari S, Akhlaghi M, Mazloomi SM, Ayaz M, Noorafshan A, Jafari P, Hojhabrimanesh A. The effect of isolated soy protein adjunctive with flaxseed oil on markers of inflammation, oxidative stress, acute phase proteins, and wound healing of burn patients; a randomized clinical trial. *Burns*. 2017

81. Grinnell F. Fibroblast–collagen-matrix contraction: Growth-factor signalling and mechanical loading. *Trends Cell Biol.* 2000;10:362-365

82. Sorrell JM, Caplan AI. Fibroblast heterogeneity: More than skin deep. *J. Cell Sci.* 2004;117:667-675

83. Eming SA, Martin P, Tomic-Canic M. Wound repair and regeneration: Mechanisms, signaling, and translation. *Sci. Transl. Med.* 2014;6:265sr266-265sr266

84. Greenwel P, Inagaki Y, Hu W, Walsh M, Ramirez F. Sp1 is required for the early response of α2 (i) collagen to transforming growth factor-β1. *J. Biol. Chem.* 1997;272:19738-19745

85. Eckes B, Zigrino P, Kessler D, Holtkötter O, Shephard P, Mauch C, Krieg T. Fibroblast-matrix interactions in wound healing and fibrosis. *Matrix Biol.* 2000;19:325-332

86. Leask A, Abraham DJ. Tgf-β signaling and the fibrotic response. *FASEB J.* 2004;18:816-827

87. Horstmeyer A, Licht C, Scherr G, Eckes B, Krieg T. Signalling and regulation of collagen i synthesis by et-1 and tgf-β1. *FEBS J.* 2005;272:6297-6309

88. Barrientos S, Stojadinovic O, Golinko MS, Brem H, Tomic-Canic M. Growth factors and cytokines in wound healing. *Wound Repair Regen*. 2008;16:585-601

89. Huang C, Fu X, Liu J, Qi Y, Li S, Wang H. The involvement of integrin β1 signaling in the migration and myofibroblastic differentiation of skin fibroblasts on anisotropic collagen-containing nanofibers. *Biomaterials*. 2012;33:1791-1800

90. Xiao L, Du Y, Shen Y, He Y, Zhao H, Li Z. Tgf-beta 1 induced fibroblast proliferation is mediated by the fgf-2/erk pathway. *Front Biosci*. 2012;17:2667-2674

91. Sriram G, Bigliardi PL, Bigliardi-Qi M. Fibroblast heterogeneity and its implications for engineering organotypic skin models in vitro. *Eur. J. Cell Biol.* 2015;94:483-512

92. Schultz GS, Ladwig G, Wysocki A. Extracellular matrix: Review of its roles in acute and chronic wounds. *World Wide Wounds*. 2005;2005:1-18

93. Tokudome Y, Nakamura K, Kage M, Todo H, Sugibayashi K, Hashimoto F. Effects of soybean peptide and collagen peptide on collagen synthesis in normal human dermal fibroblasts. *Int. J. Food Sci. Nutr.* 2012;63:689-695

94. Romano NH, Sengupta D, Chung C, Heilshorn SC. Protein-engineered biomaterials: Nanoscale mimics of the extracellular matrix. *Biochim Biophys Acta Gen Subj*. 2011;1810:339-349

95. Ascenzi P, Bocedi A, Marino M. Structure–function relationship of estrogen receptor α and β: Impact on human health. *Mol. Aspects Med.* 2006;27:299-402

96. Ashcroft GS, Dodsworth J, Van Boxtel E, Tarnuzzer RW, Horan MA, Schultz GS, Ferguson MWJ. Estrogen accelerates cutaneous wound healing associated with an increase in tgf-β1 levels. *Nat. Med.* 1997;3:1209

97. Moolman JA. Unravelling the cardioprotective mechanism of action of estrogens. *Cardiovasc. Res.* 2006;69:777-780

98. Zanella I, Marrazzo E, Biasiotto G, Penza M, Romani A, Vignolini P, Caimi L, Di Lorenzo D. Soy and the soy isoflavone genistein promote adipose tissue development in male mice on a low-fat diet. *Eur. J. Nutr.* 2015;54:1095-1107

99. Curt S, Subirade M, Rouabhia M. Production and in vitro evaluation of soy protein–based biofilms as a support for human keratinocyte and fibroblast culture. *Tissue Eng., Part A*. 2008;15:1223-1232

100. Koh TJ, DiPietro LA. Inflammation and wound healing: The role of the macrophage. *Expert Rev Mol Med*. 2011;13

101. Chien KB, Shah RN. Novel soy protein scaffolds for tissue regeneration: Material characterization and interaction with human mesenchymal stem cells. *Acta Biomater.* 2012;8:694-703

102. Shevchenko RV, Santin M. Pre-clinical evaluation of soybean-based wound dressings and dermal substitute formulations in pig healing and non-healing in vivo models. *Burns Trauma*. 2014;2:187

103. Chien KB, Makridakis E, Shah RN. Three-dimensional printing of soy protein scaffolds for tissue regeneration. *Tissue Eng., Part C*. 2012;19:417-426

104. Xu X, Jiang L, Zhou Z, Wu X, Wang Y. Preparation and properties of electrospun soy protein isolate/polyethylene oxide nanofiber membranes. *ACS Appl. Mater. Interfaces*. 2012;4:4331-4337

105. Lin L, Perets A, Har-el Ye, Varma D, Li M, Lazarovici P, Woerdeman DL, Lelkes PI. Alimentary 'green'proteins as electrospun scaffolds for skin regenerative engineering. *J. Tissue. Eng. Regen. Med.* 2013;7:994-1008

106. Thirugnanaselvam M, Gobi N, Karthick SA. Spi/peo blended electrospun martrix for wound healing. *Fibers Polym.* 2013;14:965-969

107. Sett S, Lee MW, Weith M, Pourdeyhimi B, Yarin A. Biodegradable and biocompatible soy protein/polymer/adhesive sticky nano-textured interfacial membranes for prevention of esca fungi invasion into pruning cuts and wounds of vines. *J. Mater. Chem. B*. 2015;3:2147-2162

108. Uppal R, Ramaswamy GN, Arnold C, Goodband R, Wang Y. Hyaluronic acid nanofiber wound dressing—production, characterization, and in vivo behavior. *J. Biomed. Mater. Res., Part B*. 2011;97:20-29

109. Chong BF, Blank LM, Mclaughlin R, Nielsen LK. Microbial hyaluronic acid production. *Appl. Microbiol. Biotechnol.* 2005;66:341-351

110. Murphy SV, Atala A. 3d bioprinting of tissues and organs. *Nat. Biotechnol.* 2014;32:773

111. Marini H, Polito F, Altavilla D, Irrera N, Minutoli L, Calo M, Adamo E, Vaccaro M, Squadrito F, Bitto A. Genistein aglycone improves skin repair in an incisional model of

wound healing: A comparison with raloxifene and oestradiol in ovariectomized rats. *Br. J. Pharmacol.* 2010;160:1185-1194

112. Wang C-C, Prasain JK, Barnes S. Review of the methods used in the determination of phytoestrogens. *J. Chromatogr. B*. 2002;777:3-28

113. MacQueen LA, Sheehy SP, Chantre CO, Zimmerman JF, Pasqualini FS, Liu X, Goss JA, Campbell PH, Gonzalez GM, Park S-J. A tissue-engineered scale model of the heart ventricle. *Nat Biomed Eng*. 2018:1

114. Benam KH, Dauth S, Hassell B, Herland A, Jain A, Jang K-J, Karalis K, Kim HJ, MacQueen L, Mahmoodian R. Engineered in vitro disease models. *Annu Rev Pathol*. 2015;10:195-262

115. Setchell KD. Soy isoflavones—benefits and risks from nature's selective estrogen receptor modulators (serms). *J. Am. Coll. Nutr.* 2001;20:354S-362S

116. Mendelsohn ME, Karas RH. The protective effects of estrogen on the cardiovascular system. *N. Engl. J. Med.* 1999;340:1801-1811

117. Hall G, Phillips TJ. Estrogen and skin: The effects of estrogen, menopause, and hormone replacement therapy on the skin. *J. Am. Acad. Dermatol.* 2005;53:555-568

118. Ashcroft GS, Dodsworth J, Van Boxtel E, Tarnuzzer R, Horan MA, Schultz GS, Ferguson M. Estrogen accelerates cutaneous wound healing associated with an increase in tgf-b1 levels. *Nat. Med.* 1997;3:1209-1215

119. Santin M, Ambrosio L. Soybean-based biomaterials: Preparation, properties and tissue regeneration potential. *Expert Rev. Med. Devices*. 2008;5:349-358

120. Lee J, Roh K-B, Kim S-C, Lee J, Park D. Soy peptide-induced stem cell proliferation: Involvement of erk and tgf-β1. *J. Nutr. Biochem.* 2012;23:1341-1351

121. Gerstenhaber JA, Brodsky R, Huneke RB, Lelkes PI. Electrospun soy protein scaffolds as wound dressings: Enhanced reepithelialization in a porcine model of wound healing. *Wound Medicine*. 2014;5:9-15

122. Sirotkin AV, Harrath AH. Phytoestrogens and their effects. *Eur. J. Pharmacol.* 2014;741:230-236

123. Hsia SY, Hsiao YH, Li WT, Hsieh JF. Aggregation of soy protein-isoflavone complexes and gel formation induced by glucono-delta-lactone in soymilk. *Sci. Rep.* 2016;6:35718

124. Hong H, Landauer MR, Foriska MA, Ledney GD. Antibacterial activity of the soy isoflavone genistein. *J. Basic Microbiol.* 2006;46:329-335

125. Ben Arfa A, Preziosi-Belloy L, Chalier P, Gontard N. Antimicrobial paper based on a soy protein isolate or modified starch coating including carvacrol and cinnamaldehyde. *J. Agric. Food Chem.* 2007;55:2155-2162

126. Chacko BK, Chandler RT, Mundhekar A, Khoo N, Pruitt HM, Kucik DF, Parks DA, Kevil CG, Barnes S, Patel RP. Revealing anti-inflammatory mechanisms of soy isoflavones by flow: Modulation of leukocyte-endothelial cell interactions. *Am. J. Physiol. Heart Circ. Physiol.* 2005;289:H908-H915

127. Peñta-Ramos E, Xiong Y. Antioxidant activity of soy protein hydrolysates in a liposomal system. *J. Food Sci.* 2002;67:2952-2956

128. Rieger KA, Birch NP, Schiffman JD. Designing electrospun nanofiber mats to promote wound healing–a review. *J. Mater. Chem. B*. 2013;1:4531-4541

129. Kumbar S, James R, Nukavarapu S, Laurencin C. Electrospun nanofiber scaffolds: Engineering soft tissues. *Biomed. Mater.* 2008;3:034002

130. Sell SA, Wolfe PS, Garg K, McCool JM, Rodriguez IA, Bowlin GL. The use of natural polymers in tissue engineering: A focus on electrospun extracellular matrix analogues. *Polymers*. 2010;2:522-553

131. Place ES, George JH, Williams CK, Stevens MM. Synthetic polymer scaffolds for tissue engineering. *Chem. Soc. Rev.* 2009;38:1139-1151

132. Peng YY, Glattauer V, Ramshaw JA, Werkmeister JA. Evaluation of the immunogenicity and cell compatibility of avian collagen for biomedical applications. *J. Biomed. Mater. Res., Part A*. 2010;93:1235-1244

133. Liu W, Burdick JA, van Osch GJ. Plant-derived recombinant human collagen: A strategic approach for generating safe human ecm-based scaffold. *Tissue Eng., Part A*. 2013;19:1489-1490

134. Li WJ, Laurencin CT, Caterson EJ, Tuan RS, Ko FK. Electrospun nanofibrous structure: A novel scaffold for tissue engineering. *J. Biomed. Mater. Res., Part A*. 2002;60:613-621

135. Sinha-Ray S, Zhang Y, Yarin A, Davis S, Pourdeyhimi B. Solution blowing of soy protein fibers. *Biomacromolecules*. 2011;12:2357-2363

136. Lee KY, Jeong L, Kang YO, Lee SJ, Park WH. Electrospinning of polysaccharides for regenerative medicine. *Adv. Drug Delivery Rev.* 2009;61:1020-1032

137. Miao J, Pangule RC, Paskaleva EE, Hwang EE, Kane RS, Linhardt RJ, Dordick JS. Lysostaphin-functionalized cellulose fibers with antistaphylococcal activity for wound healing applications. *Biomaterials*. 2011;32:9557-9567

138. Rodríguez K, Gatenholm P, Renneckar S. Electrospinning cellulosic nanofibers for biomedical applications: Structure and in vitro biocompatibility. *Cellulose*. 2012;19:1583-1598

139. Huang R, Li W, Lv X, Lei Z, Bian Y, Deng H, Wang H, Li J, Li X. Biomimetic lbl structured nanofibrous matrices assembled by chitosan/collagen for promoting wound healing. *Biomaterials*. 2015;53:58-75

140. Mellado P, McIlwee HA, Badrossamay MR, Goss JA, Mahadevan L, Parker KK. A simple model for nanofiber formation by rotary jet-spinning. *Appl. Phys. Lett.* 2011;99:203107

141. Golecki HM, Yuan H, Glavin C, Potter B, Badrossamay MR, Goss JA, Phillips MD, Parker KK. Effect of solvent evaporation on fiber morphology in rotary jet spinning. *Langmuir*. 2014;30:13369-13374

142. Capulli AK, Emmert MY, Pasqualini FS, Kehl D, Caliskan E, Lind JU, Sheehy SP, Park SJ, Ahn S, Weber B. Jetvalve: Rapid manufacturing of biohybrid scaffolds for biomimetic heart valve replacement. *Biomaterials*. 2017;133:229-241

143. Achouri A, Zhang W, Shiying X. Enzymatic hydrolysis of soy protein isolate and effect of succinylation on the functional properties of resulting protein hydrolysates. *Food Res. Int.* 1998;31:617-623

144. Huang Z-M, Zhang Y-Z, Kotaki M, Ramakrishna S. A review on polymer nanofibers by electrospinning and their applications in nanocomposites. *Compos. Sci. Technol.* 2003;63:2223-2253

145. Discher DE, Janmey P, Wang Y-l. Tissue cells feel and respond to the stiffness of their substrate. *Science*. 2005;310:1139-1143

146. Wells RG. The role of matrix stiffness in regulating cell behavior. *Hepatology*. 2008;47:1394-1400

147. Hutmacher DW. Scaffolds in tissue engineering bone and cartilage. *Biomaterials*. 2000;21:2529-2543

148. Xue J, He M, Liu H, Niu Y, Crawford A, Coates PD, Chen D, Shi R, Zhang L. Drug loaded homogeneous electrospun pcl/gelatin hybrid nanofiber structures for anti-infective tissue regeneration membranes. *Biomaterials*. 2014;35:9395-9405

149. Hu J, Prabhakaran MP, Tian L, Ding X, Ramakrishna S. Drug-loaded emulsion electrospun nanofibers: Characterization, drug release and in vitro biocompatibility. *RSC Adv.* 2015;5:100256-100267

150. Ekaputra AK, Prestwich GD, Cool SM, Hutmacher DW. The three-dimensional vascularization of growth factor-releasing hybrid scaffold of poly (ε-caprolactone)/collagen fibers and hyaluronic acid hydrogel. *Biomaterials*. 2011;32:8108-8117

151. Jiang J, Li Z, Wang H, Wang Y, Carlson MA, Teusink MJ, MacEwan MR, Gu L, Xie J. Expanded 3d nanofiber scaffolds: Cell penetration, neovascularization, and host response. *Adv. Healthcare Mater.* 2016;5:2993-3003

152. Chan FK-M, Moriwaki K, De Rosa MJ. Detection of necrosis by release of lactate dehydrogenase activity. *Methods Mol. Biol.* 2013:65-70

153. Scholzen T, Gerdes J. The ki-67 protein: From the known and the unknown. *J. Cell. Physiol.* 2000;182:311-322

154. Liu S, Shi-Wen X, Blumbach K, Eastwood M, Denton CP, Eckes B, Krieg T, Abraham DJ, Leask A. Expression of integrin β1 by fibroblasts is required for tissue repair in vivo. *J. Cell Sci.* 2010;123:3674-3682

155. Grose R, Hutter C, Bloch W, Thorey I, Watt FM, Fässler R, Brakebusch C, Werner S. A crucial role of β1 integrins for keratinocyte migration in vitro and during cutaneous wound repair. *Development*. 2002;129:2303-2315

156. Li J, Chen J, Kirsner R. Pathophysiology of acute wound healing. *Clin. Dermatol.* 2007;25:9-18

157. Margadant C, Sonnenberg A. Integrin–tgf-β crosstalk in fibrosis, cancer and wound healing. *EMBO Rep.* 2010;11:97-105

158. Galiano RD, Michaels V, Dobryansky M, Levine JP, Gurtner GC. Quantitative and reproducible murine model of excisional wound healing. *Wound Repair Regen*. 2004;12:485-492

159. Wang X, Ge J, Tredget EE, Wu Y. The mouse excisional wound splinting model, including applications for stem cell transplantation. *Nature protocols*. 2013;8:302

160. Griffin DR, Weaver WM, Scumpia PO, Di Carlo D, Segura T. Accelerated wound healing by injectable microporous gel scaffolds assembled from annealed building blocks. *Nat. Mater.* 2015;14:737-744

161. Khorasani H, Zheng Z, Nguyen C, Zara J, Zhang X, Wang J, Ting K, Soo C. A quantitative approach to scar analysis. *Am J Pathol*. 2011;178:621-628

162. Park E, Lee SM, Jung I-K, Lim Y, Kim J-H. Effects of genistein on early-stage cutaneous wound healing. *Biochem. Biophys. Res. Commun.* 2011;410:514-519

163. Tie L, An Y, Han J, Xiao Y, Xiaokaiti Y, Fan S, Liu S, Chen AF, Li X. Genistein accelerates refractory wound healing by suppressing superoxide and foxo1/inos pathway in type 1 diabetes. *J. Nutr. Biochem.* 2013;24:88-96

164. Ma K, Liao S, He L, Lu J, Ramakrishna S, Chan CK. Effects of nanofiber/stem cell composite on wound healing in acute full-thickness skin wounds. *Tissue Eng., Part A*. 2011;17:1413-1424

165. Gil ES, Panilaitis B, Bellas E, Kaplan DL. Functionalized silk biomaterials for wound healing. *Adv. Healthcare Mater.* 2013;2:206-217

166. Anjum F, Agabalyan NA, Sparks HD, Rosin NL, Kallos MS, Biernaskie J. Biocomposite nanofiber matrices to support ecm remodeling by human dermal progenitors and enhanced wound closure. *Sci. Rep.* 2017;7:10291

167. Levengood SL, Erickson AE, Chang FC, Zhang M. Chitosan-poly(caprolactone) nanofibers for skin repair. *J. Mater. Chem. B*. 2017;5:1822-1833

168. Xu HL, Chen PP, ZhuGe DL, Zhu QY, Jin BH, Shen BX, Xiao J, Zhao YZ. Liposomes with silk fibroin hydrogel core to stabilize bfgf and promote the wound healing of mice with deep second-degree scald. *Adv. Healthcare Mater.* 2017;6:1700344

169. Hotaling NA, Bharti K, Kriel H, Simon CG. Diameterj: A validated open source nanofiber diameter measurement tool. *Biomaterials*. 2015;61:327-338

170. Deravi LF, Su T, Paten JA, Ruberti JW, Bertoldi K, Parker KK. Differential contributions of conformation extension and domain unfolding to properties of fibronectin nanotextiles. *Nano Lett.* 2012;12:5587-5592

171. Stalder A, Kulik G, Sage D, Barbieri L, Hoffmann P. A snake-based approach to accurate determination of both contact points and contact angles. *Colloids Surf., A*. 2006;286:92-103

172. Liu X, Lin T, Gao Y, Xu Z, Huang C, Yao G, Jiang L, Tang Y, Wang X. Antimicrobial electrospun nanofibers of cellulose acetate and polyester urethane composite for wound dressing. *J. Biomed. Mater. Res., Part B*. 2012;100:1556-1565

173. Lin J, Li C, Zhao Y, Hu J, Zhang L-M. Co-electrospun nanofibrous membranes of collagen and zein for wound healing. *ACS Appl. Mater. Interfaces*. 2012;4:1050-1057

174. Thevenaz P, Ruttimann UE, Unser M. A pyramid approach to subpixel registration based on intensity. *IEEE Trans. Image Process.* 1998;7:27-41

175. Klopfenstein DR, Vale RD. The lipid binding pleckstrin homology domain in unc-104 kinesin is necessary for synaptic vesicle transport in caenorhabditis elegans. *Mol. Biol. Cell*. 2004;15:3729-3739

176. Rezakhaniha R, Agianniotis A, Schrauwen JTC, Griffa A, Sage D, Bouten Cv, Van de Vosse F, Unser M, Stergiopulos N. Experimental investigation of collagen waviness and orientation in the arterial adventitia using confocal laser scanning microscopy. *Biomech. Model. Mechanobiol.* 2012;11:461-473

177. Campbell L, Emmerson E, Davies F, Gilliver SC, Krust A, Chambon P, Ashcroft GS, Hardman MJ. Estrogen promotes cutaneous wound healing via estrogen receptor β independent of its antiinflammatory activities. *J. Exp. Med.* 2010;207:1825-1833

178. LeBlanc ES, Janowsky J, Chan BK, Nelson HD. Hormone replacement therapy and cognition: Systematic review and meta-analysis. *JAMA*. 2001;285:1489-1499

179. Thomas C, Gustafsson J-Å. The different roles of er subtypes in cancer biology and therapy. *Nat. Rev. Cancer*. 2011;11:597

180. De Wever B, Kurdykowski S, Descargues P. Human skin models for research applications in pharmacology and toxicology: Introducing nativeskin®, the "missing link" bridging cell culture and/or reconstructed skin models and human clinical testing. *Applied In Vitro Toxicology*. 2015;1:26-32

181. Pashuck ET, Stevens MM. Designing regenerative biomaterial therapies for the clinic. *Sci. Transl. Med.* 2012;4:160sr164-160sr164

182. Wu J-G, Ge J, Zhang Y-P, Yu Y, Zhang X-Y. Solubility of genistein in water, methanol, ethanol, propan-2-ol, 1-butanol, and ethyl acetate from (280 to 333) k. *J. Chem. Eng. Data*. 2010;55:5286-5288

183. Huang J, Nasr M, Kim Y, Matthews H. Genistein inhibits protein histidine kinase. *J. Biol. Chem.* 1992;267:15511-15515

184. Kadler KE, Holmes DF, Trotter JA, Chapman JA. Collagen fibril formation. *Biochem. J.* 1996;316:1-11

185. Segura T, Anderson BC, Chung PH, Webber RE, Shull KR, Shea LD. Crosslinked hyaluronic acid hydrogels: A strategy to functionalize and pattern. *Biomaterials*. 2005;26:359-371

186. Nijhof JG, Braun KM, Giangreco A, van Pelt C, Kawamoto H, Boyd RL, Willemze R, Mullenders LH, Watt FM, de Gruijl FR. The cell-surface marker mts24 identifies a novel

population of follicular keratinocytes with characteristics of progenitor cells. *Development*. 2006;133:3027-3037

187. Boekema B, Ulrich MMW, Middelkoop E. Models for cutaneous wound healing. *Wound Repair Regen*. 2017;25:347-348

188. Emmerson E, Campbell L, Davies FC, Ross NL, Ashcroft GS, Krust A, Chambon P, Hardman MJ. Insulin-like growth factor-1 promotes wound healing in estrogen-deprived mice: New insights into cutaneous igf-1r/erα cross talk. *J. Investig. Dermatol*. 2012;132:2838-2848

189. Patisaul HB, Jefferson W. The pros and cons of phytoestrogens. *Front Neuroendocrinol.* 2010;31:400-419

6 List of Publications

1. **Ahn S,** Chantre CO, Ardoña HAM, Campbell PH, Parker KK. Plant-inspired biomimetic and estrogenic fibers promote wound healing via estrogen receptor β. *in preparation*

2. **Ahn S,** Ardoña HAM, Campbell PH, Gonzalez GM, Parker KK. Alfalfa nanofibers for dermal wound healing. *submitted*

3. **Ahn S**, Ardoña HA, Lind JU, Eweje F, Kim SL, Gonzalez GM, Liu Q, Zimmerman JF, Pyrgiotakis G, Zhang Z, Beltran-Huarac J, Carpinone P, Moudgil BM, Demokritou P, Parker KK. Mussel-inspired 3d fiber scaffolds for heart-on-a-chip toxicity studies of engineered nanomaterials. *Anal. Bioanal. Chem.* 2018;410(24):6141-6154

4. Chantre CO, Campbell PH, Golecki HM, Buganza AT, Capulli AK, Deravi LF, Dauth S, Sheehy SP, Paten JA, Gledhill K, Doucet YS, Abaci HE, **Ahn S**, Pope BD, Ruberti JW, Hoerstrup SP, Christiano AM, Parker KK. Production-scale Fibronectin Nanofibers Promote Wound Closure and Tissue Repair in a Dermal Mouse Model. *Biomaterials*. 2018;166:96-108

5. **Ahn S**, Lee KY, Parker KK, Shin K. Formation of multi-component extracellular matrix protein fibers. *Sci. Rep*. 2018:8(1);1913

6. **Ahn S**, Chantre CO, Gannon AR, Lind JU, Campbell PH, Grevesse T, O'Connor BB, Parker KK. Soy protein/cellulose nanofiber scaffolds mimicking skin extracellular matrix for enhanced wound healing. *Adv. Healthcare Mater*. 2018;7(9):1701175

7. Capulli AK, Emmert MY, Pasqualini FS, Kehl D, Caliskan E, Lind JU, Sheehy SP, Park SJ, **Ahn S**, Weber B, Goss JA, Hoerstrup SP, Parker KK. JetValve: Rapid manufacturing of biohybrid scaffolds for biomimetic heart valve replacement. *Biomaterials.* 2017;133:229-241

8. Park SJ, Gazzola M, Park KS, Park S, DiSanto V, Blevins EL, Lind JU, Campbell PH, Dauth S, Capulli AK, Pasqualini FS, **Ahn S**, Cho A, Yuan H, Maoz BM, Vijaykumar R, Choi JW, Deisseroth K, Lauder GV, Mahadevan L, Parker KK. Phototactic guidance of a tissue-engineered soft-robotic ray. *Science*. 2016;353(6295):158-162

9. **Ahn S**, Deravi LF, Park SJ, Dabiri BE, Kim JS, Parker KK, Shin K. Self-organizing large-scale extracellular-matrix protein network. *Adv. Mat.* 2015;27(18):2838-2845